JAERI-M
6964

THEORETICAL INVESTIGATIONS OF LOWER HYBRID RESONANCE HEATING IN A TOKAMAK

March 1977

Hiromu MOMOTA*, Atsushi FUKUYAMA**, Masafumi AZUMI,
Masao OKAMOTO and Tomonori TAKIZUKA

日本原子力研究所
Japan Atomic Energy Research Institute

この報告書は，日本原子力研究所がJAERI-Mレポートとして，不定期に刊行している研究報告書です．入手，複製などのお問合わせは，日本原子力研究所技術情報部（茨城県那珂郡東海村）あて，お申しこしください．

JAERI-M reports, issued irregularly, describe the results of research works carried out in JAERI. Inquiries about the availability of reports and their reproduction should be addressed to Division of Technical Information, Japan Atomic Energy Research Institute, Tokai-mura, Naka-gun, Ibaraki-ken, Japan.

JAERI-M 6964

Theoretical Investigations of Lower Hybrid Resonance Heating in a Tokamak

Hiromu MOMOTA*, Atsushi FUKUYAMA,**

Masafumi AZUMI, Masao OKAMOTO and Tomonori TAKIZUKA

Division of Thermonuclear Fusion Research, Tokai, JAERI

(Received January 31, 1977)

Theoretical investigations of the lower hybrid wave heating in a tokamak have been performed systematically. The requisite power for the additional heating of a large scale tokamak, JT-60, is estimated to be about 10 MW. Linear behaviour of an incident wave is extensively examined and its physical picture is clarified. The effect of toroidicity on propagation and dispersion of a lower hybrid wave is also studied. Parametric phenomena are treated without dipole approximation and the threshold in JT-60 is also examined. The formation of the high energy ion tail attributed to a high power wave is shown by theory and a good agreement with numerical calculation is obtained.

---

*) Guest staff of JAERI: Department of Electronics, Faculty of Engineering, Kyoto University, Kyoto.

**) Department of Electronics, Faculty of Engineering, Kyoto University, Kyoto (Present address: Department of Electronics, Faculty of Engineering, Okayama University, Okayama).

JAERI－M 6964

トカマクにおける低域混合波共鳴加熱の理論的研究

日本原子力研究所東海研究所
核融合研究部

百田　弘*・福山　淳**・安積　正史・岡本　正雄・滝塚　知典

（ 1977年1月31日受理 ）

トカマクにおける低域混合波共鳴加熱（ LHRH ）に関する理論的検討を系統的に行なう。始めに，大型トカマクJT－60 の付加加熱に必要なパワーを評価し，およそ10 MW 必要であることを示す。入射波の線型的な振舞を広範囲にわたって研究し，それらの物理的描像を鮮明にする。低域混合波の伝搬や分散に及ぼすトロイダル効果についても研究する。ダイポール近似を行なわずにパラメトリック励起の解析を行ない，JT－60 におけるしきい値について調べる。 最後に大振幅入射波に帰因する高エネルギー・イオンの生成を理論的に示し，数値計算による結果とも良く一致することを示す。

* ） 客員研究員： 京都大学工学部電子工学教室
** ） 京都大学工学部電子工学教室（現住所： 岡山大学工学部電子工学教室）

Contents

	Page
§1. Introduction	1
§2. Estimations of requisite power and frequency for a large scale tokamak	2
§3. Linear phenomena	6
§3-1 Dispersion relation in a homogeneous plasma	7
§3-2 Effects of density gradient	22
§3-3 Effects of magnetic field gradient	41
§3-4 Effects of toroidicity	47
§4. Parametric decay processes	56
§4-1 Coupled dispersion relation	56
§4-2 Effects of finite wavelength of pump	60
§5. Tail formation	65
§5-1 Stochastic behaviour of a phase point	65
§5-2 Tail formation and the threshold	73
§6. Summary and discussion	77
Acknowledgement	78
References	78
Appendices	81

§1. Introduction

As is well known, an ohmic heating of a tokamak plasma is hardly effective when the temperature of this plasma becomes higher. Hence, in addition to the ohmic heating, other heating methods available for high temperature plasmas are required in order to obtain thermonuclear plasmas. In these situations, a major effort of controlled thermonuclear research is devoted to study and find out methods of additional further heating of high temperature plasmas.

Among various types of wave heating methods, LHRH (Lower Hybrid Resonance Heating) seems prospective because it possibly supplies the requisite power for a further heating and possibly couples to a plasma without any exciting coils. A number of theoretical analyses have been reported in connection with LHRH. However some discussions are based on very idealized models and disorganized. The purpose of this note is to provide an investigation on LHRH of a large scale tokamak plasma with realistic and systematic analyses.

First of all, the requisite power for an additional heating of a large scale tokamak: JT-60 [1], is introduced and the amplitude of an incident wave which characterizes the phenomena is estimated. In this situation, all the nonlinear processes are ignored.

The evolution of an incident wave energy is analysed in §3 within the framework of linear mechanism. The dispersion relation of lower hybrid wave in a homogeneous plasma is reviewed and the validity of an electrostatic approximation is justified. Then the effects of a density gradient and a magnetic field gradient are considered. Propagations, reflections and the damping of the wave is summarized. By tracing the incident ray, we will estimate the toroidal effects on the propagation of the wave in the last of this section.

This energy density of incident wave may be so large that nonlinear decay processes, especially parametric excitations, prevent the propagation of the wave energy towards the turning point. Since the wave number of a lower hybrid wave may become large, the usual dipole approximation is not applicable in our situation. A general dispersion relation for four electrostatic wave coupling in a homogeneous plasma is derived in §4. Then the effects of the finiteness of the pump wavelength on the parametric decay processes are analysed.

In §5, the formation of a high energy ion tail is analysed. This tail formation is attributed to an applied high power wave propagating perpendicularly to a magnetic field and is described in terms of "stochasticity". The threshold of an incident wave energy for the tail formation at a certain ion energy is obtained. The results are compared with numerical simulations

The results are summarized in the last section and discussions on the results are presented.

§2. Estimations of requisite power and frequency for a large scale tokamak

In this section, we evaluate basic parameters roughly for RF heating near lower hybrid frequency in JT-60 Tokamak [1]. Based on the evaluated parameters we consider the accessibility condition, position of turning point, changes of wave-numbers, intensities of electric field, potential of lower hybrid wave propagating towards the center of a plasma, and effect of impurities. It should be emphasized that the aim of the present evaluation is not to determine the parameters for designing the apparatus of the RF additional heating of JT-60, but to grasp the theoretical concept of lower hybrid resonance heating in a tokamak. The following parameters estimated roughly are nothing but one example.

Design parameters of JT-60 are as follows:

major radius	$R = 3$ m
minor radius	$a = 1$ m
toroidal magnetic field	$B = 5$ Wb/m
number density (averaged)	$\bar{n} \simeq 5\times10^{19}$ m^{-3}
plasma current	$I_p \simeq 3$ MA
ion and electron temperature (at the center)	$T \simeq 10$ keV
energy confinement time	$n\tau_E \simeq (2\sim6)\times10^{19}$ sec/m^3

First, we estimate the requisite power for RF heating in JT-60. Assuming that all the input power W is absorbed in the plasma, we consider the energy balance equation

$$2\cdot\frac{d}{dt}\left(\frac{3}{2}N_tT\right) = W - 2\cdot\frac{3}{2}N_tT/\tau_E\ , \qquad (2.1)$$

$$(N_t = 2\pi^2Ra^2N)$$

In §5, the formation of a high energy ion tail is analysed. This tail formation is attributed to an applied high power wave propagating perpendicularly to a magnetic field and is described in terms of "stochasticity". The threshold of an incident wave energy for the tail formation at a certain ion energy is obtained. The results are compared with numerical simulations

The results are summarized in the last section and discussions on the results are presented.

§2. Estimations of requisite power and frequency for a large scale tokamak

In this section, we evaluate basic parameters roughly for RF heating near lower hybrid frequency in JT-60 Tokamak [1]. Based on the evaluated parameters we consider the accessibility condition, position of turning point, changes of wave-numbers, intensities of electric field, potential of lower hybrid wave propagating towards the center of a plasma, and effect of impurities. It should be emphasized that the aim of the present evaluation is not to determine the parameters for designing the apparatus of the RF additional heating of JT-60, but to grasp the theoretical concept of lower hybrid resonance heating in a tokamak. The following parameters estimated roughly are nothing but one example.

Design parameters of JT-60 are as follows:

major radius	$R = 3$ m
minor radius	$a = 1$ m
toroidal magnetic field	$B = 5$ Wb/m
number density (averaged)	$\bar{n} \simeq 5\times10^{19}$ m^{-3}
plasma current	$I_p \simeq 3$ MA
ion and electron temperature (at the center)	$T \simeq 10$ keV
energy confinement time	$n\tau_E \simeq (2\sim6)\times10^{19}$ sec/m^3

First, we estimate the requisite power for RF heating in JT-60. Assuming that all the input power W is absorbed in the plasma, we consider the energy balance equation

$$2\cdot\frac{d}{dt}\left(\frac{3}{2}N_tT\right) = W - 2\cdot\frac{3}{2}N_tT/\tau_E\ , \qquad (2.1)$$

$$(N_t = 2\pi^2Ra^2N)$$

where N_t is the total number and N is the number density. We have assumed in Eq. (2.1) that confinement time of energy produced by RF irradiation is the same as plasma energy confinement time. From Eq. (2.1), assuming τ_E = 1 sec in the steady state, we obtain W = 10 MW to achieve the increase of T = 7 keV. The intensity of the externally applied electric field outside the plasma, E_s is estimated by calculating the Poynting vector through the surface irradiated by this electric field:

$$E_s = \left(\frac{W}{c\varepsilon_0 S} \right)^{1/2} , \qquad [\text{Volt/m}] \tag{2.2}$$

where $c = 2.998\times10^8$ m/sec is the light speed, $\varepsilon_0 = 8.854185\times10^{-12}$ F/m is the permittivity of vacuum and S is the surface area (m^2). If the RF field is irradiated all over the plasma surface, then, $S \simeq 2\pi a \cdot 2\pi R$ and we obtain $E = 5.6\times10^3$ V/m. However, in reality, the surface is localized and the intensity of external field is determined by the condition of discharge break down. It is expected that $E_s \simeq (2\sim2.5)\times10^5$ V/m can be generated [2]. The lower hybrid frequency, ω_{LH}, is given by

$$\omega_{LH} = \frac{\omega_{pi}}{(1+\omega_{pe}^2/\Omega_e^2)^{1/2}} , \tag{2.3}$$

where $\omega_{p\sigma} = (N_\sigma e_\sigma^2/m_\sigma\varepsilon_0)^{1/2}$ is the plasma frequency and $\Omega_\sigma = e_\sigma B_0/m_\sigma$ is the cyclotron frequency for the species σ. We assume that the plasma density of JT-60 is parabolic and that the pump frequency f_0 is adjusted to the lower hybrid frequency at $x_{res} = 0.2a$. (a is the radius and x_{res} is called a lower hybrid resonance point. See Fig. 2.1) Assuming $N_0 = 5\times10^{19}$ m^{-3} at the plasma center, we obtain f_0 = 1.33 GHz. ($\omega_0 = 8.34\times10^9$/sec). At the lower hybrid resonance point, $\omega_{pe}/\Omega_e \simeq 0.44$ ($\omega_{pe}^2/\Omega^2 \simeq 0.2$), then $\omega_0 = \omega_{LH}(x_{res}) \simeq \omega_{pi}(x_{res})$. Later, it will be noted that the presence of impurity ions alters the condition of pump frequency. The accessibility condition is given in terms of the index of refraction in the z-direction (the direction of the toroidal magnetic field),

$$N_z^2 = \frac{k_{0z}^2 c^2}{\omega_0^2} > 1 + \frac{\omega_{per}^2}{\Omega_e^2} , \tag{2.4}$$

where k_{0z} is the wavenumber in the z-direction of the pump field and $\omega_{per} = \omega_{pe}(x_{res})$. The validity of Eq. (2.4) will be given in §3. It is preferable that N_z is smaller, since, otherwise, the lower hybrid wave will experience an electron Landau damping during propagation. In the present

example, the right hand side of Eq. (2.4) is equal to 1.194, and we choose $N_z = 1.53$. Then, we obtain $k_{0z} \simeq 42.47\ m^{-1}$ and $\lambda_{0z} = 2\pi/k_{0z} \simeq 0.15$ m.

Using the parameters estimated above, we calculate numerically the fluid equations in order to know the behaviour of the propagation of lower hybrid wave excited externally. The numerical calculations were performed under the conditions that the density and temperature at the center $N_0 = 5\times10^{19}\ m^{-3}$ and $T_{e0} = T_{i0} = 5$ keV. The results are shown in Fig. 2.1; (a) the perpendicular wavenumber k_x versus position, (b) the electric potential field ϕ versus position, (c) the intensity of the electric field E_x versus position. It is seen from Fig. 2.1 that the turning point where the group velocity of lower hybrid wave changes its sign appears near $x = 0.5a$. The modes of cold plasma wave and warm plasma wave are designated by superscripts of "cold" and "hot", respectively, in Fig. 2.1. Linear conversion occurs near turning points which is far from the center of plasma in the present case. Fig. 2.1(a) shows the increase of perpendicular wavenumber, k_x, and $k_x\rho_i$ becomes larger and exceeds unity. According to the linear theory which will be discussed in the following section, if $k_x\rho_i$ increases enough, then the warm plasma mode is converted further into ion Bernstein wave and it suffers collisionless damping heavily to heat plasma. However, the heating of plasma bodily is not expected since the wave does not penetrate deep into the plasma in the present case. Fig. 2.1(c) shows the increase of the perpendicular component of electric field intensity, E_x.

Some remarks are given on the effects of impurity ions which are present in the plasma. It is noted in [3] that the presence of impurities alters the pump frequency slightly. If $\Omega_i \ll \omega < |\Omega_e|$ for cold plasma, then the transverse dielectric constant, ε_T, is given by

$$\varepsilon_T = 1 + \frac{\omega_{pe}^2}{\Omega_e^2} - \frac{\omega_{pi}^2}{\omega^2} - \sum_j \frac{\omega_{pj}^2}{\omega^2} \quad , \tag{2.5}$$

where the sum is over the impurity species. Lower hybrid resonance occurs when $\varepsilon_T = 0$. Then, the frequency becomes

$$\omega^2 = \frac{\omega_{pe}^2}{1+\omega_{pe}^2/\Omega_e^2} Z_i \frac{m_e}{m_i} (1 - s) \ , \tag{2.6}$$

which recovers Eq. (2.3) when $s = 0$. In Eq. (2.6), s is defined as

$$s = \sum_j C_j Z_j \left(1 - \frac{Z_j m_i}{Z_i m_j}\right) \quad , \tag{2.7}$$

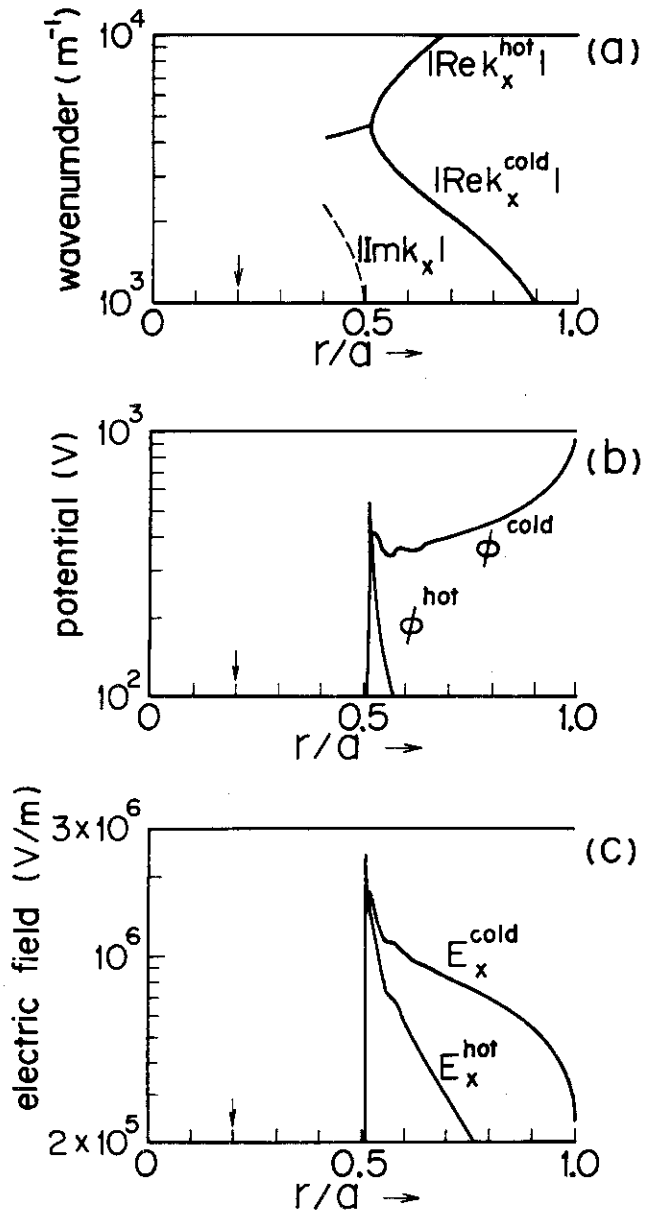

Fig. 2.1 Spatial evolution of an incident wave near the lower hybrid wave. Plasma density and temperature have parabolic profiles which vanish at the plasma edge ($r/a = 1.0$). At $r = 0$, $N = 5\times10^{19}$ m^{-3} and $T_e = T_i = 5$ keV. Incident frequency $f_0 = 1.3$ GHz and refractive index parallel to the uniform magnetic field $N_z = 1.53$ (parallel wavelength $\lambda_{0z} = 0.15$ m). The arrows indicate a lower hybrid resonance layer.

where C_j is the fractional concentration $C_j = n_j/n_e$ and Z_j and n_j are the charge number and density of the j-th impurity species.
If the impurity species are not of high atomic number and are fully ionized, then $Z_j m_i / Z_i m_j \simeq 1/2$ and $s \simeq (1/2) \sum_j C_j Z_j$. It is obvious that $0 \leq s < 1$.
From Eq. (2.6), the lower hybrid frequency becomes lower when impurities are present if we fix the position of lower hybrid resonance. In other words, for a fixed pump frequency, the lower hybrid layer shifts towards the center of the plasma when impurities exist. If there is 5 % fully ionized oxygen, then in the case of Fig. 2.1, the frequency becomes $f_0 =$ 1.06 GHz at $x_{res} = 0.2a$. With 4 % fully ionized oxygen and 4 % fully ionized carbon, $f_0 = 0.96$ GHz. The accessibility condition becomes [3]

$$N_z^2 > (1 - \frac{1}{1-s} \frac{\omega_0^2}{\Omega_e \Omega_i})^{-1} \tag{2.8}$$

In the case of Fig. 2.1, if $f_0 = 1.33$ GHz ($\omega_0 = 8.34 \times 10^9$/sec) and there is 4 % fully ionized oxygen and 4 % fully ionized carbon, then the minimum of N_z^2 is 1.3, whereas in the absence of impurity it is 1.2.

In the above discussions, we have not considered nonlinear phenomena. The parametric threshold will be shown to be $(2 \sim 5) \times 10^5$ V/m for JT-60 in §4. It is seen from Fig. 2.1 that the electric field predicted by the linear theory exceeds the parametric threshold before it reaches the turning point. If parametric instability is driven, there may be some fears that the propagation of the wave energy towards the center of plasma would be prevented which would result in peripheral heating. Some discussions about parametric instabilities will be presented later.

§3. Linear phenomena

Many authors have been studying linear phenomena of lower hybrid waves such as dispersion relation, damping, propagation, accessibility, linear mode conversion and ray trajectories [4-26]. Also, some experimental works have been carried out [33-40]. The purpose of the present section is to review and advance the linear theories of plasma waves near the lower hybrid frequency for the purpose of the investigations of the additional heating by LHRH in tokamaks. Especially, we clarify the linear processes of the waves in JT-60 device. The work presented here will also serve the investigation of nonlinear phenomena which will be discussed in the sections

where C_j is the fractional concentration $C_j = n_j/n_e$ and Z_j and n_j are the charge number and density of the j-th impurity species.
If the impurity species are not of high atomic number and are fully ionized, then $Z_j m_i / Z_i m_j \simeq 1/2$ and $s \simeq (1/2) \sum_j C_j Z_j$. It is obvious that $0 \leq s < 1$.
From Eq. (2.6), the lower hybrid frequency becomes lower when impurities are present if we fix the position of lower hybrid resonance. In other words, for a fixed pump frequency, the lower hybrid layer shifts towards the center of the plasma when impurities exist. If there is 5 % fully ionized oxygen, then in the case of Fig. 2.1, the frequency becomes $f_0 =$ 1.06 GHz at $x_{res} = 0.2a$. With 4 % fully ionized oxygen and 4 % fully ionized carbon, $f_0 = 0.96$ GHz. The accessibility condition becomes [3]

$$N_z^2 > (1 - \frac{1}{1-s} \frac{\omega_0^2}{\Omega_e \Omega_i})^{-1} \tag{2.8}$$

In the case of Fig. 2.1, if $f_0 = 1.33$ GHz ($\omega_0 = 8.34 \times 10^9$/sec) and there is 4 % fully ionized oxygen and 4 % fully ionized carbon, then the minimum of N_z^2 is 1.3, whereas in the absence of impurity it is 1.2.

In the above discussions, we have not considered nonlinear phenomena. The parametric threshold will be shown to be $(2 \sim 5) \times 10^5$ V/m for JT-60 in §4. It is seen from Fig. 2.1 that the electric field predicted by the linear theory exceeds the parametric threshold before it reaches the turning point. If parametric instability is driven, there may be some fears that the propagation of the wave energy towards the center of plasma would be prevented which would result in peripheral heating. Some discussions about parametric instabilities will be presented later.

§3. Linear phenomena

Many authors have been studying linear phenomena of lower hybrid waves such as dispersion relation, damping, propagation, accessibility, linear mode conversion and ray trajectories [4-26]. Also, some experimental works have been carried out [33-40]. The purpose of the present section is to review and advance the linear theories of plasma waves near the lower hybrid frequency for the purpose of the investigations of the additional heating by LHRH in tokamaks. Especially, we clarify the linear processes of the waves in JT-60 device. The work presented here will also serve the investigation of nonlinear phenomena which will be discussed in the sections

§4 and 5, since the analysis of the evolution of an incident wave energy in this section will be useful for studying the possibilities of the parametric instability and ion tail formation.

The dispersion relation of the lower hybrid wave in a homogeneous plasma is reviewed and the validity of an electrostatic approximation is justified in §3-1. Then the effects of density and magnetic field inhomogeneities are considered in §3-2 and §3-3. The results will be applied to a large scale tokamak, JT-60, to clarify the propagation, reflections and dampings of an incident lower hybrid wave in JT-60. Finally, we will estimate the toroidal effects on the propagation of the wave by ray tracing.

§3-1 Dispersion relation in a homogeneous plasma

(1) Cold plasma approximation

The local properties of plasma waves in a weakly inhomogeneous plasma can be explained to a great extent by means of a dispersion relation in a homogeneous plasma. Section §3-1 deals with the local dispersion relation of plasma waves near the lower hybrid frequency.

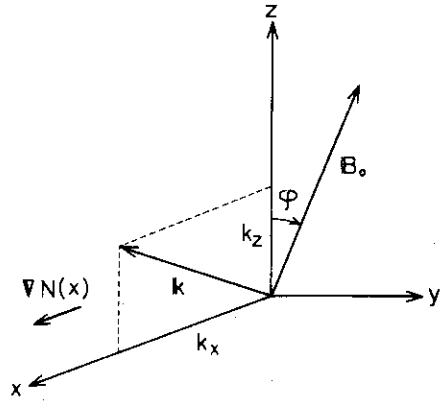

Fig.3.1 Magnetized plasma of slab geometry.

We shall consider a magnetized plasma of the slab geometry illustrated in Fig. 3.1. The plasma is uniform in the y-z plane, while the plasma density N increases in the x direction. The applied static magnetic field has two components $(0, B_0\sin\psi, B_0\cos\psi)$. It is assumed that the amplitude of the plasma wave is small enough for a linear theory to be employed and that the wave has a form of a stationary plane wave, $\exp i(k_x x + k_z z - \omega t)$; the quantities which can be determined externally such as ω and k_z are

assumed to be real and only k_x is considered to be complex.

In the cold plasma approximation, the dielectric tensor ε takes the form,

$$\overleftrightarrow{\varepsilon} = \begin{bmatrix} 1-h & i\alpha h\cos\psi & -i\alpha h\sin\psi \\ -i\alpha h\cos\psi & 1-h-\beta h\sin^2\psi & -\beta h\sin\psi\cos\psi \\ i\alpha h\sin\psi & -\beta h\sin\psi\cos\psi & 1-h-\beta h\cos^2\psi \end{bmatrix} , \tag{3.1}$$

where

$$\left.\begin{aligned} h &= \frac{\omega_{pe}^2}{\omega^2-\Omega_e^2} + \frac{\omega_{pi}^2}{\omega^2-\Omega_i^2} , \\ \alpha h &= \frac{\omega_{pe}^2}{\omega^2}\frac{\omega\Omega_e}{\Omega_e^2-\omega^2} + \frac{\omega_{pi}^2}{\omega^2}\frac{\omega\Omega_i}{\Omega_i^2-\omega^2} , \\ \beta h &= \frac{\omega_{pe}^2}{\omega^2}\frac{\Omega_e^2}{\Omega_e^2-\omega^2} + \frac{\omega_{pi}^2}{\omega^2}\frac{\Omega_i^2}{\Omega_i^2-\omega^2} . \end{aligned}\right\} \tag{3.2}$$

The wave number vector and the frequency of an electromagnetic wave must satisfy the dispersion relation,

$$D(\omega,\vec{k}) = \det \overleftrightarrow{D}(\omega,\vec{k}) = 0 , \tag{3.3}$$

where the dispersion tensor $\overleftrightarrow{D}$ is defined by

$$\overleftrightarrow{D}(\omega,\vec{k}) = \frac{c^2}{\omega^2}(\vec{k}\vec{k} - k^2\overleftrightarrow{I}) + \overleftrightarrow{\varepsilon} . \tag{3.4}$$

The dispersion curves in the typical plasma frequency regions are shown in Fig. 3.2 for $k_x = 0$, Fig. 3.3 for $k_z = 0$ and Fig. 3.4 for finite k_z, respectively.

When the waves propagate perpendicularly to the static magnetic field ($k_z = 0$, $\psi = 0$), they can be split into the ordinary and the extraordinary modes. The latter mode

$$\frac{k_x^2c^2}{\omega^2} = \frac{\varepsilon_{xx}^2 - \varepsilon_{xy}^2}{\varepsilon_{xx}} , \tag{3.5}$$

shows hybrid resonances when $\varepsilon_{xx} = 0$, i.e. $h = 1$; and it has two branches the resonance frequency of which are called the upper hybrid frequency ω_{UH} ($\omega_{UH} > |\Omega_e|$) and the lower hybrid frequency ω_{LH} ($\sqrt{\Omega_i|\Omega_e|} > \omega_{LH} > \Omega_i$), respectively. While the upper hybrid resonance is mainly related to the

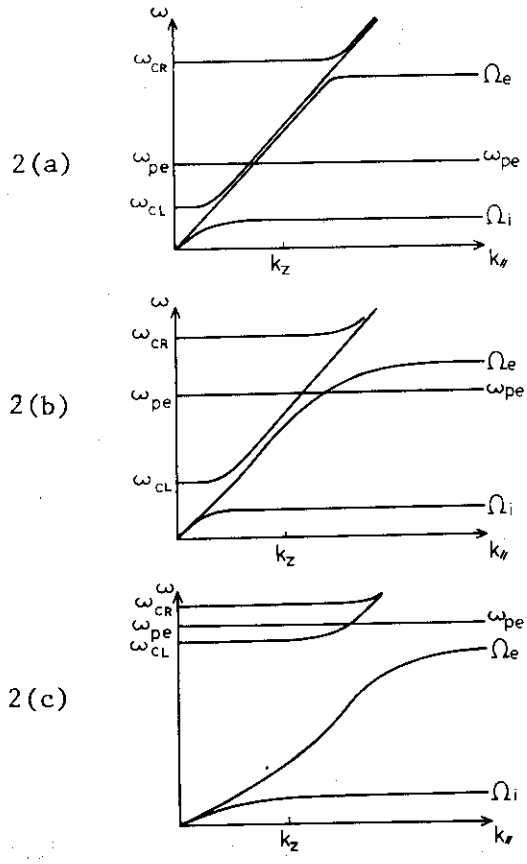

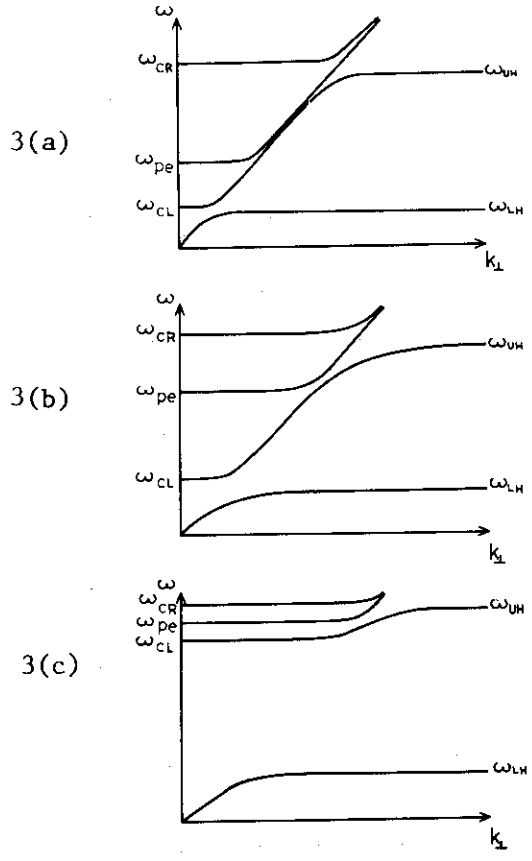

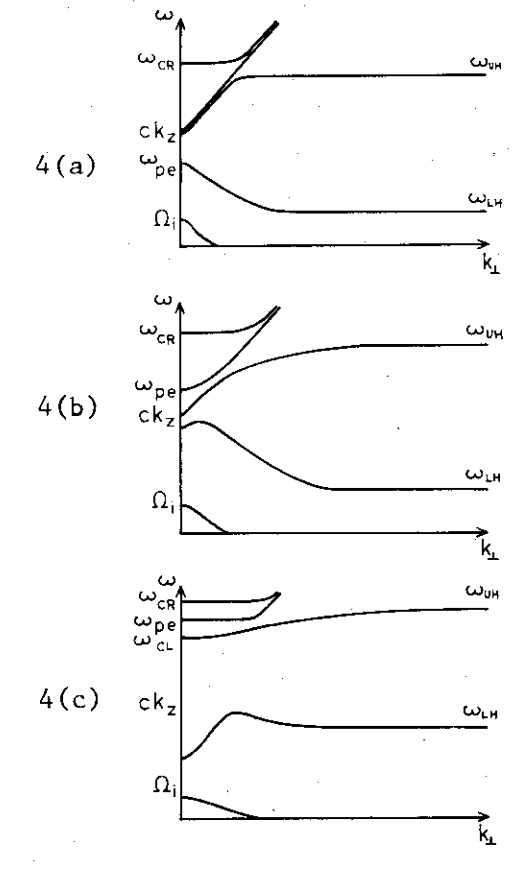

Fig.3.2 Dispersion curves in the typical plasma frequency regions for $k_x=0$; (a) $\Omega_i<\omega_{pe}<\sqrt{\Omega_i|\Omega_e|}$, (b) $\sqrt{\Omega_i|\Omega_e|}<\omega_{pe}<|\Omega_e|$, (c) $|\Omega_e|<\omega_{pe}$.

Fig.3.3 Dispersion curves in the typical plasma frequency regions for $k_z=0$.

Fig.3.4 Dispersion curves in the typical plasma frequency regions for nonzero k_z.

motion of electrons, the lower hybrid resonance (LHR) with which we will be concerned has relation to both electrons and ions. If we assume that $\Omega_i \ll \omega < |\Omega_e|$, the LH frequency, ω_{LH}, can be approximated by

$$\omega_{LH}^2 \simeq \frac{\omega_{pi}^2}{1 + \frac{\omega_{pe}^2}{\Omega_e^2}} \quad , \tag{3.6}$$

and in the other way for a given frequency $\omega < \sqrt{\Omega_i |\Omega_e|}$, LHR occurs where the plasma density satisfies

$$\frac{\omega_{pe}^2}{\Omega_e^2} = \frac{\omega_{per}^2}{\Omega_e^2} \equiv q \ , \tag{3.7}$$

where

$$q = \frac{(\frac{\omega^2}{\Omega_i^2} - 1)(1 - \frac{m_e^2}{m_i^2}\frac{\omega^2}{\Omega_i^2})}{(\frac{m_i}{m_e} - \frac{\omega^2}{\Omega_i^2})(1 + \frac{m_e}{m_i})} \simeq \frac{\omega^2}{\Omega_i |\Omega_e| - \omega^2} \quad , \tag{3.8}$$

and the suffix r indicates the value at the LHR. However, as is shown from the dispersion curve in Fig. 3.3, the extraordinary wave cannot propagate in the plasma where $\omega_{pe} < \omega_{per}$; therefore a wave cannot reach the LHR from outside of a confined plasma.

On the other hand, when there exists nonzero k_z determined by a wave source the LHR is accessible to the wave from the lower density side. The condition for the accessibility is obtained in the following. The dispersion relation Eq. (3.3) is a quadratic equation with respect to k_x^2; and the coefficients (3.2) may be approximated by

$$\left.\begin{aligned} h &= \frac{\omega_{pe}^2}{\omega_{per}^2} = \frac{N}{N_r} \ , \\ \alpha &= \frac{\omega_{per}^2}{\omega}\frac{\Omega_e - \Omega_i}{\Omega_e^2 - \omega^2} + \frac{\Omega_i}{\omega} \simeq \frac{\omega_{per}^2}{\omega\Omega_e} \simeq O(\sqrt{\frac{m_i}{m_e}}) \quad , \\ \beta &= \frac{\omega_{per}^2}{\omega^2}\frac{\Omega_e^2 - \Omega_i^2}{\Omega_e^2 - \omega^2} + \frac{\Omega_i^2}{\omega^2} \simeq \frac{\omega_{per}^2}{\omega^2} \simeq O(\frac{m_i}{m_e}) \ , \end{aligned}\right\} \tag{3.9}$$

in the frequency range $\Omega_i \ll \omega \ll |\Omega_e|$. Except the extremely low density region $\omega_{pe} \sim \omega$, the solution to Eq. (3.3) can be simplified on the assumption that $\beta h >> 1$ to

$$\frac{k_x^2c^2}{\omega^2} \simeq \frac{\beta h}{2(1-h)}\left[\frac{k_z^2c^2}{\omega^2}\cos^2\psi - (1-h+qh) \pm \sqrt{\{\frac{k_z^2c^2}{\omega^2}\cos^2\psi - (1-h+qh)\}^2 - 4(1-h)qh}\right], \tag{3.10}$$

and the branch related to the LHR takes the upper sign. In order that the wave can propagate without considerable reflection, the r.h.s. of Eq. (3.10) must be real and positive. The sufficient condition for such a solution to exist can be easily obtained from Eq. (3.10),

$$\left|\frac{k_z c}{\omega}\cos\psi\right| > \sqrt{1-h} + \sqrt{qh}\ , \tag{3.11}$$

and for $0 < h < 1$ the r.h.s. takes its maximum value $\sqrt{1+q}$ at $h = \frac{q}{1+q}$. Therefore the accessiblity condition of the LHR from the lower density side is given as

$$\frac{k_z^2c^2}{\omega^2}\cos^2\psi\Big|_{h=\frac{q}{1+q}} > 1 + \frac{\omega_{per}^2}{\Omega_e^2} \simeq \frac{\Omega_i|\Omega_e|}{\Omega_i|\Omega_e|-\omega^2}\ . \tag{3.12}$$

Near the plasma boundary $\omega_{pe} \sim \omega$, the solution to Eq. (3.3) which leads to the LHR is approximated by

$$\frac{k_x^2c^2}{\omega^2} \simeq (\beta h\cos^2\psi - 1)\frac{k_z^2c^2}{\omega^2} - (\beta h - 1). \tag{3.13}$$

It should be noted here that the wave which satisfies the accessibility condition is evanescent where $\omega_{pe} < \omega$.

When the wave approaches the LHR, the x-component of the electric field E_x increases as well as k_x, so that the solution obtained from the electrostatic approximation,

$$\frac{k_x^2c^2}{\omega^2} = \frac{\beta h}{1-h}\cos^2\psi\,\frac{k_z^2c^2}{\omega^2}\ , \tag{3.14}$$

can be a good approximation. Comparing Eq. (3.14) with Eq. (3.10), we get a condition for the electrostatic approximation.

$$\left|\frac{k_z c}{\omega}\cos\psi\right| \gg \sqrt{1-h} + \sqrt{qh}\ . \tag{3.15}$$

Therefore if the accessibility condition Eq. (3.12) is well satisfied, the electrostatic approximation can be employed in the investigation of the LH waves.

The comparison of the exact real solution to Eq. (3.3) with the

solution from the electrostatic approximation is illustrated in Fig. 3.5, for an example of $\omega/\Omega_i = 30$, $\psi = 0$ and a mass number $A = 1$; in this case the accessibility condition (3.12) shows $k_{//}c/\omega = 1.3998$. There still exist a narrow evanescent gap for $k_{//}c/\omega = 1.4$, nevertheless the figure shows that the approximated analysis Eq. (3.12) gives a good criterion.

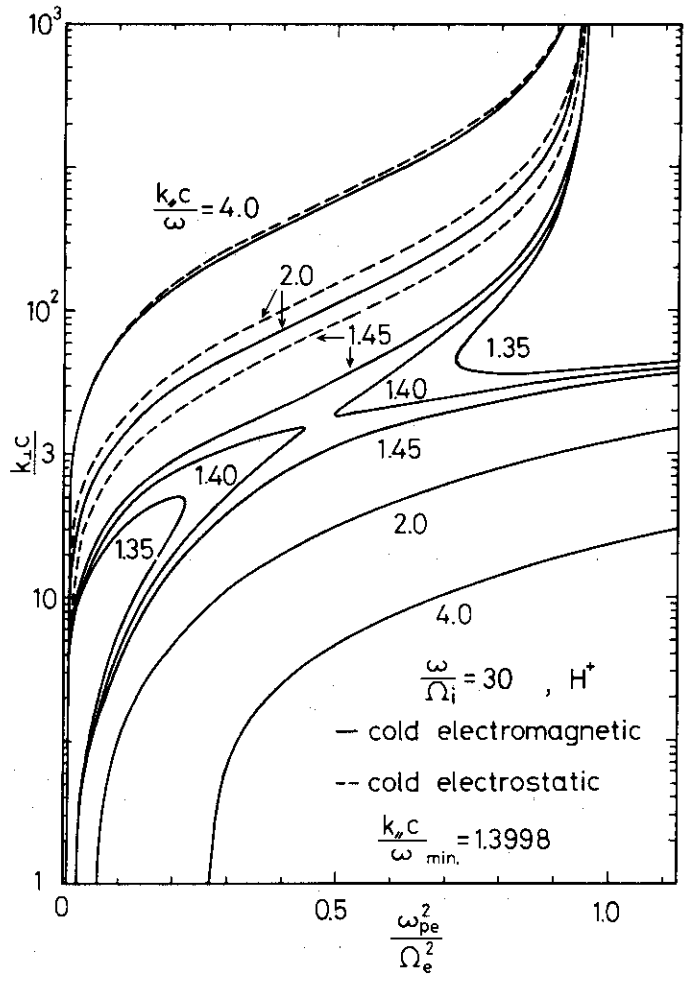

Fig. 3.5 The comparison of the exact real solutions to Eq. (3.3) with electrostatic approximation.

(2) Electrostatic approximation in a hot plasma

(2)-1 Dispersion relation in a hot plasma

With an increase of k_x, the effect of a finite Larmor radius becomes important in the dispersion relation of plasma waves. Assuming that the electrostatic approximation can be applied, we shall investigate the longitudinal dispersion in a magnetized collisionless plasma composed of

electrons and one species of ions with Maxwellian velosity distributions. The longitudinal dispersion relation derived from the Vlasov and Poisson equations is [30]

$$D_L \equiv \frac{\vec{k}\cdot\overleftrightarrow{D}\,\vec{k}}{k^2} = 1 + \chi_e + \chi_i = 0 \ , \tag{3.16}$$

where

$$\chi_\sigma = \frac{\omega_{p\sigma}^2}{k^2}\frac{m_\sigma}{T_\sigma}\left[1 + \sum_{n=-\infty}^{\infty}\frac{\omega}{\omega - n\Omega_\sigma}\left(W\left(Z_{\sigma n}\right) - 1\right)\Lambda_n(\lambda_\sigma)\right] \ , \tag{3.17}$$

$$Z_{\sigma n} = \frac{\omega - n\Omega_\sigma}{k_{//}\, v_{T\sigma}} \ , \qquad \lambda_\sigma = \frac{k_\perp^2 v_{T\sigma}^2}{\Omega_\sigma^2} \ ,$$

$$k_\perp^2 = k_x^2 + k_z^2 \sin^2\psi \ , \qquad k_{//} = k_z \cos\psi$$

and the thermal velosity $v_{T\sigma} = \sqrt{T_\sigma/m_\sigma}$. The properties of the plasma dispersion function $W(z)$ and the function $\Lambda_n(\lambda)$ defined by

$$\Lambda_n(\lambda) = I_n(\lambda)e^{-\lambda} \ , \tag{3.18}$$

with the aid of the modified Bessel function $I_n(\lambda)$ are summarized in Appendix A.

In the frequency range $\omega \ll |\Omega_e|$, the terms except $n = 0$ in the summation of the electron susceptivity χ_e may be neglected. The electron Landau damping caused by the imaginary part of $W(\omega/k_{//}v_{Te})$ prevents the effective ion heating; therefore we shall consider only the case of small electron Landau damping,

$$\frac{\omega}{k_{//}\, v_{Te}} \gg 1 \ . \tag{3.19}$$

Making use of the ion Larmor radius $\rho_i = v_{Ti}/\Omega_i$, we may rewrite this condition as

$$k_{//}\rho_i\left(\frac{T_e}{T_i}\right)^{1/2}\left(\frac{1+q}{q}\right)^{1/2} \ll 1 \ , \tag{3.20}$$

where $q \sim O(1)$ has been defined in Eq. (3.8).

If $k_\perp \rho_i \gg 1$ and $k_{//}\rho_i \gg 1$, the summation in the ion part χ_i can be approximated by the integral and the unmagnetized ion susceptivity,

$$\chi_i = \frac{\omega_{pi}^2}{k^2}\frac{m_i}{T_i} W\left(\frac{\omega}{kv_{Ti}}\right) , \tag{3.21}$$

is derived. Though this assumption is inadequate to the following analysis as the condition (3.20) leads to $k_{//}\rho_i \ll 1$, a discussion about it will be given in (2)-4 of §3-1 in connection with the effect of rare collisions.

On the assumption that $k_{//}\rho_i \ll 1$, we may neglect the terms involving $W(Z_{in})$ except a new integers of n nearest to ω/Ω_i; the rest terms in χ_i are summed up to a function,

$$f_{\omega^*}(\lambda_i) = \sum_{n=-\infty}^{\infty} \frac{\omega^*}{\omega^* - n} \Lambda_n(\lambda_i), \tag{3.22}$$

where $\omega^* = \omega/\Omega_i$. The behavior of this function is investigated in detail in Ref. [29]. When $\omega^* \gg 1$ and $\lambda_i \gg 1$, with the aid of the Hadamard expansion $f_{\omega^*}(\lambda_i)$ can be approximated by

$$f_{\omega^*}(\lambda_i) = 1 - \mathrm{Re}W\left(\frac{\omega^*}{k_\perp \rho_i}\right) + \mathrm{Im}W\left(\frac{\omega^*}{k_\perp \rho_i}\right) \cot \omega^*\pi \tag{3.23}$$

while when $\lambda_i \ll \omega^*$ and $\omega^* \gg 1$, $f_{\omega^*}(\lambda_i)$ can be expanded to

$$f_{\omega^*}(\lambda_i) = 1 + \frac{\lambda_i}{\omega^{*2}-1} + \frac{3\lambda_i^2}{(\omega^{*2}-1)(\omega^{*2}-4)} , \tag{3.24}$$

which corresponds to the asymptotic expansion of $1 - \mathrm{Re}\ W(\omega^*/k_\perp\rho_i)$. Since $\mathrm{Im}\,W(\omega^*/k_\perp\rho_i)$ is considerably small for $\omega^* \gg k_\perp\rho_i$, Eq. (3.23) is a good approximation as long as $\omega^* \gg 1$. Furthermore the following approximation is valid for $k\rho_i \ll 1 \ll \omega^*$.

$$\mathrm{Re}\,W\left(\frac{\omega^*}{k_\perp \rho_i}\right) + W\left(\frac{\omega^*}{k_{//}\rho_i}\right)\Lambda_0(k_\perp^2\rho_i^2) \simeq \mathrm{Re}\,W\left(\frac{\omega^*}{k\rho_i}\right) , \tag{3.25}$$

As a result of above discussion, provided $\Omega_i \ll \omega \ll |\Omega_e|$, $k_{//}\rho_i \ll 1$ and Eq. (3.20), one may approximate D_L by the following expression;

$$D_L = 1 + \frac{\omega_{pe}^2}{k^2}\frac{m_e}{T_i}\left[1 + W(z_{e0} - 1)\Lambda_0(\lambda_e)\right]$$

$$+ \frac{\omega_{pi}^2}{k^2}\frac{m_i}{T_i}\left[\mathrm{Re}\,W\left(\frac{\omega^*}{k\rho_i}\right) - \mathrm{Im}\,W\left(\frac{\omega^*}{k_\perp\rho_i}\right)\cot\omega^*\pi + {\sum_n}' \frac{\omega^*}{\omega^*-n} W\left(\frac{\omega^*-n}{k_{//}\rho_i}\right)\Lambda_n(k_\perp^2\rho_i^2)\right], \tag{3.26}$$

here the summation Σ' in the last term was taken over the few integers near ω^*. If ω^* is particularly close to an integer n_0, $\cot\omega^*\pi$ and the terms for $n = n_0$ in Σ' behave singularly in Eq. (3.26); however the corresponding terms in the exact equation (3.16),

$$\frac{\omega^*}{\omega^*-n_0}\left[W\left(\frac{\omega^*-n_0}{k_{//}\rho_i}\right) - 1\right] \Lambda_{n_0}(k_\perp^2\rho_i^2) \quad , \tag{3.27}$$

shows no singularity because $W(Z_{in}) - 1$ tends to zero faster than $\omega^* - n_0$. Therefore a more appropriate form of D_L near the ion cyclotron harmonics is

$$D_L = 1 + \frac{\omega_{pe}^2}{k^2}\frac{m_e}{T_e}\left[1 + (W(Z_{i0}) - 1)\Lambda_0(\lambda_e)\right] \tag{3.28}$$

$$+ \frac{\omega_{pi}^2}{k^2}\frac{m_i}{T_i}\left[\mathrm{Re}\, W\left(\frac{\omega^*}{k\rho_i}\right) + \frac{\omega^*}{\omega^*-n_0}\left\{W\left(\frac{\omega^*-n_0}{k_{//}\rho_i}\right) - 1\right\}\Lambda_{n_0}(k_\perp^2\rho_i^2)\right] .$$

On the basis of these approximations of D_L, the nature of the wave near the LH frequency is analyzed in the following subsections.

(2)-2 Warm-plasma approximation

We shall show in this subsection that the cold plasma mode Eq. (3.14) change the sign of its group velocity near the LHR by means of the warm plasma approximation ($k\rho_i \ll \omega^*$). Since $k_\perp\rho_i$ is not small compared with unity, we assume that Re $k_\perp \gg$ Im $k_\perp$; otherwise strong damping takes place before the waves propagate a few ion Larmor radii; therefore Re $k_\perp$ may be derived as a solution of Re $D_L = 0$.

As long as $k_\perp\rho_i \lesssim \omega^{*1/2}$, the effect of the ion cyclotron harmonics may be neglected since $\Lambda_{n0}(k_\perp^2\rho_i^2)$ in their terms is fairly small compared with unity. Moreover assuming that $\lambda_e = k_\perp^2\rho_i^2(T_e/T_i)(m_e/m_i) \ll 1$ which is compatible with $k_\perp\rho_i \lesssim \omega^{*1/2}$, we obtain a warm plasma approximation;

$$\mathrm{Re}D_L = -\frac{1}{k^2}\left[\left(3\frac{\omega_{pi}^2}{\omega^4}\frac{T_i}{m_i} + \frac{3}{4}\frac{\omega_{pe}^2}{\Omega_e^4}\frac{T_e}{m_e}\right)k_\perp^4 - \left(1 + \frac{\omega_{pe}^2}{\Omega_e^2} - \frac{\omega_{pi}^2}{\omega^2}\right)k_\perp^2 - \left(1 - \frac{\omega_{pe}^2}{\omega^2}\right)k_{//}^2\right]. \tag{3.29}$$

The dispersion relation Re $D_L = 0$ shows

$$\omega^2 = \frac{\omega_{pi}^2}{1 + \frac{\omega_{pe}^2}{\Omega_e^2}\left(1 - \frac{3}{4}\frac{k_\perp^2 v_{Te}^2}{\Omega_e^2}\right)}\left[1 + \frac{m_i}{m_e}\frac{k_{//}^2}{k_\perp^2} + 3\frac{k_\perp^2 v_{Ti}^2}{\omega^2}\right] , \tag{3.30}$$

and this dispersion curve is illustrated in Fig. 3.6 as well as that from the cold plasma approximation. It is clear that for smaller $k_\perp \rho_i$ than some critical value the phase velocity $\omega/k_\perp$ and the group velocity $\partial\omega/\partial k_\perp$ perpendicular to the magnetic field have opposite signs, i.e. a backward wave, and that for larger $k_\perp \rho_i$ they have the same signs, i.e. a forward wave. On the other hand the waves are always forward waves along the magnetic field.

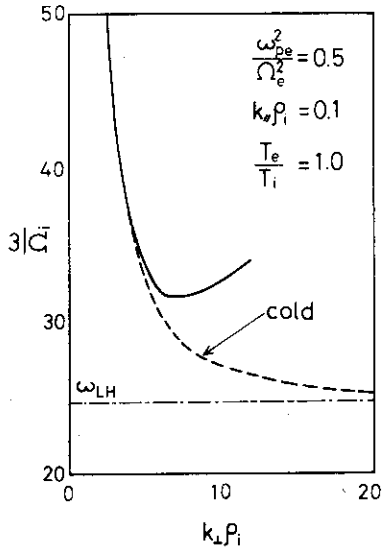

Fig. 3.6 Dispersion relation derived from Eq. (3.30).

We may transform Eq. (3.29) to a dimensionless form;

$$(k_\perp \rho_i)^4 - \frac{1-h}{h}\frac{m_i}{m_e}\frac{1}{(1+q)s^2}(k_\perp \rho_i)^2 + \left(\frac{m_i}{m_e}\right)^2 \frac{1}{s^2}(k_{/\!/}\rho_i)^2 = 0 \ , \qquad (3.31)$$

where

$$s^2 = 3\left(\frac{1+q}{q} + \frac{1}{4}\frac{T_e}{T_i}\frac{q}{1+q}\right) = 3\left(\frac{\Omega_i|\Omega_e|}{\omega^2} + \frac{1}{4}\frac{T_e}{T_i}\frac{\omega^2}{\Omega_i|\Omega_e|}\right), \qquad (3.32)$$

in order to obtain the density dependence of $k_\perp \rho_i$ for given ω^* and $k_{/\!/}\rho_i$. At the critical density ${\omega_{pet}}^2$ smaller than ${\omega_{per}}^2$, the cold plasma mode joins with the mode of larger $k_\perp \rho_i$ and changes the sign of its group velocity. Where the density is lower than ${\omega_{pet}}^2$ there exists two real positive ${k_\perp}^2{\rho_i}^2$, while in higher density there are only complex conjugate solutions which means spatially damped oscillations. The density and $k_\perp \rho_i$ at the critical point (turning point) can be easily obtained from the double root of Eq. (3.31);

$$\frac{{\omega_{per}}^2}{{\Omega_e}^2} = \frac{8}{1+2(1+q)k_{/\!/}\rho_i s} = \frac{\omega^2}{\Omega_i|\Omega_e|(1+2k_{/\!/}\rho_i s) - \omega^2} \ , \qquad (3.33)$$

$$k_\perp^2 \rho_i^2 \big|_{\omega_{pe}^2 = \omega_{pet}^2} = \frac{m_i}{m_e} \frac{k_{//} \rho_i}{s} \quad . \tag{3.34}$$

The ω^* and $k_{//}\rho_i$ dependence on $\omega_{pet}^2/\Omega_e^2$ is illustrated in Fig. 3.7 for $T_e/T_i = 1$. When $k_{//}\rho_i$ increases and/or ω^* decreases, the turning point shifts to the lower density. Since ω^2 must be smaller than $\Omega_i|\Omega_e|$, the electron tempera ture does not considerably change the location of the turning point unless $T_e \gg T_i$.

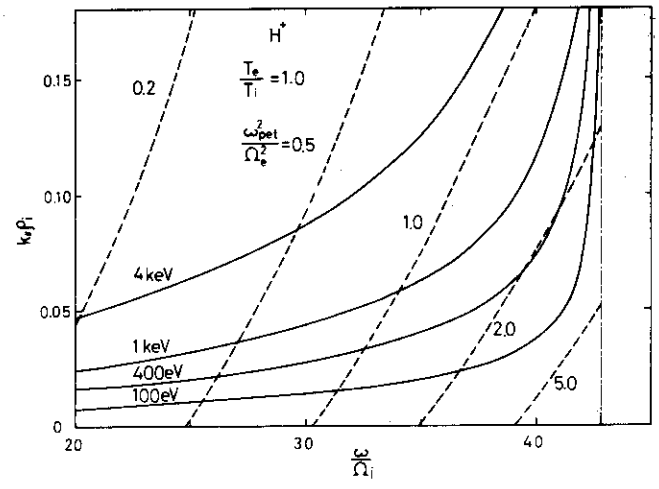

Fig. 3.7 $k_{//}\rho_i$ vs. ω/Ω_i for the case $T_e = T_i$. Accessibility conditions are satisfied above the solid lines for a given temperature. Dotted lines show the densities at the turning point.

(2)-3 Dispersion relation in the vicinity of higher harmonics

In this subsection, taking account of the ion cyclotron harmonics we shall make an qualitative analysis of D_L. In order to make an analysis clear, D_L is devided into two parts; the first part is

$$D_0 = 1 + \frac{\omega_{pe}^2}{k^2} \frac{m_e}{T_e} [1 + (W(Z_{e0}) - 1)\Lambda_0(\lambda_e)] + \frac{\omega_{pi}^2}{k^2} \frac{m_i}{T_i} \mathrm{Re}\, W\left(\frac{\omega^*}{k\rho_i}\right), \tag{3.35}$$

and the second part D_1 is composed of the singular part of $f_{\omega^*}(\lambda_i)$ and the terms which involves $W(Z_{in})$ in Eq. (3.16). If ω^* falls halfway between the two successive integers, n_0 and n_0+1, the term in Re D_1 on each side of ω^* cancels one another, so that Re D_1 is almost zero. On the contrary, if ω^* is close to an integer n_0, D_1 is approximated from Eq. (3.28) as follows,

$$D_1 = \frac{\omega_{pi}^2}{k^2} \frac{m_i}{T_i} \frac{\omega^*}{\omega^* - n_0} \left(W\left(\frac{\omega^* - n_0}{k_{//}\rho_i}\right) - 1\right)\Lambda_{n_0}(k_\perp^2 \rho_i^2) \quad . \tag{3.36}$$

The ω^* dependence of Eq. (3.36), i.e.

$$w_{n_0}(\omega^*) = \frac{\omega^*}{\omega^*-n_0}\left[W\left(\frac{\omega^*-n_0}{k_{\parallel}\rho_i}\right) - 1\right], \tag{3.37}$$

is illustrated in Fig. 3.8. The real part of $w_{n_0}(\omega^*)$ is an odd function with respect to ω^*-n_0 and takes its maximum value at about $n_0 - 1.3\, k_{\parallel}\rho_i$. Since $\mathrm{Im}\, W\left(\frac{\omega^*-n}{k_{\parallel}\rho_i}\right)$ is an odd function with respect to ω^*-n, Im D_1 must be a summation of Im $w_n(\omega^*)$ over all integers n. However, with $k_{\parallel}\rho_i \ll 1$, only the n_0-th term is dominant because

$$\mathrm{Im}\; w_n(\omega^*) = \sqrt{\frac{\pi}{2}}\,\frac{\omega^*}{k_{\parallel}\rho_i}\exp\left(-\frac{(\omega^*-n_0)^2}{2k_{\parallel}^2\rho_i^2}\right) . \tag{3.38}$$

It should be noted that when $k_{\parallel}\rho_i = 0$, the following approximation

$$D_1 = -\frac{\omega_{pi}^2}{k^2}\frac{m_i}{T_i}\,\omega^*\pi\,\cot(\omega^*\pi)\Lambda_{n_0}(k_{\perp}^2\rho_i^2) , \tag{3.39}$$

leads to the usual ion Bernstein wave [27] propagating perpendicularly to the magnetic field. On the other hand in the case of $k_{\parallel}\rho_i \gg 1$, Re D_1 is averaged to zero and Im D_1 are summed up so as to make up the ion Landau damping (Appendix B); therefore we recover the unmagnetized ion approximation, Eq. (3.21).

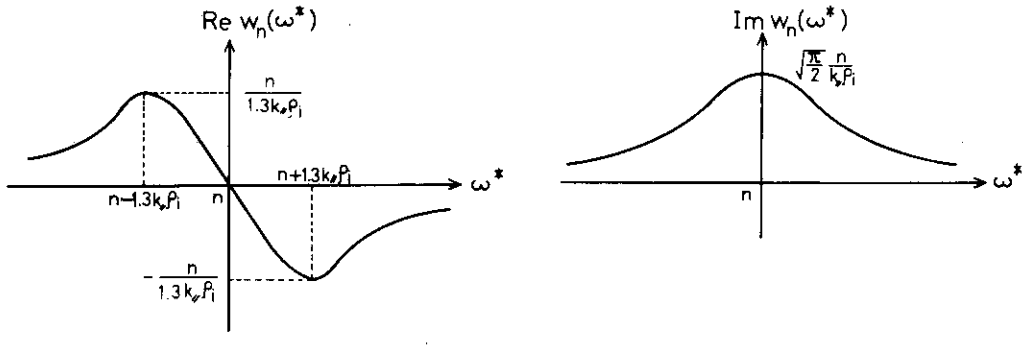

Fig. 3.8 Properties of Eq. (3.37).

The function D_0 is approximated by Eq. (3.29) for $k_{\perp}\rho_i \ll \omega^*$; and when $k_{\perp}\rho_i \gg \omega^*$, D_0 approaches

$$D_0 \to 1 + \frac{\omega_{pe}^2}{k^2}\frac{m_e}{T_e} + \frac{\omega_{pi}^2}{k^2}\frac{m_i}{T_i} . \tag{3.40}$$

Knowing the behavior of D_0 and D_1 with respect to $k_{\perp}^2\rho_i^2$, we can obtain the root of Re $D_L = 0$ from the intersecting point of the curves

$y = D_0(k_\perp^2\rho_i^2)$ and $y = D_1(k_\perp^2\rho_i^2)$. Fig. 3.9 shows the qualitative results in the cases a) $\omega^* = n_0 + \delta$ $(0 < \delta \ll 1)$, b) $\omega^* = n_0 \pm 1/2$ and c) $\omega^* = n_0 - \delta$. It can be seen that there exists the second turning point between the first turning point in the warm plasma approximation and the plasma boundary and that its location shifts toward higher density when ω^* approaches $n_0 - 1.3k_{//}\rho_i$ and toward lower density when ω^* approaches $n_0 + 1.3k_{//}\rho_i$. The numerical example will be given in (2)-5 of §3-1.

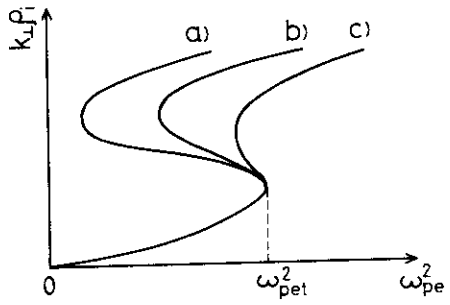

Fig. 3.9 Shifts of the second turning point. (a) $\omega^* = n_0 + \delta$, (b) $\omega^* = n_0 \pm 1/2$, (c) $\omega^* = n_0 - \delta$.

(2)-4 Linear damping mechanism

The linear damping mechanism of the LH wave contains the electron Landau damping, the ion cyclotron damping and the modified ion Landau damping which occurs when the cyclotron damping overlaps each other because of $k_{//}\rho_i$ larger than unity or when small but considerable collisions randomize the cyclotron harmonics component of the ion motion, in addition to the ordinary collisional damping.

The electron Landau damping which results from Im $W(\omega/k_{//}v_{Te})$ has a negligible dependence of $k_\perp$ as long as $\lambda_e = k_\perp^2\rho_e^2 \ll 1$. Therefore the large electron Landau damping which is almost independent of the plasma density causes strong damping of the waves near the plasma surface. The condition of the small electron Landau damping has been given in Eq. (3.20).

The ion cyclotron damping originated in Im $W(\frac{\omega^*-n_0}{k_{//}\rho_i})$ strongly localizes in $|\omega^*-n_0| \lesssim k_{//}\rho_i$ in as much as $k_{//}\rho_i \ll 1$; since it includes the factor $\Lambda_{n_0}(k_\perp^2\rho_i^2)$, the damping substantially appears when $k^2\rho_i^2 \gtrsim n_0$. As is mentioned in (2)-3 of §3-1 for $k_{//}\rho_i \gtrsim 1$ the width of the cyclotron damping is broaden and overlaps each other to form the Landau damping.

Though we have assumed that the ion-ion collision frequency is small enough for the collisional damping to be neglected ($\nu_{ii} \ll \Omega_i$), small collisions which cannot cause the considerable damping can restore the Landau damping. When $k_\perp\rho_i \gg 1$, the wavelength is short compared with the ion Larmor radius; so that the memory of the collective motion of an ion can be lost by a small-angle scattering due to the Coulomb collision. In other

words if the velocity variation Δv within one ion cyclotron period Ω_i^{-1} gives rise a phase mismatching $k_\perp \Delta v/\Omega_i$ which exceeds unity, the ion feels no successive acceleration and the energy obtained in the last acceleration dissipates into the thermal motion of ions. Therefore the collision restored Landau damping can occur under the condition [28,5]

$$\nu_{eff} = \left(\frac{v}{\Delta v}\right)^2 \nu_{ii} = k_\perp^2 \rho_i^2 \nu_{ii} > \Omega_i \quad . \tag{3.41}$$

In this case the unmagnetized ion approximation can be applied. The ion-ion collision frequency used above is given for an ion of a charge number Z and a mass number A as [31]

$$\nu_{ii} = 3.46\times10^{-13} \frac{Z^2 \ell n \Lambda \cdot N_i}{A^{1/2} \; T_i^{3/2}} \qquad [\sec^{-1}] \; , \tag{3.42}$$

where the ion density N_i and the temperature T_i are measured by m^{-3} and eV, respectively.

As a result, the dominant damping mechanism of the LH waves is considered to be the collisional damping for $\nu_{ii} > \Omega_i$, the collision restored Landau damping for $\Omega_i > \nu_{ii} > \Omega_i / k_\perp^2 \rho_i^2$ and the cyclotron damping for $\nu_{ii} < \Omega_i / k_\perp^2 \rho_i^2$.

(2)-5 Summaries of dispersion

In this subsection, we summarize the numerical calculations of the dispersion relation on the assumption that Re $k_\perp \rho_i \gg$ Im $k_\perp \rho_i$. Two models are utilized in calculations; in the unmagnetized model, the ion susceptibility χ_i is approximated by Eq. (3.21); and in the magnetized model only the nearest integers, i.e. n_0 and n_0+1 with $n_0 < \omega^* < n_0+1$, are taken into account as contributions of the ion cyclotron harmonics, that is,

$$\chi_i = \frac{\omega_{pi}^2}{k^2} \frac{m_i}{T_i} \left[\mathrm{Re}\, W\left(\frac{\omega^*}{k\rho_i}\right) + \sum_{\substack{n=n_0, \\ n_0+1}} \left\{ \frac{\omega^*}{\omega^*-n} W\left(\frac{\omega^*-n}{k_{//}\rho_i}\right) - 1 \right\} \Lambda_n (k_\perp^2 \rho_i^2) \right]. \tag{3.43}$$

Figure 3.10 shows the ω^* dependence of the dispersion curve in the unmagnetized ion model, and Fig. 3.11 shows the $k_{//}\rho_i$ dependence. The arrow in the right direction means the damping rate before the turning and the arrow in the left direction after the turning. The mark + in the figure indicates the turning point predicted by Eqs. (3.33) and (3.34), which fairly agrees with the numerical result except for large $k_{//}\rho_i$. The discrepancy is considered to be due to the higher order terms of $k_\perp^2 \rho_i^2/\omega^2$ in

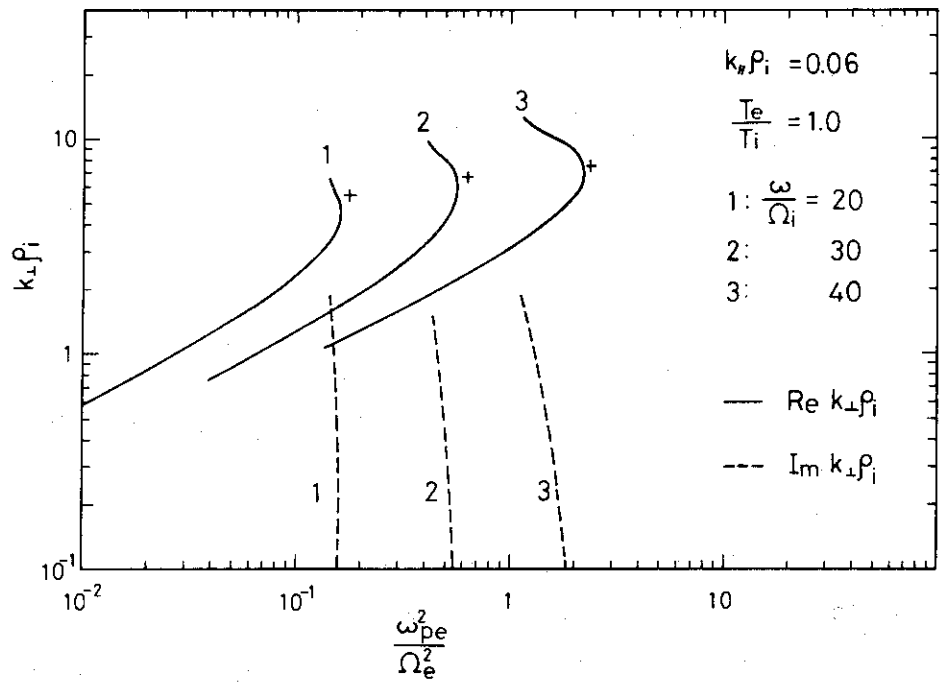

Fig. 3.10 Dispersion curves for various ω/Ω_i in the unmagnetized ion model.

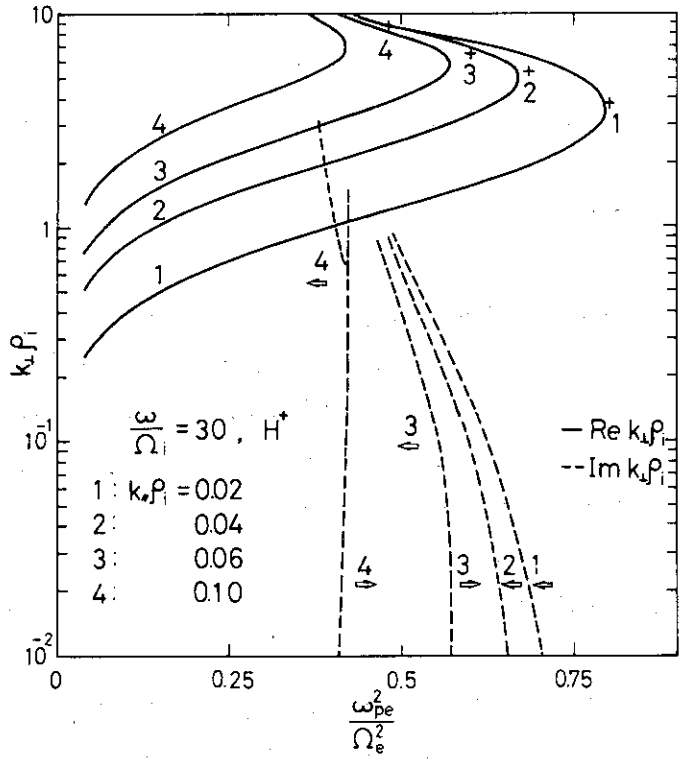

Fig. 3.11 Dispersion curves for various $k_{\parallel}\rho_i$ in the unmagnetized ion model.

Eq. (3.29). With the decrease of ω^* and the increase of $k_\parallel \rho_i$, the location where the strong ion Landau damping appears after the turning, approaches the turning point and at last strong damping occurs before the turning. The dependence on T_e is shown in Fig. 3.12. It can be seen from Eqs. (3.32) and (3.33) that the change of T_e affects the location of the turning point only if

$$\frac{T_e}{T_i} \gtrsim 4 \frac{\Omega_i^2 \Omega_e^2}{\omega^4} \quad . \tag{3.44}$$

Since for the parameter of Fig. 3.12, the r.h.s. of Eq. (3.44) equals 12.6, the shift of the turning point for $T_e/T_i = 10$ is reasonable. One more distinction for larger T_e/T_i is that the large electron Landau damping spreads to the lower density region.

In Fig. 3.13, the results from the magnetized ion model is plotted, which agree with the qualitative result in Fig. 3.9. The cyclotron damping appears near the harmonics; the location where Im $k_\perp \rho_i$ exceeds 10^{-1} is indicated by a circle in Fig. 3.13. On the other hand, no significant damping appears in the frequency $|\omega^* - n| \gtrsim 3k_\parallel \rho_i$ and therefore after the twice turning the short wavelength wave propagates into the high density region.

§3-2 Effects of density gradient

(1) W.K.B. approximation

In order to calculate the local power absorption of the wave energy or to evaluate the nonlinear effect of the wave, it is necessary to know the spatial variation of the wave amplitude. This problem may be solved by the W.K.B. approximation except near the turning point.

The one dimensional energy conservation for a single wave is expressed as

$$\frac{\partial W}{\partial t} + \frac{\partial}{\partial x} (v_W W) + 2\gamma W = 0 \ , \tag{3.45}$$

where W denotes the wave energy density, v_W the energy flow velocity and γ the damping ratio (real and positive). The W.K.B. approximation of the first order shows that the energy density and the energy flow velocity are approximated, with the aid of the dispersion tensor $\overleftrightarrow{D}$ defined by Eq. (3.4), by [23]

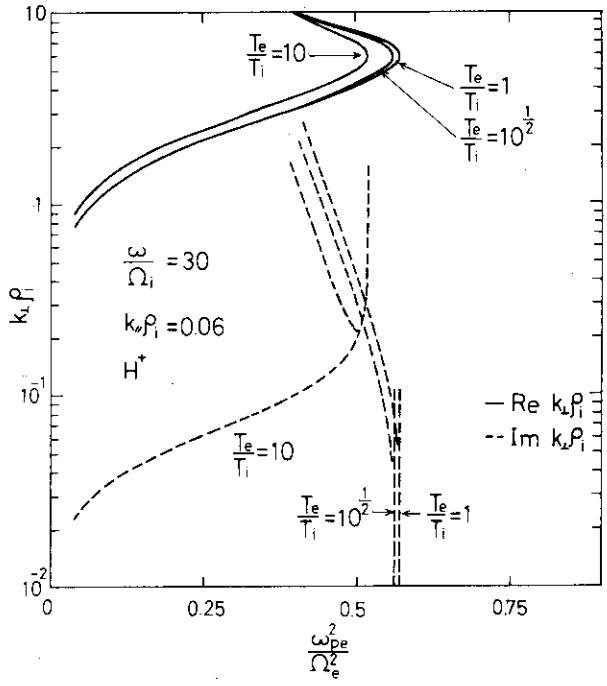

Fig.3.12 Dispersion curves for various T_e/T_i in the unmagnetized ion model.

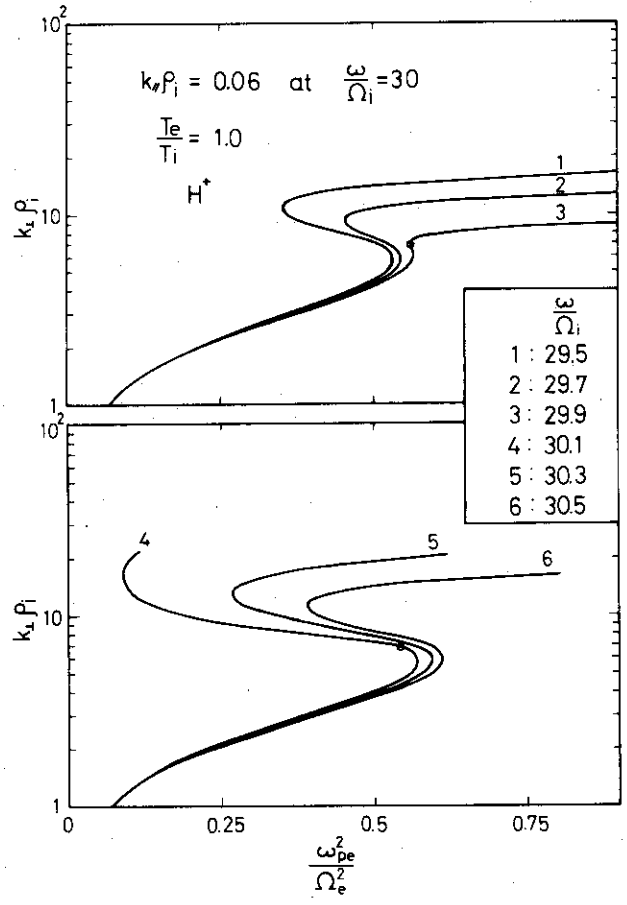

Fig.3.13 Dispersion curves for various ω/Ω_i close to 30 in the magnetized ion model.

$$W = \frac{\partial(\omega D_{\alpha\beta})}{\partial\omega} \frac{\varepsilon_0 E_\alpha {}^* E_\beta}{2} , \tag{3.46}$$

$$v_W = \frac{\partial\omega}{\partial k_x} = - \frac{\partial D/\partial k_x}{\partial D/\partial\omega} = v_g . \tag{3.47}$$

Provided that $\omega \gg \gamma$, the damping rate γ can be obtained also from $D = \det \overleftrightarrow{D}$ as follows:

$$\gamma = \frac{ImD}{\frac{\partial D}{\partial\omega}} . \tag{3.48}$$

Deriving the group velocity v_g and the damping rate as a function of x by means of the local dispersion relation $D(\omega, k_x, k_z; x) = 0$, we may easily calculate the energy density.

$$W(x) = \frac{W(x_0)v_g(x_0)}{v_g(x)} \exp \int_{x_0}^{x} (- \frac{2\gamma(x)}{v_g(x)}) dx . \tag{3.49}$$

In the case of an electrostatic wave, the energy density of the electric field W_E has the following relation to W:

$$W = \omega \frac{\partial D}{\partial\omega} \frac{\varepsilon_0 |E|^2}{2} = \omega \frac{\partial D}{\partial\omega} W_E . \tag{3.50}$$

Therefore the absolute values of the electric field $|E|$ and the potential $|\phi| = |E|/k$ can be calculated. Moreover we may obtain the absorbed power density

$$P_{abs}(x) = 2\gamma(x)W(x) = v_g(x_0)W(x_0) \frac{2\gamma(x)}{v_g(x)} \exp \int_{x_0}^{x} (- \frac{2\gamma(x)}{v_g(x)}) dx . \tag{3.51}$$

It may be noted that $\gamma(x)/v_g(x)$ is equivalent to Im k_x as long as $\gamma \ll \omega$ and $Imk_x \ll Rek_x$.

The W.K.B. approximation is valid only if the inequality

$$\frac{1}{k_x} \frac{dk_x}{dx} \ll k_x , \tag{3.52}$$

is satisfied. The weakness of the inhomogeneity compared with the wavelength is not sufficient for this condition to be satisfied, because near the turning point dk_x/dx goes to infinity. Using Eq. (3.31) to calculate dk_x/dx, we find that (3.52) is equivalent to

$$(k_x L_N)^2 (1 - \frac{N(x)}{N_t})(1 + \frac{N(x)}{N_t} - 2\frac{N(x)}{N_r}) \gg 1 \ , \tag{3.53}$$

where

$$L_N^{-1} = \frac{1}{N(x)} \frac{dN(x)}{dx} \ , \tag{3.54}$$

and N_t and N_r is the plasma density at the turning point and the LHR, respectively.

Far from the turning point, the solution to Eq. (3.31) can be approximated by

$$k_{\perp 1}^2 = \frac{m_i}{m_e}(1+q)\frac{h}{1-h}k_{\parallel}^2 \ , \tag{3.55}$$

$$k_{\perp 2}^2 = \frac{m_i}{m_e}\frac{1}{(1+q)s^2}\frac{1-h}{h}\frac{1}{\rho_i^2} \ . \tag{3.56}$$

The first solution corresponds to the mode before turning (cold plasma mode) and the second to the mode after turning (warm plasma mode). Using Eqs. (3.55), (3.56) and the W.K.B. approximation, we find the density dependence of the wave potential in the case of negligible damping;

$$\phi_1 \propto \frac{1}{h^{1/4}(1-h)^{1/4}} \sim \frac{1}{x^{1/4}(x_r-x)^{1/4}} \ , \tag{3.57}$$

$$\phi_2 \propto \frac{h^{1/4}}{(1-h)^{3/4}} \sim \frac{x^{1/4}}{(x_r-x)^{3/4}} \ . \tag{3.58}$$

In the last expression we have assumed the linear density profile and $\omega_{pe}^2 = 0$ at $x = 0$.

(2) Asymptotic solution near the turning point

The W.K.B. approximation fails to describe the mode conversion at the turning point and the solution diverges at $x = x_t$ since $v_g(x_t) = 0$. It comes from the fact that the phase correlation between the two waves has been neglected in the W.K.B. approximation. This section deals with this problem from another approach [17-21].

(2)-1 Differential equation near the turning point

The dispersion relation near the turning point Eq. (3.31) has a form

$$k_\perp^4 - (k_1^2 + k_2^2)k_\perp^2 + k_1^2k_2^2 = 0 \ , \tag{3.59}$$

and this algeblaic equation in a homogeneous plasma is a reduced form of the forth order differential equation in a weakly inhomogeneous plasma:

$$\frac{d^4\phi}{dx^4} + \frac{d}{dx}(k_1^2 + k_2^2)\frac{d\phi}{dx} + (k_1^2 \cdot k_2^2) = 0 \ . \tag{3.60}$$

This equation can be derived from the MHD equations and Poisson's equation on the assumption that $k_\perp v_{Ti} \ll \omega$ and $k_\perp v_{Te} \ll \Omega_e$. In Eq. (3.60), terms in the first and the third derivatives are neglected because these are less important in a gentle inhomogeneity, i.e. $k_\perp l_N \gg 1$. In the neighborhood of the turning point $x = x_t$, the spatial variation of Re $(k_1^2+k_2^2)$ can be approximated by a linear dependence on x. By the following transformation:

$$\begin{aligned}
\kappa^3 &= \mathrm{Re}\,\frac{d(k_1^2+k_2^2)}{dx}\Big|_{x=x_t} \ , \\
\mu &= \mathrm{Re}\ k_1^2k_2^2\big|_{x=x_t}/\kappa^4 \ , \\
\varepsilon &= \mathrm{Im}(k_1^2+k_2^2)\big|_{x=x_t}/\kappa^2 \ , \\
u &= \kappa(x - x'_r) \ ,
\end{aligned} \tag{3.61}$$

where

$$x'_r = x_t - \mathrm{Re}(k_1^2+k_2^2)\big|_{x=x_t}/\kappa^3$$

Eq. (3.60) becomes a dimensionless equation;

$$\frac{d^4\phi}{du^4} + \frac{d}{du}(u + i\varepsilon)\frac{d\phi}{du} + \mu\phi = 0 \ . \tag{3.62}$$

Here we have neglected the spatial variation of Im $(k_1^2+k_2^2)$ and the imaginary part of $k_1^2k_2^2$ in Eq. (3.59). The validity of these assumptions will be discussed in (2)-4 of §3-2.

Comparing Eq. (3.59) with Eq. (3.31), we obtain the relations between the transformed and the real quantities:

$$\begin{aligned}
\kappa^3 &= -\frac{m_i}{m_e}\frac{1+2(1+q)k_\parallel\rho_i s}{(1+q)s^2}\frac{1}{\rho_i^2 L_N} \ , \\
\mu &= \left(\frac{m_i}{m_e}\right)^2\frac{k_\parallel^2\rho_i^2}{s^2}\frac{1}{\kappa^4\rho_i^4} \ ,
\end{aligned} \tag{3.63}$$

$$\varepsilon = (-\kappa N_L)\, \mathrm{Im}\, D_L \ ,$$

where L_N is the scale length of the density gradient at $x = x_t$.

(2)-2 Asymptotic solution

By the general Laplace transformation, the integral representation of the solution to Eq. (3.62) has a form (Appendix C),

$$\phi(u) = \int_C \frac{1}{p} \exp\left[\frac{p^3}{3} + (u+i\varepsilon)p - \frac{\mu}{p}\right]dp = \int_C \frac{1}{p} e^{f(p)}dp \ , \tag{3.64}$$

where the contour C in the complex p plane is chosen such that the difference of the values

$$V(p) = p \exp\left[\frac{p^3}{3} + (u+i\varepsilon)p - \frac{\mu}{p}\right] \ , \tag{3.65}$$

at the end points of C is zero.

The contour integration in Eq. (3.64) may be carried out approximately by the method of steepest descents (the saddle point integration technique). The integration along the contour through the four different saddle points ($f'(p) = 0$), which are shown in Fig. 3.14, corresponds to the four linearly independent solutions. In Fig. 3.14(a) for $u > 2\mu^{1/2}$ and $\varepsilon = 0$, the contours C_i are selected so that $V(p)$ at the end points may be zero and Im $f(p)$ be constant along a contour. These contours C_i which have the same end points are deformed as illustrated in Fig. 3.14(b) for $-2\mu^{1/2} < u < 2\mu^{1/2}$ and in Fig. 3.14(c) for $u < -2\mu^{1/2}$. Here we have assumed a positive but infinitely small ε to make a discussion definitely. By denoting the integral along the countour C_i by I_i and the contribution from the saddle point P_j by J_j, we obtain the following relations,

$$\begin{bmatrix} I_1 \\ I_2 \\ I_3 \\ I_4 \end{bmatrix} = \begin{bmatrix} J_a \\ J_b \\ J_c \\ J_d \end{bmatrix} \longleftrightarrow \begin{bmatrix} J_a+J_b \\ J_a \\ J_c \\ J_c+J_d \end{bmatrix} \longleftrightarrow \begin{bmatrix} J_a + \frac{1}{2}J_b + \frac{1}{2}J_c + \frac{1}{2}J_d \\ J_a - \frac{1}{2}J_b + \frac{1}{2}J_c \\ J_a - \frac{1}{2}J_b - \frac{1}{2}J_c \\ J_a + \frac{1}{2}J_b - \frac{1}{2}J_c - \frac{1}{2}J_d \end{bmatrix} \ . \tag{3.66}$$

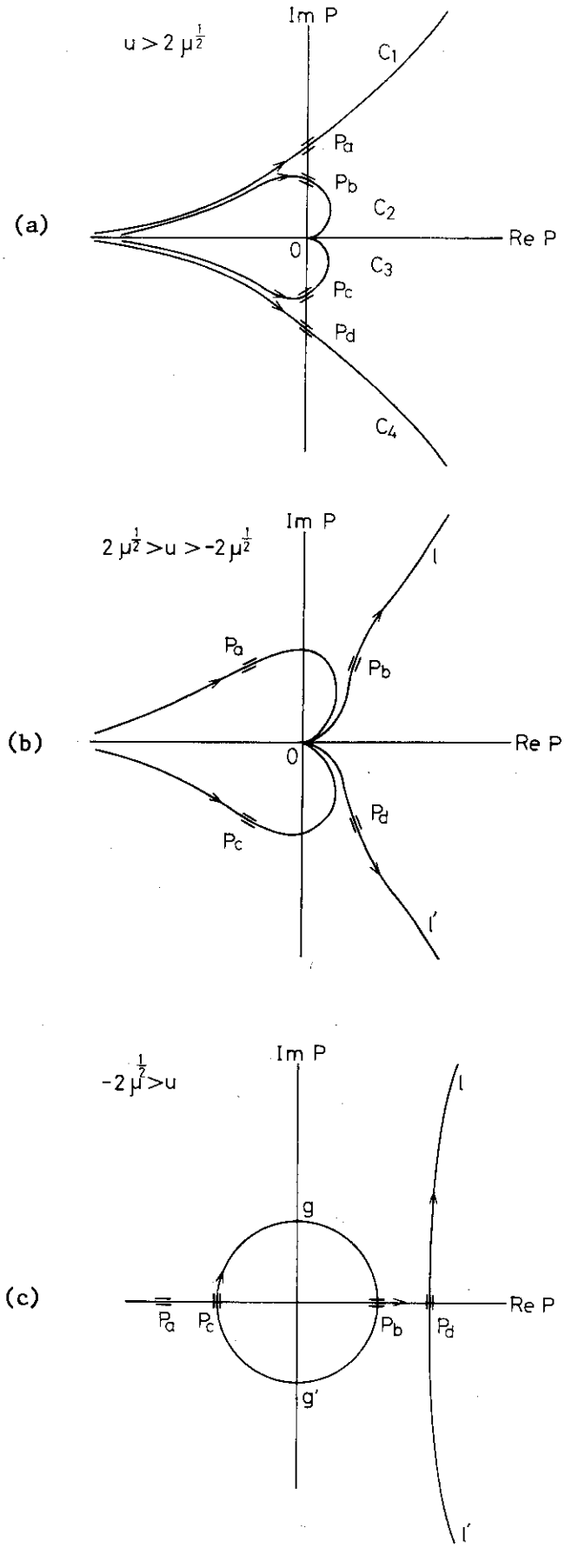

Fig. 3.14 Contours of integration:
(a) $u > 2\mu^{1/2}$,
(b) $2\mu^{1/2} > u > -2\mu^{1/2}$,
(c) $-2\mu^{1/2} > u$.
Contours C_i in (a) are deformed in (b):
$C_1(-\infty, P_a, 0, P_b, \ell)$, $C_2(-\infty, P_a, 0)$,
$C_3(-\infty, P_c, 0)$, $C_4(-\infty, p_c, 0, P_d, \ell')$.

And also in (c):
$C_1(-\infty, P_a, P_c, g, P_b, P_d, \ell)$,
$C_2(-\infty, P_a, P_c, g, P_b, 0)$,
$C_3(-\infty, P_a, P_c, g', P_b, 0)$,
$C_4(-\infty, P_a, P_c, g', P_b, P_d, \ell')$.

The first column of the r.h.s. is for $2\mu^{1/2} < u$, the second for $-2\mu^{1/2} < u < 2\mu^{1/2}$ and the last for $u < -2\mu^{1/2}$. Since the general solution which contains four arbitrary constants A_i has a form $\sum_i A_i I_i$, the connection formulae are found to be

$$
\begin{aligned}
& A_1 J_a + A_2 J_b + A_3 J_c + A_4 J_d \\
\longleftrightarrow\ & (A_1+A_2) J_a + (+A_1) J_b + (A_3+A_4) J_c + (+A_4) J_d \\
\longleftrightarrow\ & (A_1+A_2+A_3+A_4) J_a + \frac{1}{2}(A_1-A_2-A_3+A_4) J_b + \frac{1}{2}(A_1+A_2-A_3-A_4) J_c \\
& + \frac{1}{2}(A_1-A_4) J_a .
\end{aligned}
\tag{3.67}
$$

The constants A_i are determined from the boundary conditions. The boundary conditions are so chosen that i) for $u \to -\infty$ (high density limit) ϕ vanishes and ii) for $u \to \infty$ (low density limit), there exists an incoming solution which corresponds to the cold plasma mode. The properties of the contribution from each saddle point shows that for $u < -2\mu^{1/2}$, J_a and J_c are exponentially growing mode; therefore their coefficients must be zero;

$$
A_1 = -A_2 \qquad \text{and} \qquad A_3 = -A_4 . \tag{3.68}
$$

And that for $u \gg 2\mu^{1/2}$, J_a is the outgoing warm-plasma mode, J_b the incoming cold-plasma mode, J_c the outgoing cold-plasma mode and J_d the incoming warm-plasma mode. Using Eqs. (3.68), we conclude that the incoming wave of one mode is fully converted into the other outgoing mode. The contributions from the saddle points have been calculated in a usual manner [32] on the assumption that $\mu^{3/4} \gg 1$. With the aid of the boundary condition ii), we obtain the asymptotic solutions,

$$
\begin{aligned}
\phi = & \frac{\sqrt{\pi}[(z+1)^{1/2}-(z-1)^{1/2}]^{1/2}}{2^{3/4}\mu^{3/8}(z-1)^{1/4}(z+1)^{1/4}} \exp\left[i\frac{2\sqrt{2}}{3}\mu^{3/4}\{(z+1)^{3/2}+(z-1)^{3/2}\}\right] e^{-i\frac{\pi}{4}} \\
& + \frac{\sqrt{\pi}[(z+1)^{1/2}+(z-1)^{1/2}]^{1/2}}{2^{3/4}\mu^{3/8}(z-1)^{1/4}(z+1)^{1/4}} \exp\left[i\frac{2\sqrt{2}}{3}\mu^{3/4}\{(z+1)^{3/2}-(z-1)^{3/2}\}\right] e^{i\frac{\pi}{4}} ,
\end{aligned}
\qquad (\text{for } z > 1) \tag{3.69}
$$

$$\phi = \frac{\sqrt{\pi}}{2^{1/2}\mu^{3/8}(1-z)^{1/4}(1+z)^{1/4}} \exp[-\frac{2\sqrt{2}}{3}\mu^{3/4}(1-z)^{3/2} + i\frac{2\sqrt{2}}{3}\mu^{3/4}(1+z)^{3/2}]e^{i\frac{1}{4}\cos^{-1}z},$$

$$(\text{for } -1 < z < 1) \qquad (3.70)$$

$$\phi = \frac{\sqrt{\pi}[(-z+1)^{1/2}-(-z-1)^{1/2}]^{1/2}}{2^{3/4}\mu^{3/8}(-z+1)^{1/4}(-z-1)^{1/4}} \exp[-\frac{2\sqrt{2}}{3}\mu^{3/4}\{(-z+1)^{3/2}+(-z-1)^{3/2}\}]e^{-i\pi/2}$$

$$+ \frac{\sqrt{\pi}[(-z+1)^{1/2}+(-z-1)^{1/2}]^{1/2}}{2^{3/4}\mu^{3/8}(-z+1)^{1/4}(-z-1)^{1/4}} \exp[-\frac{2\sqrt{2}}{3}\mu^{3/4}\{(-z+1)^{3/2}-(-z-1)^{3/2}\}],$$

$$(\text{for } z < -1) \qquad (3.71)$$

where

$$z = \frac{u}{2\mu^{1/2}} \quad . \qquad (3.72)$$

When $u >> 2\mu^{1/2}$, the r.h.s. of Eq. (3.69) is approximated by

$$\phi = \frac{\sqrt{\pi}}{u^{3/4}} \exp[i\frac{2}{3}u^{3/2}]e^{-i\frac{\pi}{4}} + \frac{\sqrt{\pi}}{u^{1/4}\mu^{1/4}} \exp[i\,2\mu^{1/2}u^{1/2}]e^{i\frac{\pi}{4}}$$

$$= \frac{\sqrt{\pi}}{u^{3/4}} \exp\int^{x} -i|k_2|dx\, e^{-i\frac{\pi}{4}} + \frac{\sqrt{\pi}}{u^{1/4}\mu^{1/4}} \exp\int^{x} -i|k_1|dx\, e^{+i\frac{\pi}{4}}, \qquad (3.73)$$

where we have assumed $|k_1| \ll |k_2|$; therefore k_1 and k_2 are the wave numbers of the cold-plasma mode and the warm-plasma mode, respectively. It is noted that since the cold plasma wave is a backward wave the second term means an incoming wave. Using the relation $u \propto (x_r - x)$, we find that the x-dependence of the wave amplitudes in Eq. (3.73) coincides with those in Eqs. (3.57) and (3.58) as long as $x \gg |x_r - x|$; hence the solutions (3.73) join smoothly with the W.K.B. solutions. The amplitude ratio between the incoming and the outgoing waves are obtained by comparing each terms:

$$\frac{|\phi_{out}|}{|\phi_{in}|} = \frac{\mu^{1/4}}{u^{1/2}} \quad . \qquad (3.74)$$

(2)-3 Solution at the turning point

Since the solutions (3.69) and (3.70) depend on u as $(u-2\mu^{1/2})^{-1/4}$ near the turning point $u = 2\mu^{1/2}$, they diverge at the turning point. It may be noted that this x-dependence $(x-x_t)^{-1/4}$ can also be obtained in the

W.K.B. approximation. However the asymptotic method is able to derive the solution at the turning. The divergence near $u = 2\mu^{1/2}$ is due to the smallness of $f''(p)$ at the saddle point where two saddle points are very close to each other; therefore instead of the usual "two-legs" saddle point method, the "three-legs" method must be utilized. With $u = 2\mu^{1/2}$, $f(p)$ is expanded near the saddle point $p_0 = i\mu^{1/4}$, as follows:

$$f(p) = f(p_0) + f'''(p_0)\frac{(p-p_0)^3}{6} . \tag{3.75}$$

The integral J_0 along the contour determined by the boundary condition illustrated in Fig. 3.15 is obtained;

$$J_0 = \int_{C_0} \frac{1}{p_0} e^{f(p_0)+\frac{1}{6}f'''(p_0)(p-p_0)^3} dp$$

$$= \frac{e^{f(p_0)}}{p_0[f'''(p_0)]^{1/3}} \int_{-\infty}^{0} e^{\frac{1}{6}\tau^3} d\tau \cdot [e^{i\frac{2}{3}\pi} - e^{-i\frac{2}{3}\pi}]$$

$$= \frac{\Gamma(1/3)}{3^{1/6}2^{2/3}\mu^{1/4}} \exp\left(i\frac{8}{3}\mu^{3/4}\right) , \tag{3.76}$$

where Γ is the Gamma function.

As we have set $A_1 = 1$ in Eq. (3.69), it is easy to see $\phi(2\mu^{1/2}) = J_0$. Since the solution in Eq. (3.69) approaches

$$\phi \to \frac{\sqrt{\pi}}{\mu^{1/4}(u-2\mu^{1/2})^{1/4}} \exp\left(i\frac{8}{3}\mu^{3/4}\right), \tag{3.77}$$

with $u \to 2\mu^{1/2}$, the "two-legs" saddle point method breaks down in the region,

$$|u-2\mu^{1/2}| < \frac{2^{2/3}3^{2/3}\pi^2}{\Gamma(1/3)^4} \sim 2.52 . \tag{3.78}$$

(2)-4 Conversion rate

The damping near the turning point is important because the energy density becomes large there; therefore Im D_L must be included in the investigation. With positive ε, the contour of integration is deformed near the turning point as illustrated in Fig. 3.16. For certain critical value $u = u_c$, one contour intersects another contour at the saddle point

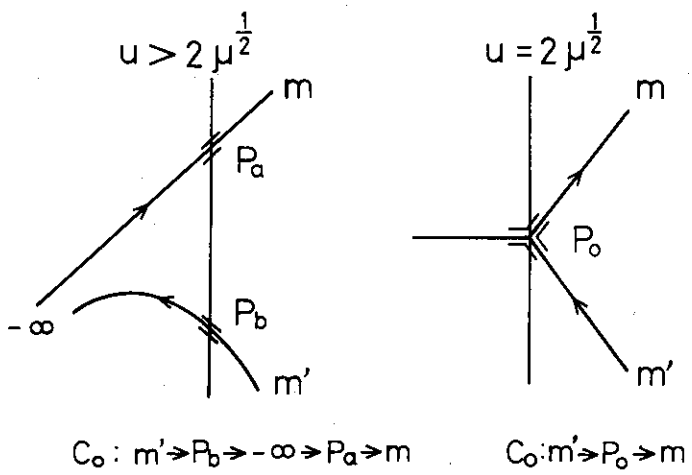

Fig. 3.15 Contour deformation near the turning point for $\varepsilon=0$. The contour C_0 $(m', P_b, -\infty, P_a, m)$ for $u > 2\mu^{1/2}$ is deformed to C_0' (m', P_0, m) for $u = 2\mu^{1/2}$.

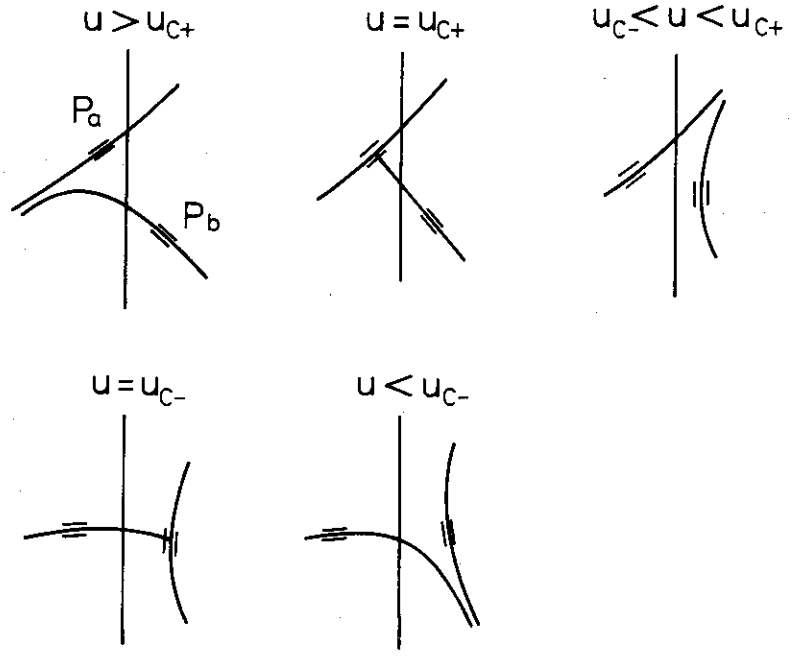

Fig. 3.16 Contour deformation near the turning point for $\varepsilon > 0$.

of the latter. Since Im $f(p_1) \simeq$ Im $f(p_2)$ at the critical points, it is easy to obtain

$$u_{c\pm} = 2\mu^{1/2} \pm \frac{\varepsilon}{\sqrt{3}} \quad . \tag{3.79}$$

Without a discussion about the behavior of the wave for $u < u_{c+}$, we may estimate the conversion rate which is the ratio between the amplitudes of the outgoing wave ϕ_{out} and the incoming wave ϕ_{in}.

Even if finite ε is included, Eq. (3.69) is valid for $u \geq u_{c+}$ by the new definition,

$$z = \frac{u + i\varepsilon}{2\mu^{1\ 2}} \quad . \tag{3.80}$$

Then, we can calculate the conversion ratio R at $u = u_{c+}$ for $\mu \gg \varepsilon^2$,

$$R = \frac{|\phi_{out}|}{|\phi_{in}|} = \exp\left(-\frac{2^{5/2}}{3^{7/4}}\varepsilon^{3/2}\right) \quad . \tag{3.81}$$

It may be noted that R^2 means the conversion rate of the wave energy, as long as $k_1 \simeq k_2$ at $u = u_{c+}$. The potential at $u = u_{c+}$ is also obtained;

$$|\phi| = \frac{\sqrt{\pi}\ 3^{1/8}}{2^{3/4}\mu^{1/4}\varepsilon^{1/4}} \exp\left(-\mu^{1/4}\varepsilon + i\frac{8}{3}\mu^{3/4}\right)\sqrt{R+\frac{1}{R}} \quad . \tag{3.82}$$

There are two limitations on the result Eqs.(3.81) and (3.82); that is, first, for small ε the "two-legs" method breaks down under the condition (3.78). Therefore when

$$\varepsilon < \frac{2^{2/3}3^{7/6}\pi^2}{\Gamma(1/3)^4} \sim 4.36, \tag{3.83}$$

Eq. (3.82) is not correct but Eq. (3.81) is still useful because the conversion ratio is independent of the phase defference of the waves. Second, for large ε the critical point u_{c+} is far from the turning point; hence the x dependence of ε and the imaginary part of $k_1^2k_2^2$ becomes considerable. In fact a numerical calculation shows that the inequality $k_{1i}/k_{1r} \ll k_{2i}/k_{2r}$ takes place near the turning point; this corresponds to that the imaginary part of $k_1^2k_2^2$ cannot be neglected. However, for large ε the wave strongly damps before arriving at the turning point in a weakly inhomogeneous plasma. In this case, it is unnecessary to consider the turning.

(3) Summary of wave propagations

The numerical calculation is carried out for two cases, that is,

Case A : $a/\rho_i = 100$, $\omega_{pe}^2/\Omega_e^2 = 1.0$, at $x = a$,
(linear density profile)

Case B : $a/\rho_i = 1500$, $\omega_{pe}^2/\Omega_e^2 = 0.4$, at $x = a$,
(parabolic density profile)

where a is the distance from the plasma boundary to the maximum density. These conditions correspond to, for example,

Case A' : $N_{max} = 10^{19}$ m^{-3}, $B_0 = 1$T, $a = 10^{-1}$ m,
$T_i = 100$ eV, $\rho_i = 10^{-3}$ m ,

Case B' : $N_{max} = 10^{20}$ m^{-3}, $B_0 = 5$T, $a = 1$ m,
$T_i = 1$ keV, $\rho_i = 6.5\times10^{-4}$ m .

First, the unmagnetized ion model is employed. Fig. 3.17 shows an example of spatial variation of electric field E_x and potential ϕ in Case A. The variation of ϕ is small except near the plasma boundary and the turning point; therefore E_x is almost propotional to $k_\perp\rho_i$. After the turning E_x and ϕ are strongly damped by the ion Landau damping. The conversion ratio R at the critical point is calculated to be 70.5 %; however the reflection ratio of the energy flux $v_{gx}W$ is 58 %, which is more than R^2. This is due to the difference of $\partial D/\partial\omega$ between the incoming and the outgoing waves at the critical point. The energy absorbed at the critical point is considered to be dissipated into ion not only at the critical point $u = u_{c+}$ but in the region $u_{c-} < u < u_{c+}$, for the wave amplitude remains considerable there. The lowest curve in Fig. 3.17 shows that the reflected energy is absorbed between $x/a = 0.48$ and the turning point. The absorbed power density P_{abs} which is the gradient of $v_{gx}W$ takes its maximum value at $x/a = 0.54$.

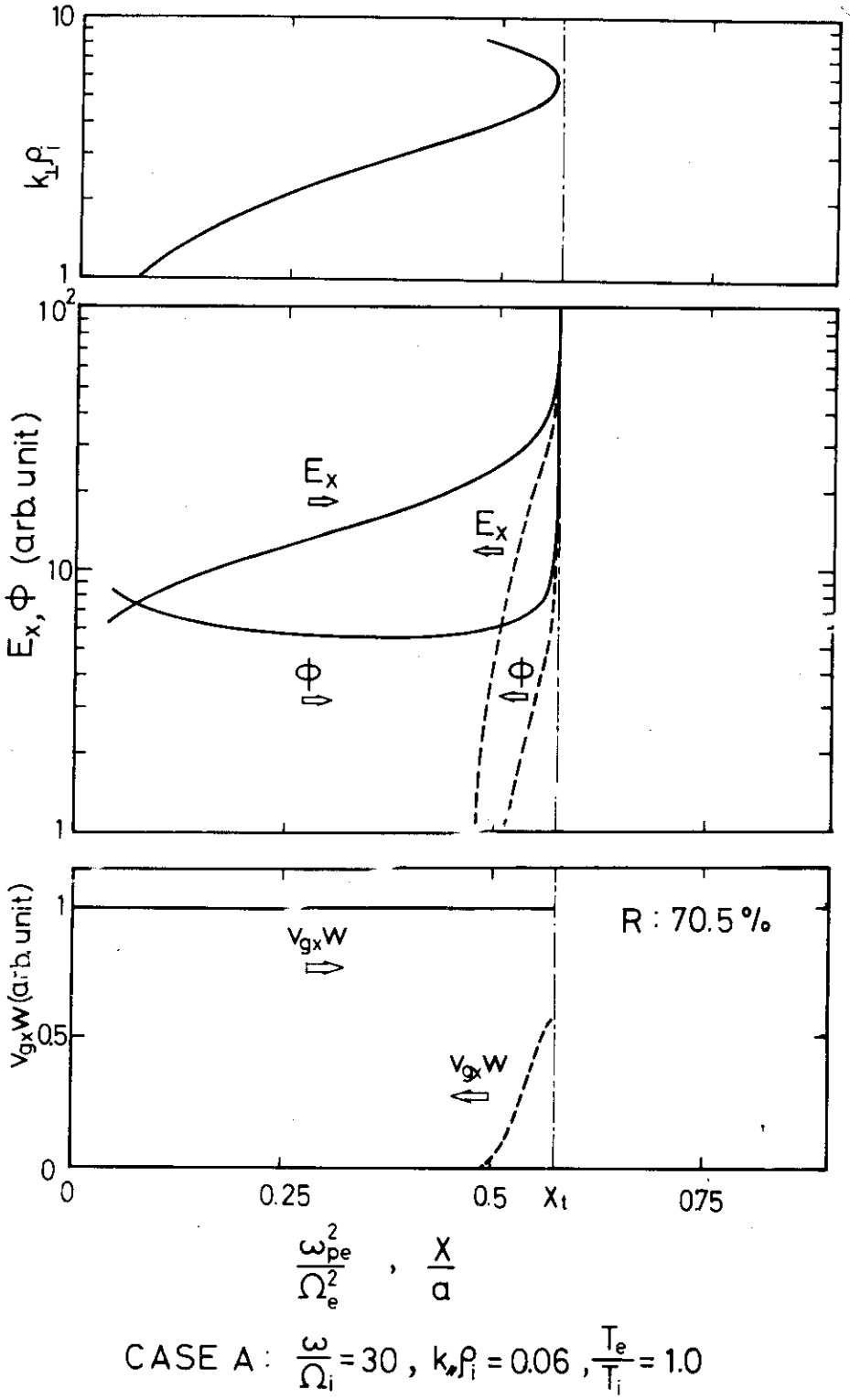

Fig.3.17 An example of spatial variations of electric field E_x, potential ϕ and energy flux $v_{gx}W$ in the case A (unmagnetized ion model).

The spatial distributions of P_{abs} for various $k_{\parallel}\rho_i$ values are described in Fig. 3.18 and Fig. 3.19. As $k_{\parallel}\rho_i$ decreases, the turning point shifts toward the high density side. For $k_{\parallel}\rho_i = 0.15$ power absorption spreads over a wide region in addition to near the turning point. For $0.08 \leq k_{\parallel}\rho_i \leq 0.12$ the absorption is highly localized in the vicinity of the turning point; the upward arrows indicate overscale of P_{abs}. With the further decrease of $k_{\parallel}\rho_i$, some of the incident energy flux is reflected and absorbed after turning as indicated by the broken line. It should be noted that the location where the absorption occurs after turning is almost independent of $k_{\parallel}\rho_i$, which is a property of the warm plasma mode. With $T_e/T_i = 10^{1/2}$, the electron Landau damping appears for large $k_{\parallel}\rho_i$; however for smaller $k_{\parallel}\rho_i$ the change of electron temperature has no influence on the phenomena.

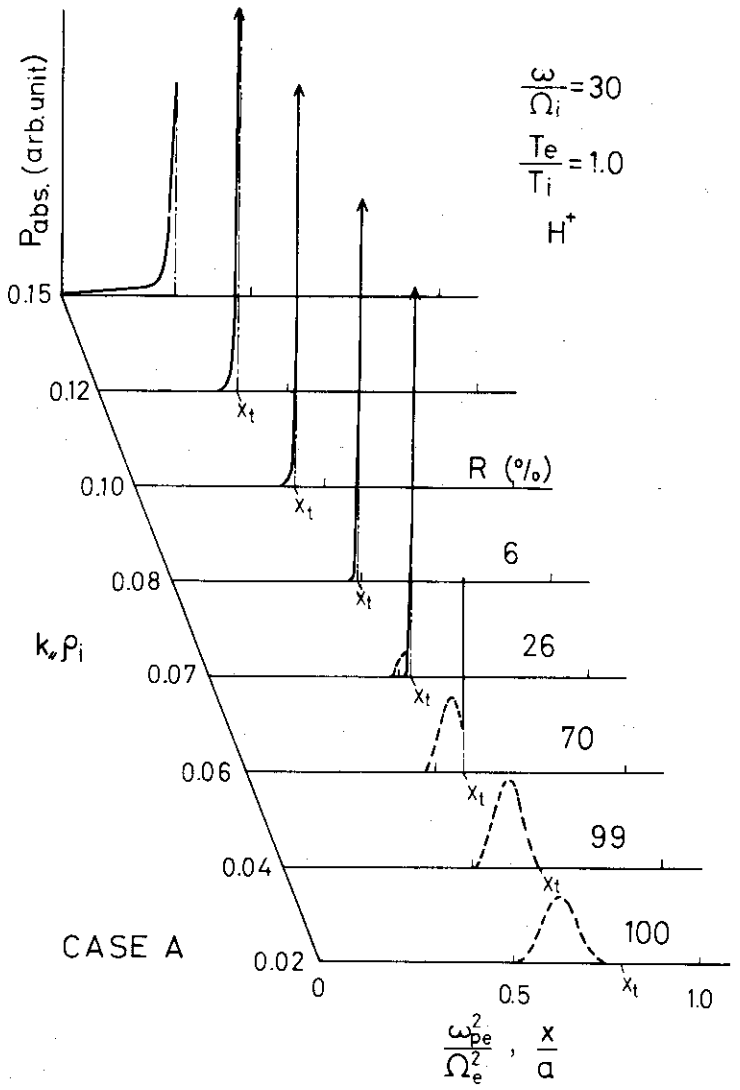

Fig. 3.18 The spatial distributions of absorbed power P_{abs} for various $k_{\parallel}\rho_i$ in the case A (unmagnetized ion model).

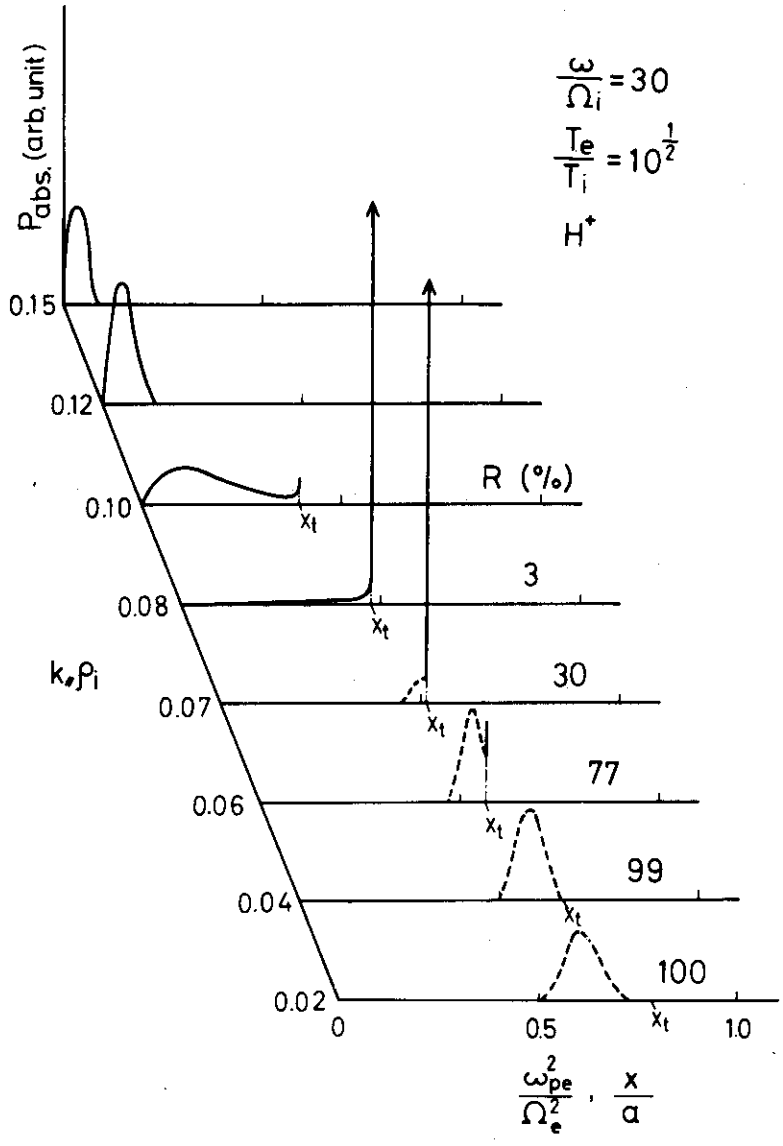

Fig.3.19 The spatial distributions of absorbed power P_{abs} for various $k_{\parallel}\rho_i$ in the case A (unmagnetized ion model, $T_e = 10^{1/2}T_i$).

The lower limit of $k_{\parallel}\rho_i$ is determined by the accessibility condition; in the case A' at $\omega/\Omega_i = 30$, the minimum $k_{\parallel}\rho_i$ equals 0.013.

Next we consider the case B. It is shown in Fig. 3.20 that because of the parabolic density profile E_x and ϕ changes more gently near the turning point compared with Fig. 3.17. For the parameter of Fig. 3.20, the wave energy is almost absorbed before turning. The location of power absorption is demonstrated in Fig. 3.21 for various frequency. The parameter $k_x\rho_i$ is so chosen that the turning occurs at $x/a \simeq 0.8$. The spreading of absorption region for large ω^* and $k_x\rho_i$ is considered to be due to the large a/ρ_i as well as the parabolic density profile. The minimum $k_z\rho_i$ in the case B' equalls 0.0316. When T_e/T_i is large, the electron Landau damping appears in a similar way to Fig. 3.19. Furthermore the effect of shear is examined on the linear shear.

$$\cos\psi = \frac{1}{7.5}\,\frac{a-x}{a} \quad . \tag{3.84}$$

However only a little decrease of the electron Landau damping is observed.

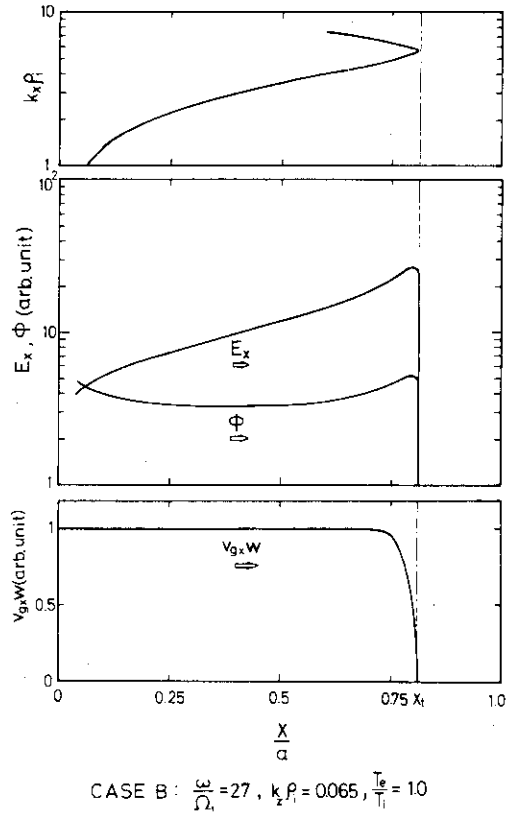

Fig. 3.20 An example of spatial variations of electric field E_x, potential ϕ and energy flux $v_{gx}W$ in the case B (unmagnetized ion model).

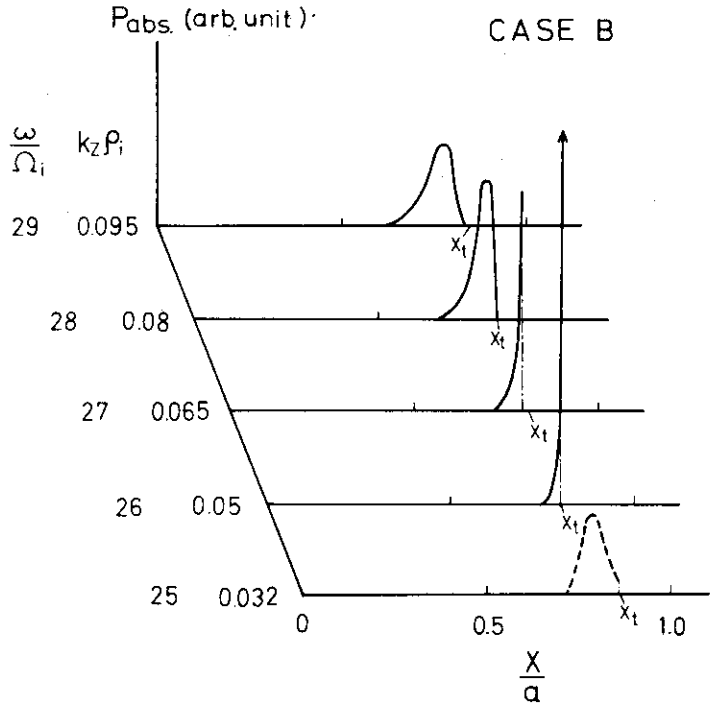

Fig.3.21 The spatial distributions of absorbed power P_{abs} in the case B (unmagnetized ion model).

The results of the magnetized ion model in the case B is summarized in Fig. 3.22. The parameters are selected so that the wave first turns at $x/a \simeq 0.9$. The end of the horizontal line which starts from $x = 0$ indicates the first turning point; the oblique line means the wave after the first turning and ends at the second turning; the wave after the second turning is shown by the horizontal line which starts from the second turning point. The thick line denotes the location of power absorption. For small $k_z\rho_i$, there are wide pass bands, where the waves propagate beyond the maximum density. With the increase of $k_z\rho_i$ the width of the pass band becomes narrower and finally the pass band vanishes at $k_z\rho_i=0.1$. When the frequency approaches of the harmonics, the power absorption first appears near the second turning point and spreads between the first and the second turning; then it is localized in the vicinity of the first turning point and at last the wave is absorbed before arriving at the first turning point. The width of absorbed band is approximately

$$|\omega^* - n| \lesssim 4 \cdot k_\parallel \rho_i \quad , \tag{3.85}$$

in the case B. It may be noted that the damping rate just at the cyclotron harmonics is $(2\pi k_\parallel \rho_i)^{-1}$ times larger than that of the ion Landau damping.

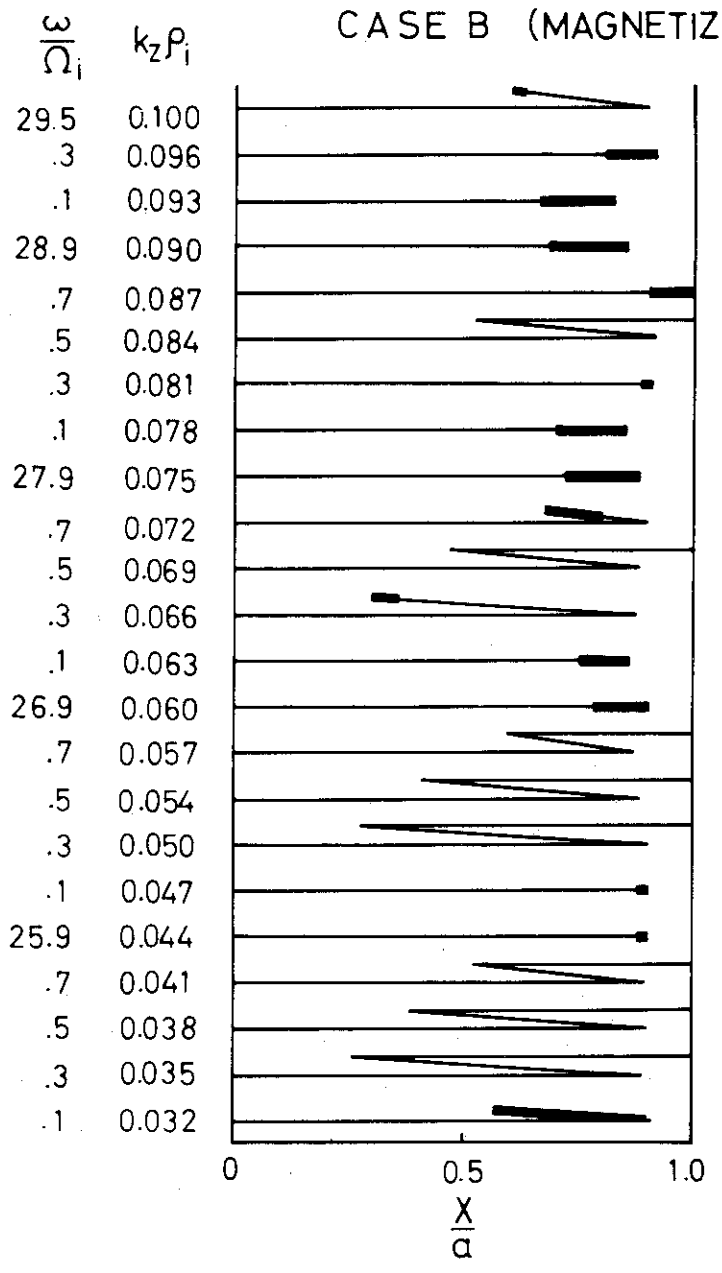

Fig. 3.22 The results of the magnetized ion model in the case B. The thick line denotes the location of appreciable power absorption.

In the cases A' and B', the main damping process is considered to be the ion cyclotron damping; because

Case A' : $\Omega_i = 9.58\times10^7$ [sec^{-1}], $\nu_{ii} = 4.97\times10^4$ [sec^{-1}] ,

Case B' : $\Omega_i = 4.79\times10^8$ [sec^{-1}], $\nu_{ii} = 1.83\times10^4$ [sec^{-1}] ,

therefore the collision restored Landau damping is not expected to take place.

§3-3 Effect of magnetic field gradient

As we have seen in §3-2(3), the waves in the pass band traverse the plasma without significant damping if a magnetic field gradient is not taken account of. However in an actual low β toroidal machine like a tokamak the magnetic field is almost proportional to R^{-1} where R is the distance from the toroidal axis; hence there exists a magnetic field gradient perpendicular to the magnetic field. In this case the LH wave which propagates across the ion cyclotron harmonics suffers a localized damping. We shall discuss on the effect of the magnetic field gradient.

(1) Damping through the passage of cyclotron harmonics

The contribution of the singular part D_1 to the dispersion relation is small when $k_\perp \rho_i \ll \omega^*$. If we assume the solution of the form $k_\perp = k_{\perp 1} + k_{\perp 0}$ where $k_{\perp 0}$ is a solution of $D_0(k_\perp) = 0$, the correction $k_{\perp 1}$ due to $D_1(k_\perp)$ may be expressed as

$$k_{\perp 1} = - \frac{D_1(k_{\perp 0})}{\partial D_0(k_{\perp 0})/\partial k} \quad , \tag{3.86}$$

which is valid only if $|k_{\perp 1}| \ll |k_{\perp 0}|$. Using Eq. (3.36) as D_1, we find that the dispersion curve is distorted near the cyclotron harmonics.

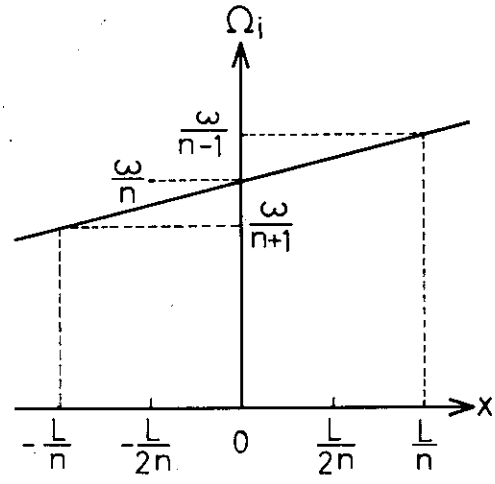

Fig. 3.23 The illustration of magnetic field gradient.

In the rest of this section, we shall calculate the damping rate when the wave goes across one of the cyclotron harmonics. The magnetic field is assumed to satisfy the resonance condition $\Omega_i = \omega/n$ at $x = 0$, i.e.

$$\Omega_i = \frac{\omega}{n}\left(1+\frac{x}{L}\right) , \tag{3.87}$$

as illustrated in Fig. 3.23; we consider the propagation from $-L/2n$ to $L/2n$. Moreover we assume that $n \gg 1$ and $k_\parallel \rho_i \ll 1$; therefore the change of D_0 during the propagation is negligible and the cyclotron harmonics are sufficiently separated from the neighboring harmonics. By the use of Eqs. (3.36) and (3.86), the imaginary part of $k_{\perp 1}$ is found to be

$$\mathrm{Im}\ k_{\perp 1} = -\frac{1}{\dfrac{\partial D_0}{\partial k_\perp}}\sqrt{\frac{\pi}{2}}\frac{\omega_{pi}^2}{k^2}\frac{m_i}{T_i}\frac{\omega}{k_\parallel v_{Ti}}\exp\left(-\frac{(\omega-n\Omega_i)^2}{2k_\parallel^2 v_{Ti}^2}\right)\Lambda_n(k_{\perp 0}^2\rho_i^2). \tag{3.88}$$

Denoting the averaged damping ratio by $\overline{k_i}$, we may calculate the damping during the propagation to obtain

$$\begin{aligned}\overline{k_i} &= \frac{n}{L}\int_{-\frac{L}{2n}}^{\frac{L}{2n}} \mathrm{Im}\ k_{\perp 1}\, dx \\ &= -\frac{1}{\partial D_0/\partial k_\perp|_{x=0}}\,\pi\,\frac{\omega_{pi}^2}{k^2}\frac{m_i}{T_i}\,n\,\Lambda n(k_{\perp 0}^2\rho_i^2|_{x=0}) .\end{aligned} \tag{3.89}$$

Here the integration has been extended to infinity on the assumption that $k_\parallel \rho_i \ll 1$. Comparing this result with the unmagnetized ion approximation,

$$\mathrm{Im}\ k_\perp = -\frac{1}{\dfrac{\partial D_0}{\partial k_\perp}}\,\pi\,\frac{\omega_{pi}^2}{k^2}\frac{m_i}{T_i}\frac{1}{\sqrt{2\pi}}\frac{\omega^*}{k\rho_i}\exp\left(-\frac{1}{2}\left(\frac{\omega^*}{k\rho_i}\right)^2\right) , \tag{3.90}$$

and using the approximated form of $\Lambda_n(\lambda)$ in Appendix A, we conclude that for $k_\perp \rho_i \gg \omega^{*1/2}$ the two expressions coincide and for $k_\perp \rho_i \lesssim \omega^{*1/2}$ the averaged cyclotron damping exceeds the Landau damping.

In the case of the LH wave the above discussions can be applied to the damping before the turning; because near and after the turning, $k_\perp \rho_i$ is so large that $k_{\perp 1}$ becomes as large as $k_{\perp 0}$.

(2) Damping near the cyclotron harmonics

Since $\partial D_0/\partial k_\perp$ approaches zero near the turning point, the distortion

of the dispersion curve from the warm plasma approximation becomes large as illustrated in Fig. 3.23. If a cyclotron harmonics resonance occurs near the turning point, i.e. $\omega_{pe}^2 \lesssim \omega_{pet}^2$, there is a possibility that the turning occurs at the cyclotron harmonics. This condition may be evaluated as follows. As $-D_1$ has its maximum value $-D_{1max}$ at $\omega \simeq n_0 + 1.3k_\parallel\rho_i$, there exists a solution of $D_0 + D_1 = 0$ if $D_0 < -D_{1max}$. Using Eq. (3.34) for $k_\perp\rho_i$, we find that if the cyclotron harmonics resonance appears in the region

$$\frac{\omega_{pet}^2 - \omega_{pe}^2}{\omega_{pe}^2} < \frac{\omega_{pet}^2}{\omega_{per}^2} \frac{\omega^* s}{1.3k_\parallel^2\rho_i^2} \Lambda_n \left(\frac{m_i}{m_e} \frac{k_\parallel\rho_i}{s}\right) , \tag{3.91}$$

the wave changes the sign of its group velocity. For example if $\omega/\Omega_i = 30$, $k_\parallel\rho_i = 0.08$ and $T_e/T_i = 1$, this condition is calculated to be

$$\frac{\omega_{pet}^2 - \omega_{pe}^2}{\omega_{pe}^2} \lesssim 0.13 \quad . \tag{3.92}$$

It should be noted that the cyclotron damping at the turning point is strong in this case.

After the turning, $k_\perp$ becomes so large that the wave which approaches the cyclotron harmonics resonance is strongly damped regardless of the density. Therefore the wave which experiences the turning damps between the two neighboring ion cyclotron harmonics.

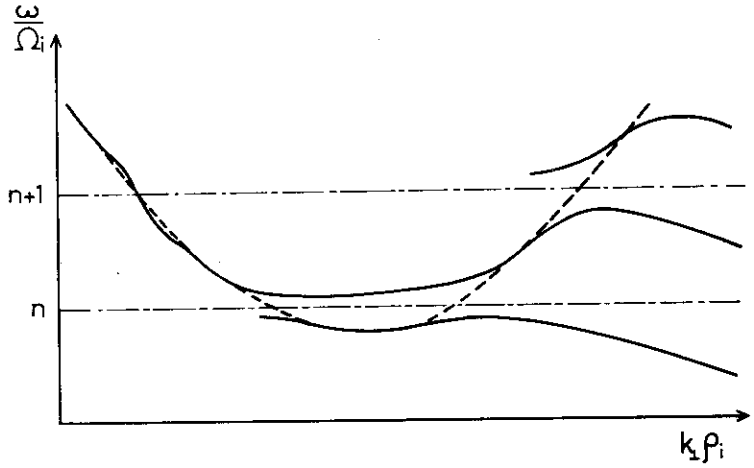

Fig. 3.24 The distortion of the dispersion curve near the cyclotron harmonics.

(3) Local dispersion relation of lower hybrid waves in JT-60

In order to investigate the propagation and the collisionless damping of lower hybrid waves in JT-60 device, we numerically solve the local dispersion relation of electrostatic waves, taking account of inhomogenities of plasma density and magnetic field. For simplicity, we employ the slab model, where plasma parameters depend on only x and the magnetic field is parallel to the z-axis and has the dependence $B = B_t\ (1-x/R)$ (R is the major radius of a torus). (The effects of two dimensional inhomogenity are studied in §3-4.) We make the electrostatic approximation and assume that the parallel wavelength is much larger than the ion Larmor radius (for example, $k_{//}\rho_i \sim 3\times10^{-2}\ N_{//}$ in JT-60, where the parallel refractive index, $N_{//}$, is of order unity). Under these approximations the dispersion relation of lower hybrid waves in a homogeneous plasma, Eqs. (3.16) and (3.17) are reduced to

$$D = 1 + \frac{\omega_{pe}^2}{k^2}\frac{m_e}{T_e}\left[1 + (W(z_{e0})-1)\Lambda_0(\lambda_e)\right]$$

$$+ \frac{\omega_{pi}^2}{k^2}\frac{m_i}{T_i}\left[1 - \sum_{\ell\neq n,n+1}\frac{\omega}{\omega-\ell\Omega_i}\Lambda_\ell(\lambda_i) + \sum_{\ell=n,n+1}\frac{\omega}{\omega-\ell\Omega_i}(W(z_{i\ell})-1)\Lambda_\ell(\lambda_i)\right], \tag{3.93}$$

where $n = [\omega/\Omega_i]$. For given frequency $Re\omega$ and parallel wavenumber $k_{//}$, Eq. (3.93) has been solved numerically, changing the plasma parameters. The summation of ion cyclotron harmonics has been taken up to $|\ell_{max}| = 50$. Results are shown in Fig. 3.25. Typical parameters used in these calculations are the followings: $N_e(0) = 5\times10^{19}\ m^{-3}$, $T_e(0) = T_i(0) = 1$ keV, $B_t = 5\ Wb/m^2$, $R = 3$ m, $f = 1.4$ GHz and $k_{//} = 50\ m^{-1}$. The plasma density and temperature are assumed to be parabolic. The incident wave excited by an external source propagates into the high density region with increasing perpendicular wavenumber and it is converted to the plasma wave due to the finite temperature effect, before it reaches the resonance layer. The reflected wave has a very short wavelength ($k_\perp\rho_i \gg 1$) and propagates as the ion Bernstein wave. As is well known, ion Bernstein waves are possible only within the frequency band between two adjacent harmonics of ion cyclotron frequency ($n\Omega_i < \omega < (n+1)\Omega_i$; n is the integer). In our case, the frequency of the wave is fixed and the ion cyclotron frequency varies spatially due to the inhomogenity of the magnetic field, which implies that the ion Bernstein wave is spatially trapped within the narrow region ($\Delta \sim \frac{\Omega_i}{\omega} R$) between two adjacent

(a)

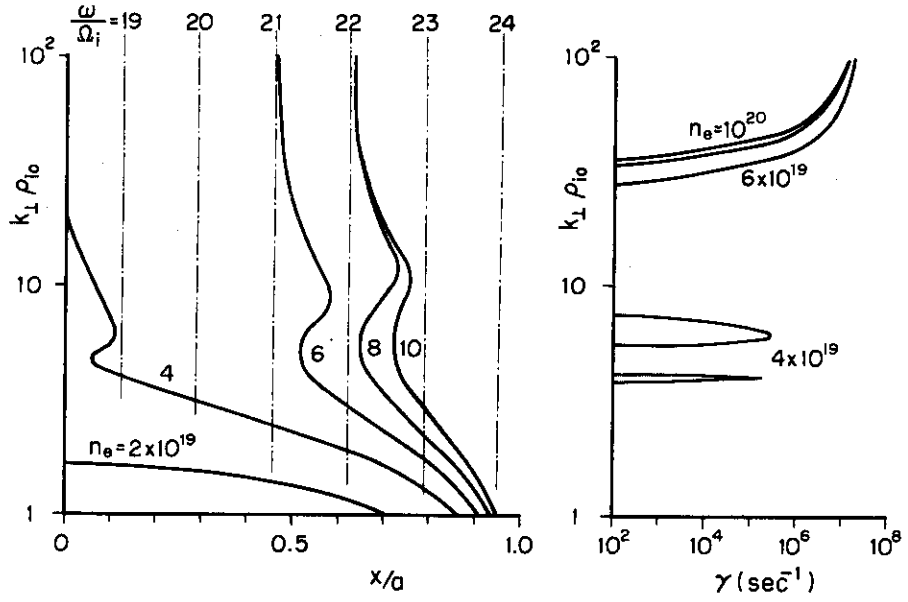
ω/Ωi=19 20 21 22 23 24
10²
k⊥ ρio
10
1
0 0.5 1.0
x/a
4
6
8
10
ne=2x10¹⁹
ne=10²⁰
6x10¹⁹
4x10¹⁹
10² 10⁴ 10⁶ 10⁸
γ (sec⁻¹)

(b)

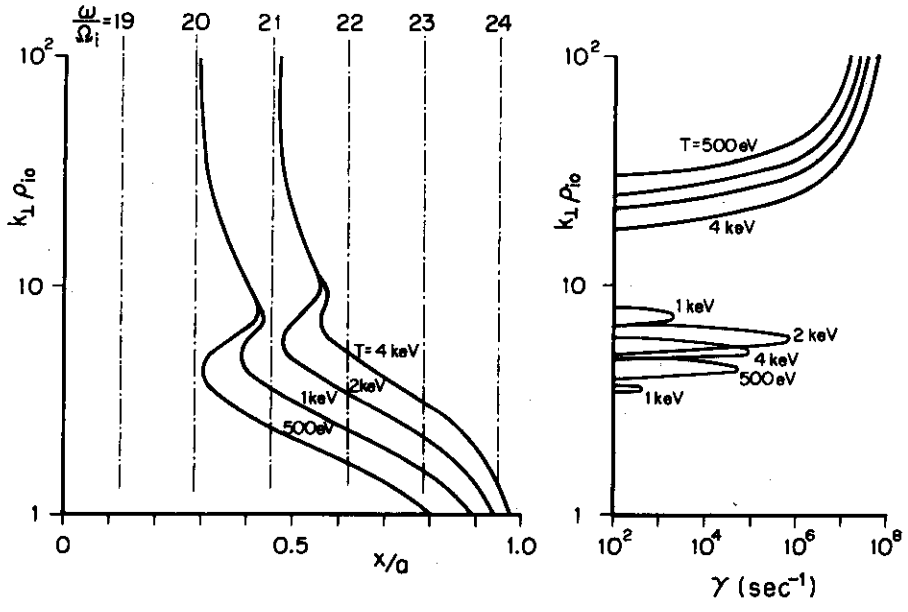
ω/Ωi=19 20 21 22 23 24
10²
k⊥ ρio
10
1
0 0.5 1.0
x/a
T=4 keV
2keV
1keV
500eV
T=500eV
4 keV
1 keV
2 keV
4 keV
500eV
1keV
10² 10⁴ 10⁶ 10⁸
γ (sec⁻¹)

(c)

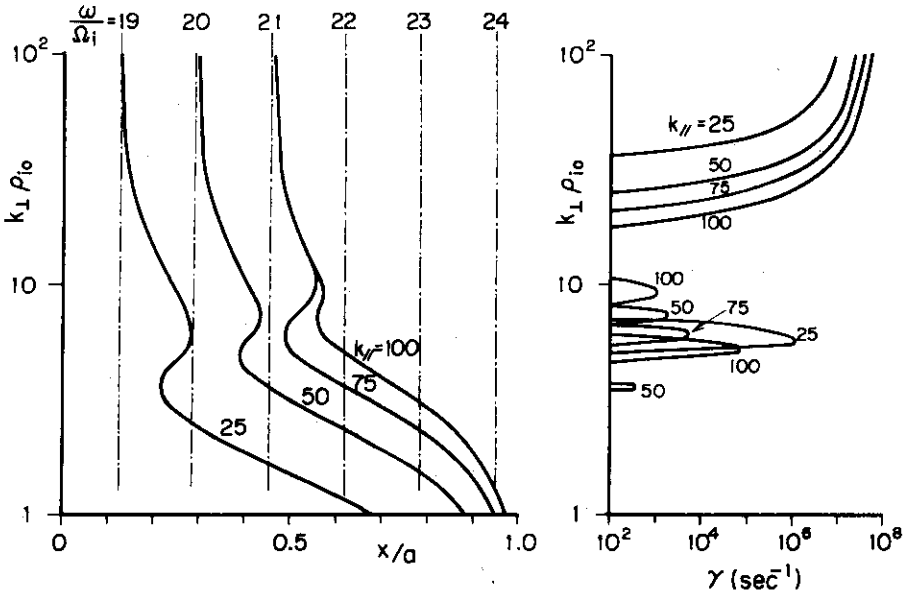

(d)

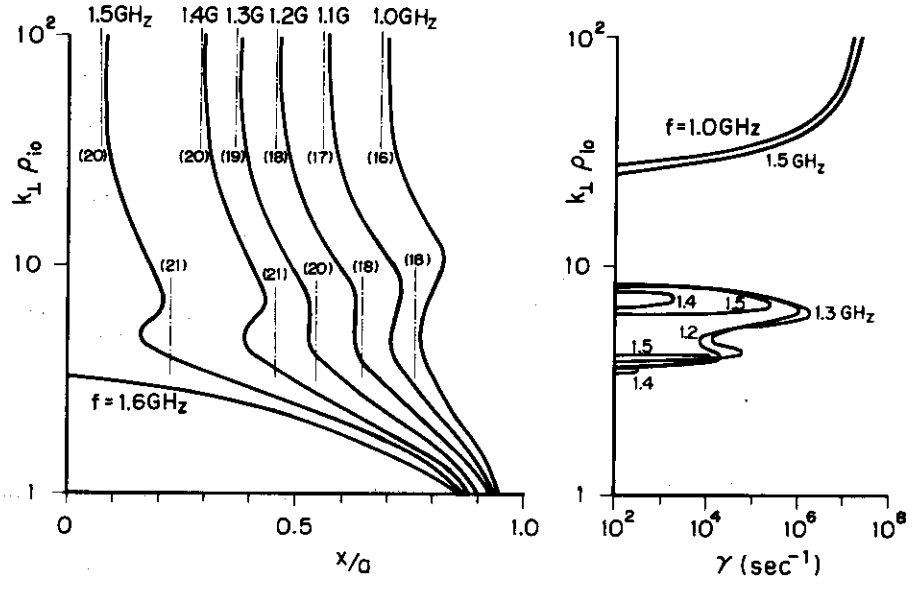

Fig.3.25 Local dispersion relations of lower hybrid waves in the presence of density, temperature and magnetic field gradients. Dependences on (a) $N_e(0)$, (b) $T(0)$, (c) $k_{//}$, and (d) f are illustrated. Standard parameters are $N_e(0) = 5\times10^{19}$ m^{-3} $T_e(0) = T_i(0) = 1$ keV, $B_t = 5Wb/m^2$, $R = 3m$, $f = 1.4GHz$ and $k_{//} = 50m^{-1}$. Dashed lines and integers denote the ion cyclotron harmonic layers and the harmonic numbers, respectively.

layers of ion cyclotron harmonics (which are indicated by dashed lines and integers). When the wavelength becomes short, the wave approaches the layer of the higher harmonic, and suffers the strong ion cyclotron damping. The damping rate is up to the order of the ion cycrotron frequency. Therefore, the heating region of lower hybrid waves in a tokamak is strongly localized near the ion cyclotron harmonic layer. The cyclotron damping is also possible for small $k_\perp \rho_i$, but it strongly depends on the behaviour of the dispersion curve near the ion cyclotron harmonic layer.

§3-4 Effects of toroidicity

The propagation of lower hybrid waves in an inhomogeneous plasma was first studied by Briggs and Parker [25]. They have shown experimentally and theoretically that the wave excited by a point source propagates deep into the plasma along a conical trajectory or the so-called lower hybrid cone, which gradually bends to the magnetic field line with increasing plasma density, so that it is parallel to the magnetic field at the resonance layer. In a one dimensional plasma, the resonance layer is also parallel to the magnetic field, so that the trajectory tends to be tangent to the resonance layer and the field of the incident cold wave has a singularity at this layer. This singularity should lead to the mode conversion of the incident wave or the nonlinear filamentation of lower hybrid cones [56,57]. However, in a plasma with two or three dimensional inhomogeneity, the problem is more complicated, because the resonance surface does not coincide with the magnetic surface. The singularities of the field of an electromagnetic wave in a cold plasma, whose parameters depend on two co-ordinates, were investigated by Piliya and Fedrov [24]. They have shown that singularities are possible only at the points, where the magnetic field is tangent to the resonance surface. Ohkubo et al. [26] numerically calculated two dimensional characteristics of partial differential equation of electrostatic lower hybrid wave in JIPP T-II device.

In this section, we study the propagation of waves near lower hybrid frequency in JT-60. We employ the method of geometric optics [22,23] and solve the problem in three dimensional space, taking account of two dimensional inhomogeneity of plasma parameters. Finite temperature effects on the wave propagation are also investigated.

Under assumptions of geometric optics, an electromagnetic wave in a weakly inhomogeneous plasma propagates along the trajectory, which is described

by the following ordinary differential equations, or the ray equations,

$$\frac{d\vec{r}}{dt} = \vec{v}_g = \frac{\partial D}{\partial \vec{k}} \Big/ \frac{\partial D}{\partial \omega} , \quad \frac{d\vec{k}}{dt} = - \frac{\partial D}{\partial \vec{r}} \Big/ \frac{\partial D}{\partial \omega} , \tag{3.94}$$

where $D = D(\vec{r}, \vec{k}, \omega)$ is the dispersion relation in a homogeneous nondissipative plasma. We have assumed that the medium does not change in time, so that the frequency ω is constant along the trajectory. The wave energy $W = \frac{\varepsilon_0 \omega}{2} \frac{\partial}{\partial \omega} D|E|^2$ is determined by the energy conservation law,

$$\frac{dW}{dt} = -W(\vec{\nabla} \cdot \vec{v}_g + 2\gamma) , \tag{3.95}$$

where γ is the local damping rate, which is neglected in the following calculations.

We apply the theory to waves near lower hybrid frequency in an axisymmetric low-β tokamak plasma with circular cross section. Using the quasi-toroidal co-ordinates (r, θ, ϕ) with metric $(d\ell)^2 = (dr)^2 + (rd\theta)^2 + (Rd\phi)^2$, where $R = R_0 + r\cos\theta$ is the major radius of a torus, the magnetic field is given by

$$\vec{B} = \frac{R_0}{R} [B_t \vec{e}_\phi + B_p(r) \vec{e}_\theta], \quad B_p \ll B_t$$

and the plasma density, temperature and current density depend on only r. The deformation of magnetic surface due to toroidal effects is not essential in our problem so that it has been neglected. Under electrostatic and fluid approximations, the dispersion relation of waves near lower hybrid frequency is given by

$$D = -\left(\frac{T_e}{m_e} \frac{\omega_{pe}^2}{\Omega_e^4} + \frac{T_i}{m_i} \frac{\omega_{pi}^2}{\omega^4}\right) k_\perp^4 + \left(1 - \frac{\omega_{pi}^2}{\omega^2} + \frac{\omega_{pe}^2}{\Omega_e^2}\right) k_\perp^2 - \frac{\omega_{pe}^2}{\omega^2} k_{/\!/}^2 = 0 , \tag{3.96}$$

where $k_{/\!/} = k_\phi + k_\theta B_p/B_t$ and $\vec{k}_\perp = \vec{k}_{/\!/} - \vec{k}\,\vec{B}/B$. The dispersion relation depends on two co-ordinates r and θ because of the poloidal variation of the magnetic field.

First, we consider the wave propagation in a cold plasma. Setting $T_e = T_i = 0$ in Eq. (3.96) and assuming that $k_r \gg k_\theta$, k_ϕ and $B_p/B_t \gg (k_{/\!/}/k_\perp)^2$,

$$\frac{dr}{d\theta} = -\mathrm{sgn}(k_r) q(r) R_0 \frac{\omega}{\omega_{pe}} \sqrt{\varepsilon} , \quad \frac{d\phi}{d\theta} = q(r) , \tag{3.97}$$

where $q(r) = B_t r/B_p(r)R_0$ is the safety factor and ε is the dielectric constant

$$\varepsilon = 1 + \frac{\omega_{pe}^2}{\Omega_e^2} - \frac{\omega_{pi}^2}{\omega^2} \quad . \tag{3.98}$$

The resonance surface $\varepsilon = 0$ shifts toward the major axis of a torus by $\Delta R \simeq -(\frac{\omega}{\omega_{pi}})^4 (\frac{\omega_{pe}}{\Omega_e})^2 \frac{a^2}{R}$ due to the inhomogeneity of the magnetic field. Equation (3.97) shows that the wave excited by an external source propagates along the magnetic field line and penetrates into the plasma with decreasing radial velocity $v_{gr}/v_g \sim \sqrt{\frac{m_e}{m_i}}\,\varepsilon$. Because of the toroidal shift of the resonance surface, the trajectory intersects the resonance surface and terminates at this point. The only exceptions are the innermost and the outermost point on the resonance surface, where the magnetic field is tangent to the resonance surface. Piliya and Fedrov have shown that the innermost point is the singular point of the saddle type, while the outermost point is the singular point of the focus type or the node type for $(\frac{r_s}{R_0}) \gtrless \frac{1}{16}\,(q\,\frac{r_s N_e'}{N_e}\,\frac{\Omega_e}{\omega_{pe}})^2$, respectively.

The wavenumbers along the trajectory is given by

$$\frac{1}{\omega}\frac{dk_r}{dt} \simeq -\frac{1}{2}\frac{N_e'/N_e}{1+\omega_{pe}^2/\Omega_e^2} \quad ,$$

$$\frac{1}{\omega}\frac{d}{dt}(rk_\theta) \simeq -\left[\frac{\omega_{pe}^2/\Omega_e^2}{1+\omega_{pe}^2/\Omega_e^2} + \frac{m_i/m_e \cdot k_{/\!/}k_\phi/k^2}{1+m_i/m_e \cdot k_{/\!/}^2/k^2}\right]\frac{r\sin\theta}{R} \quad , \tag{3.99}$$

$$\frac{1}{\omega}\frac{d}{dt}(Rk_\phi) = 0 \quad .$$

The radial wavenumber monotonically increases along the trajectory as in a cylindrical plasma, while the poloidal and toroidal wavenumbers change due to the toroidicity, which implies that the parallel wavenumber is not constant along the trajectory. (The last equation of Eq. (3.99) shows the conservation of the toroidal mode number which is due to the axisymmetry of the plasma.) In the neighborhood of the resonance surface, neglecting terms proportional to ε, the variation of $k_{/\!/}$ is given by

$$\frac{1}{\omega}\frac{dk_{/\!/}}{dt} \simeq -\frac{\omega_{pe}^2/\Omega_e^2}{1+\omega_{pe}^2/\Omega_e^2}\cdot\frac{B_p}{B_t}\cdot\frac{\sin\theta}{R} \quad . \tag{3.100}$$

Assuming $\frac{dr}{dt} \simeq 0$, Eq. (3.100) yields the solution $k_{//}^2 \propto \varepsilon$, which implies that the parallel wavenumber goes to zero at the resonance surface. Because $k_\perp^2 = (\omega_{pe}/\omega)^2 \cdot k_{//}^2/\varepsilon$, the perpendicular wavenumber remains within the finite value at $\varepsilon = 0$. In other words, the refractive index in a tokamak plasma does not have singularities, except at the outermost point of the resonance surface, where the assumption $\frac{dr}{dt} \simeq 0$ is invalid.

In a plasma with finite temperature, the branch of the outgoing plasma wave $k_\perp^2 \simeq \frac{m_i}{T_i} (\omega^4/\omega_{pi}^2)\ \varepsilon$ appears and this branch intersects the branch of the incident cold wave. Then the incident wave is converted to the plasma wave and comes back to the plasma boundary. Although the theories of the mode conversion have been restricted within a plasma with one dimensional inhomogeneity, the mode conversion may also take place in a toroidal plasma, because the intersection of two branches is possible even if the reflactive index does not have singularities. Because the incident wave can not come to the resonance surface, the toroidal effects on the incident wave are not important. The reflected wave strongly interacts with cyclotron motions of ions because of the short wavelength ($k_\perp \rho_i \ll 1$), so that the inhomonegeity of the magnetic field plays an important role on this wave (see §3-3).

For the numerical analysis of the wave propagation in JT-60 device, Eqs. (3-94) and (3-95) have been integrated by the predictor-corrector method. Typical results are shown in Figs. 3-26 to 3-30. The parameters used in these calculations are the following: $R_0 = 3$ m, $a = 1$ m, $B_t = 5$ Wb/m^2, $q(a) = 3$, $N_e(0) = 5\times10^{19}$ m^{-3} and $T_e(0) = T_i(0) = 0$ or 1 keV. The profiles of the electron density, temperatures and the current density are taken to be parabolic and impurity ions are neglected, for simplicity. Figure 3-26 shows trajectories of waves with different frequency in a cold plasma, projected on the poloidal and toroidal planes. The waves are excited by sources located at the outermost point of the torus, but initial positions of integrations are at the points slightly inside of the plasma column, which is indicated by asteristks in figures. The initial values of poloidal and toroidal wavenumbers are $k_\theta = 0$ and $k_\phi = 50$ m^{-1}, respectively, and the radial wavenumber is determined by the dispersion relation Eq. (3-96). The wave excited by the external source enters the plasma perpendicularly to the magnetic field. Then the wave propagates to the magnetic axis in the spiral form, rotating around the minor and major axis of the torus, until the trajectory intersects the resonance surface, which is plotted by the dashed line. When the frequency increases, the resonance surface shrinks to the magnetic axis and shifts toward the major axis of torus. The critical

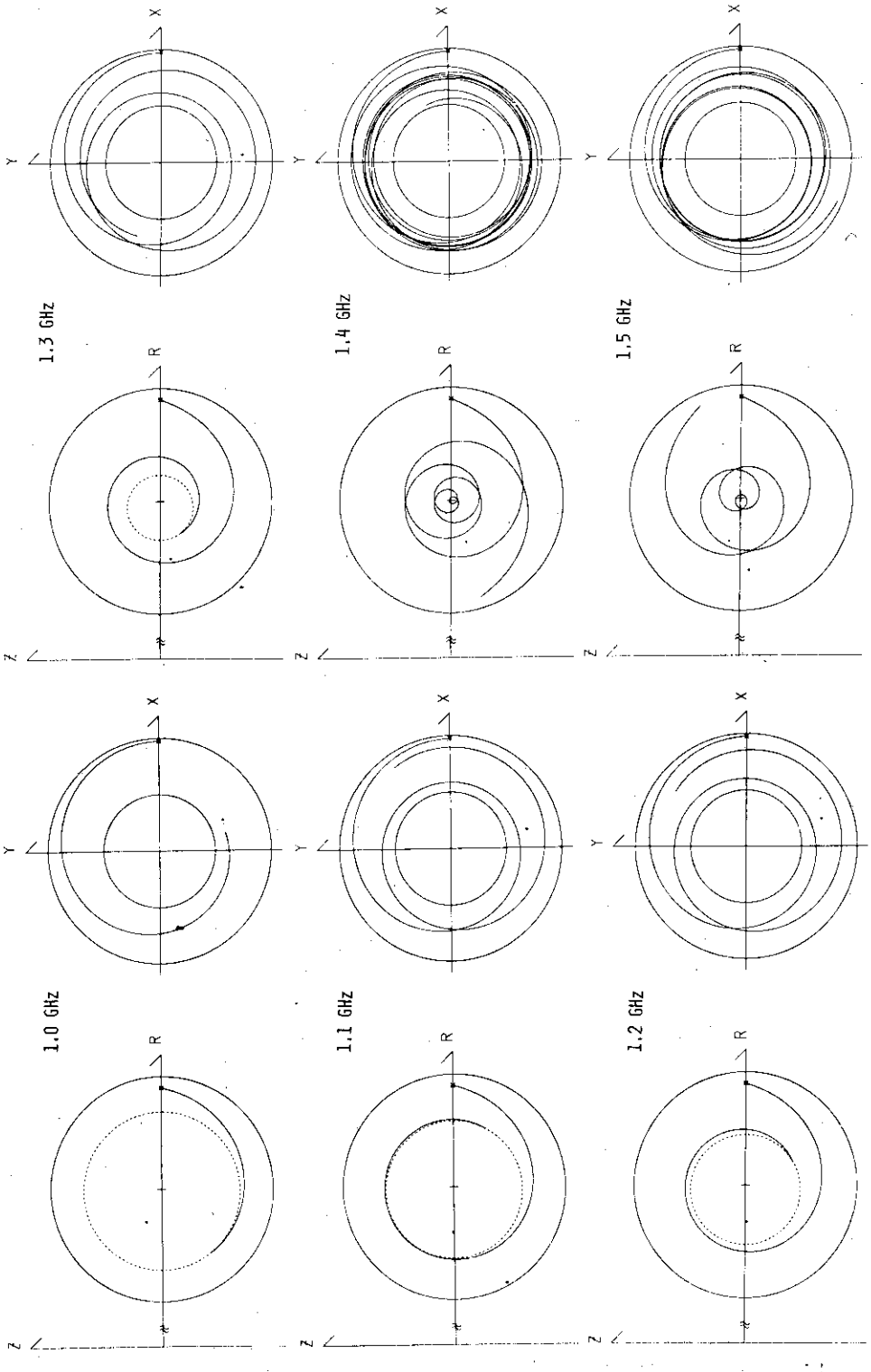

Fig. 3.26 Ray trajectories of lower hybrid waves in a cold plasma. Trajectories are projected on the poloidal and the toroidal planes. Parameters are $R_0 = 3m$, $a = 1m$, $B_t = 5Wb/m^2$, $q(a) = 3$, $N_e(0) = 5\times10^{19}\ m^{-3}$. Initial positions of trajectories are indicated by asteristks and initial values of k_θ and k_ϕ are $k_\theta = 0$ and $k_\phi = 50m^{-1}$, respectively. The resonance surfaces are indicated by dotted lines.

resonance frequency is 1.33 GHz in our parameters and the shift is $\Delta R \sim -0.04$ m. The off-resonance wave continues to propagate to the magnetic axis, but the direction of the perpendicular wavenumber rotates by π near the magnetic axis and the wave comes back again to the plasma boundary with $k_r < 0$. The sign of $k_{//}$ does not change along the trajectory so that the wave experiences many rotations around the major axis. When the frequency increases, the average radial velocity increases and the rotation numbers around the minor and major axis decrease. Figure 3-27 shows trajectories of waves excited by ten sources with equal spacing. Trajectories of resonance waves terminate only at the localized region of the lower part of the resonance surface. Because of the symmetry of Eq. (3.94), the terminal points of waves with initial wavenumber $k_\phi = -50$ m^{-1} are localizated at the upper part. This localization of terminal points is due to the toroidal shift of the resonance surface, so that this effect is strong for high frequency waves or weak magnetic field. Moreover, it is noted that there is the concentration, or the focusing, of trajectories near the trajectory passing through the innermost point of the resonance surface, and the wave can not penetrate inside of this critical surface. This focusing of trajectories is due to the dependence of the radial group velocity on ε. Figure 3-28 shows the variations of ε, $k_{//}$, $k_\perp$ and W along the trajectory. The toroidicity causes the variation of the parallel wavenumber, which abruptly goes to zero near the resonance surface ($\varepsilon = 0$), and, as the result, the perpendicular wavenumber does not have singularities on the resonance surface. The group velocity tends to be zero when $\varepsilon \to 0$, so that the wave energy has the singularity on the resonance surface. Therefore, we can expect that the nonlinear effects play important roles on the wave propagation near the resonance surface, as in a cylindrical plasma [24]. Effects of plasma temperatures on the wave propagation are shown in Figs. 3-29 and 3-30. The incident waves with resonance frequency are converted to the plasma waves with short wavelength and come back to the plasma boundary perpendicularlly to the magnetic surface. The reflection point strongly depends on the parallel wavenumber and the ion temperature. Because the mode conversion takes place at the points away from the resonance surface, the localization and the concentration of trajectories do not occur. The off-resonance wave with $f = 1.4$ GHz is also converted to the plasma wave because the perpendicular wavenumber in a cold plasma has enough large to intersect with the branch of the plasma wave.

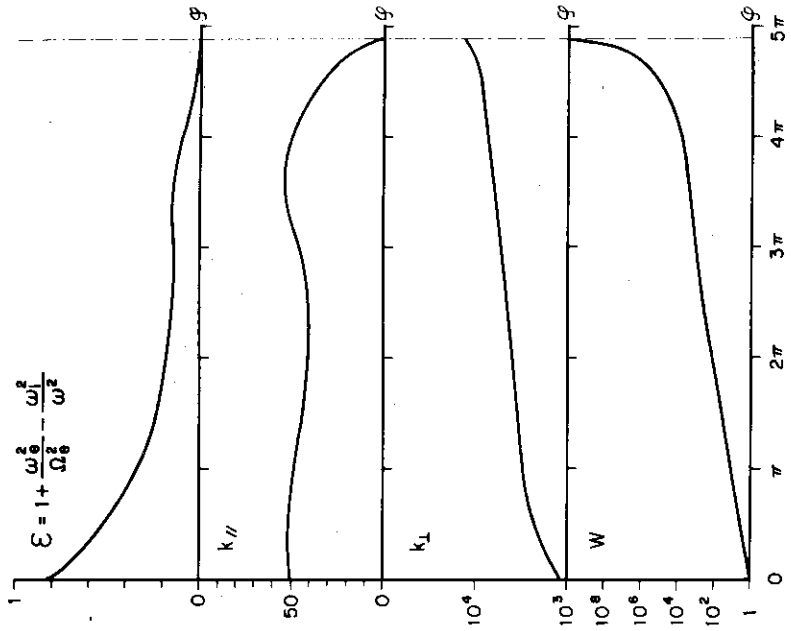

Fig.3.28 Variations of ε, $k_{//}$, $k_{\perp}$ and W along the trajectory.

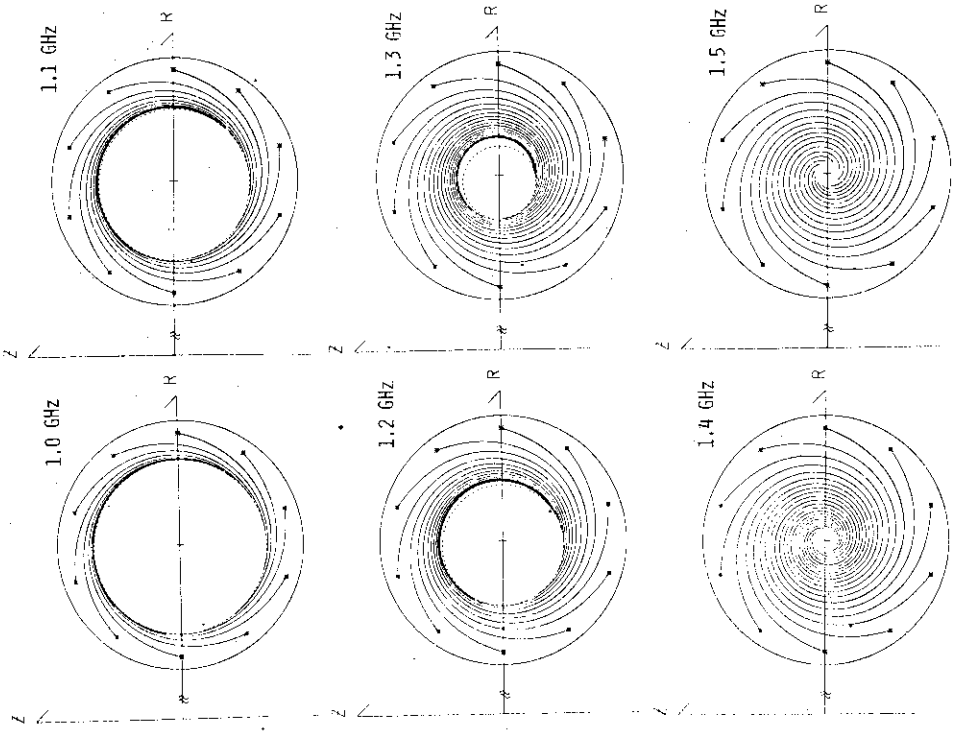

Fig.3.27 Pay trajectories of waves excited by ten sources with equal spacing. For waves with frequency f = 1.4 and 1.5 GHz, outgoing waves do not plotted for simplicity.

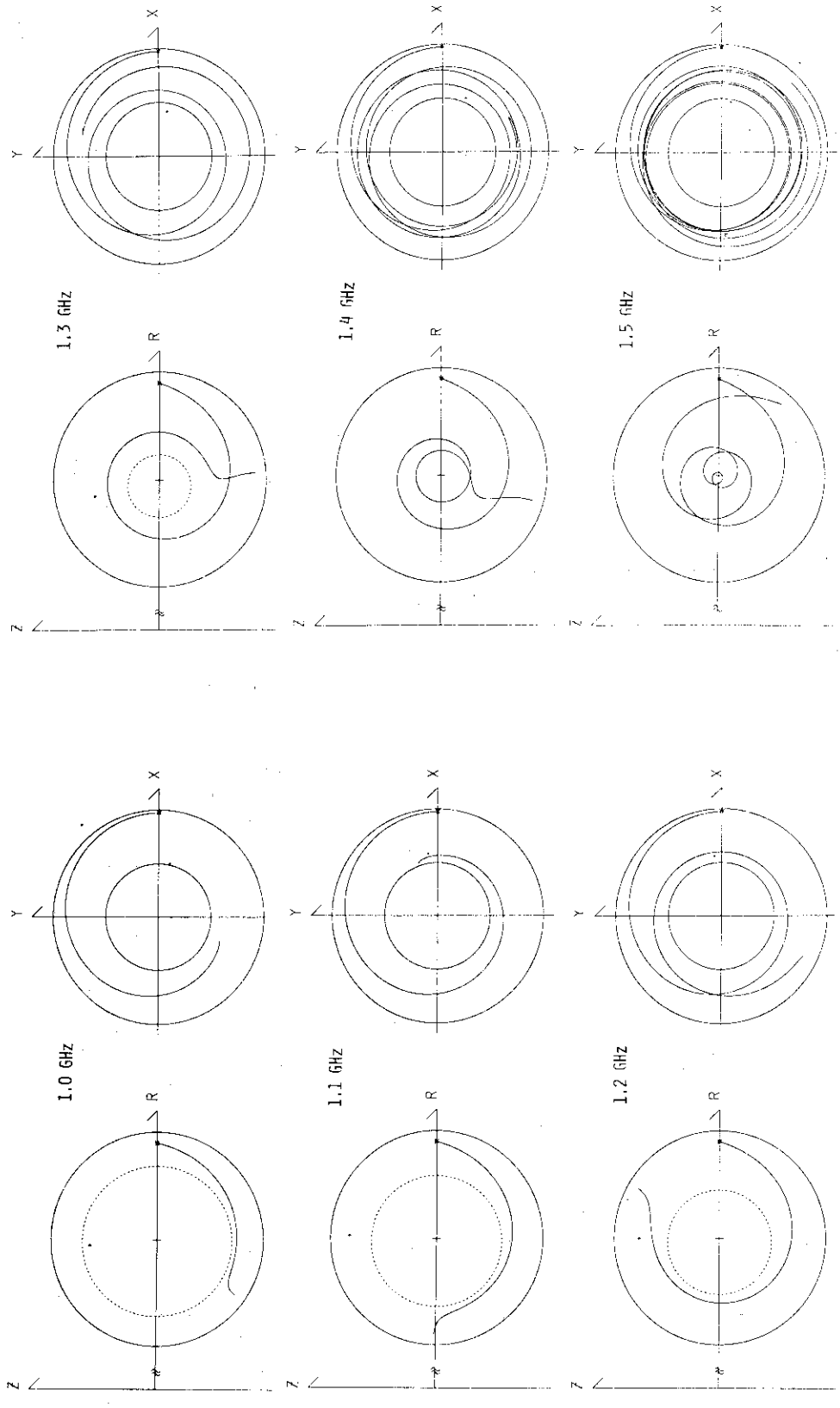

Fig. 3.29 Ray trajectories of lower hybrid waves in a warm plasma. $T_e(0)=T_i(0)=1$ keV. and other parameters are the same as in Fig.3.26. Incident cold waves are reflected as plasma waves before they reach the resonance surface.

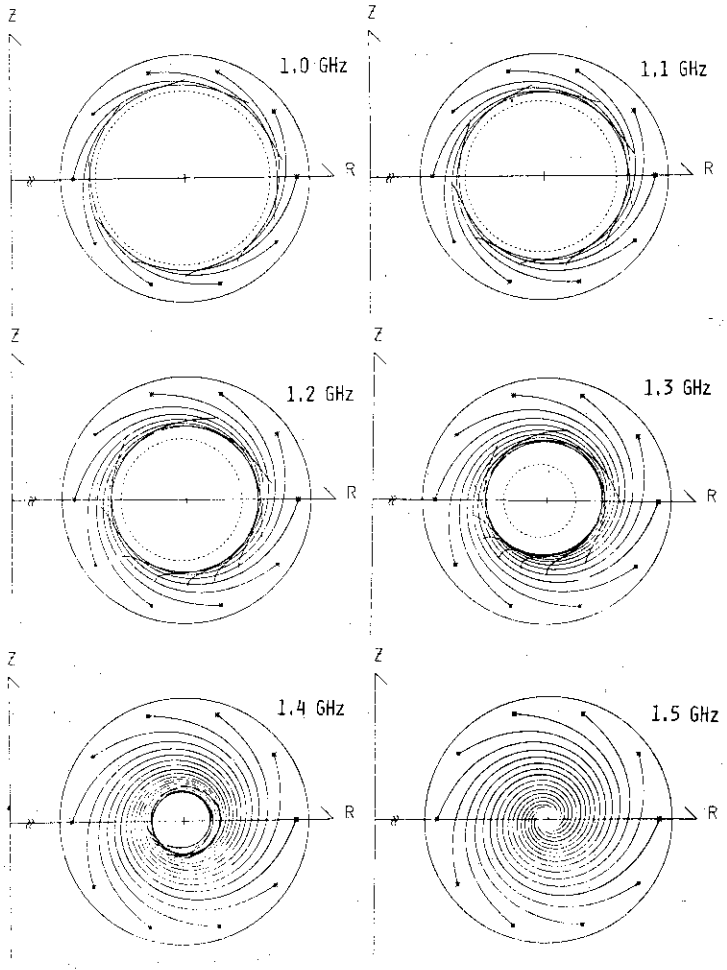

Fig.3.30 Ray trajectories of waves excited by ten sources with equal spacing in a warm plasma. Outgoing waves do not plotted for simplicity.

In the result, one can see in the above calculations:

i) The resonance surface shifts toward the major axis of a torus due to the toroidicity and trajectories intersect with the resonance surface.

ii) The shift of the resonance surface leads to the localization of terminal points and the concentration of trajectories. These effects are strong for high frequency waves or the weak magnetic field.

iii) The parallel wavenumber is not constant and goes to zero at the resonance surface, so that the reflactive index does not have singularities.

iv) The wave energy is singular on the resonance surface, and the ponderomotive force may lead to the filamentation of trajectories.

v) The effect of toroidicity is important only near the resonance surface, so that the propagation of the off-resonance wave is essentially the same as in a cylindrical plasma.

vi) The finite temperature effect causes a trajectory to be apart from the resonance surface and reduces the toroidal effect on the incident cold wave.

§4. Parametric decay processes

As shown in the end of §2, the externally excited lower hybrid wave propagating toward the center of a plasma may become so strong enough before it reaches the turning point to drive non-linear phenomena, especially parametric excitation. Lower hybrid parametric excitations have been considered theoretically [41-55] and numerically [58-61] by many authors. Almost of the investigations assume the pump of infinite wavelength. However, in a tokamak, as shown in Fig. 2.1, the pump is converted to an electrostatic lower hybrid wave with sufficiently large amplitude at a point far from the turning point. Then the pump which drives parametric instability should be treated as a lower hybrid wave.

In this section, we consider the parametric decay of an electrostatic lower hybrid wave with finite wavelength without the dipole approximation. We derive a general dispersion relation for four electrostatic wave coupling assuming the homogeneous plasma. The dispersion relation is analysed to investigate the effect of the finiteness of pump wavelength on the threshold. It will be shown that the non-dipole approximation has an insignificant effect on low frequency modes (ion Bernstein wave, electrostatic ion cyclotron wave, high and low frequency ion sound waves and ion quasi modes). However, the finiteness of pump wavelength affects on the high frequency mode coupling.

§4-1 Coupled dispersion relation

We start with the Vlasov and Poisson equations,

$$\frac{\partial f_\sigma}{\partial t} + \vec{v}\cdot\vec{\nabla} f_\sigma + \frac{e_\sigma}{m_\sigma}\{-\vec{\nabla}\phi + \vec{v}\times\vec{B}_0\}\cdot\frac{\partial f_\sigma}{\partial \vec{v}}$$
$$= -\nu_\sigma(f_\sigma - f_\sigma^{(0)}) + \frac{f_\sigma^{(0)}}{n_0}\int (f_\sigma - f_\sigma^{(0)})d\vec{v}\ , \qquad (4.1)$$

$$\nabla^2\phi = -\frac{1}{\varepsilon_0}\sum_\sigma e_\sigma \int f_\sigma d\vec{v}\ . \qquad (4.2)$$

We have assumed the Crook type collision model (BGK model [62]) in Eq. (4.1). Notations in Eqs. (4.1) are usual one. We expand the distribution function f_σ by powers of the electric potential

$$f_\sigma = f_\sigma^{(0)} + f_\sigma^{(1)} + f_\sigma^{(2)} + \cdots\cdots \qquad (4.3)$$

Then, Eq. (4.1) can be solved successively. We assume the equilibrium distribution function $f_\sigma^{(0)}$ be Maxwellian;

$$f_\sigma^{(0)} = \frac{N_0}{(\sqrt{\pi} v_{T\sigma})^3} \exp\left(-\frac{v^2}{v_{T\sigma}{}^2}\right) \quad . \tag{4.4}$$

We solve Eq. (4.1) to the second order accuracy in the electric potential to derive a coupled dispersion relation for the discussions of parametric instabilities excited by pump electric field with finite wavelength. Fourier-expanding the potential ϕ and distribution f_σ, we first obtain the first order distribution function $f_\sigma^{(1)}$ and then $f_\sigma^{(2)}$ is calculated. Substitution of $f_\sigma^{(1)}$ and $f_\sigma^{(2)}$ for the poisson equation (4.2) yields the equation for the waves

$$D_L(\vec{k},\omega)\phi(\vec{k},\omega) + \sum_{\substack{\vec{k}=\vec{k}'+\vec{k}'' \\ \omega=\omega'+\omega''}} D_{NL}(\vec{k}',\omega',\vec{k}'',\omega'')\phi(\vec{k}',\omega')\phi(\vec{k}'',\omega'') = 0. \tag{4.5}$$

Here D_L is the linear dielectric constant given by Eq. (3.16);

$$D_L(\vec{k},\omega) = 1 + \sum_\sigma \chi_\sigma(\vec{k},\omega) \ ,$$

$$\chi_\sigma(\vec{k},\omega) = \frac{\omega_{p\sigma}^2 m_\sigma}{k^2 T_\sigma} \frac{1 + \sum_n \frac{\omega+i\nu_\sigma}{\omega+i\nu_\sigma-n\Omega_\sigma}[W(z_{\sigma n})-1]\Lambda_n(\lambda_\sigma)}{1 + \sum_n \frac{i\nu_\sigma}{\omega+i\nu_\sigma-n\Omega_\sigma}[W(z_{\sigma n})-1]\Lambda_n(\lambda_\sigma)} \quad . \tag{4.6}$$

In the limit $\nu_\sigma \to 0$, Eq. (4.6) becomes Eq. (3.17). By the integration of $f_\sigma^{(2)}$ over velocity space, we obtain by usual method

$$D_{NL}(\vec{k}',\omega',\vec{k}'',\omega'') = \sum_\sigma \frac{1}{2\varepsilon_0} \frac{e_\sigma}{T_{\sigma 0}} \frac{\omega_{p\sigma}^2}{k^2} \int_0^\infty u_\perp du_\perp \int_{-\infty}^\infty du_\parallel$$

$$\times \sum_{\ell,m,n} \frac{1}{k_\parallel u_\parallel + m\Omega_\sigma - \omega} J_m(\eta_\sigma)\Big[\frac{1}{2}\{J_{n-1}(\eta_\sigma)e^{-i(\delta-\delta')} + J_{n+1}(\eta_\sigma)e^{i(\delta-\delta')}\}k_\perp' \frac{\partial}{\partial u_\perp}$$

$$+ \frac{1}{2}\{J_{n-1}(\eta_\sigma)e^{-i(\delta-\delta')} - J_{n+1}(\eta_\sigma)e^{i(\delta-\delta')}\} \frac{k_\perp'(n-m)}{u_\perp} + J_n(\eta_\sigma)k_\parallel' \frac{\partial}{\partial u_\parallel}\Big]$$

$$\times e^{i(n-m)(\delta-\delta'')} J_\ell(\eta_\sigma'') J_{\ell+n-m}(\eta_\sigma'') \frac{k_\parallel'' u_\parallel + \ell\Omega_\sigma}{k_\parallel'' u_\parallel + \ell\Omega_\sigma - \omega''} f_\sigma^{(0)} \tag{4.7}$$

where $u_\perp = \sqrt{v_x^2+v_y^2}$, $u_\parallel = v_z$, $\eta_\sigma = k_\perp u_\perp/\Omega_\sigma$, $\delta = \tan^{-1}(k_y/k_x)$ and J_m the Bessel

function. We have derived Eq. (4.7) assuming that the effect of collisions is small enough to be negligible in $f_0^{(2)}$. This corresponds to assuming that collision terms are of the order of ϕ.

We proceed to derive the coupled dispersion relation from Eq. (4.5) together with Eqs. (4.6) and (4.7). Let us retain three monochromatic modes $(\vec{k}, \omega; \pm\vec{k}_0, \pm\omega_0)$ and two coupled modes $(\vec{k} \pm \vec{k}_0, \omega \pm \omega_0)$, where modes $(\pm\vec{k}_0, \pm\omega_0)$ are those of pump electric field,

$$\vec{E}_0(\vec{r},t) = 2\vec{\varepsilon}_0 \cos(\vec{k}_0\cdot\vec{r} - \omega_0 t) \ . \tag{4.8}$$

The electric potential of Eq. (4.8) is

$$\phi_0(\vec{r},t) = \bar{\phi}_0 \sin(\vec{k}_0\cdot\vec{r} - \omega_0 t) \ , \tag{4.9}$$

$$\bar{\phi}_0 = -2\vec{k}_0\cdot\vec{\varepsilon}_0/k_0^2 \ .$$

Equation (4.5) yields the dispersion relation for four modes coupling,

$$D_L(\vec{k},\omega) = (\frac{\bar{\phi}_0}{2})^2 \{ \frac{D_{NL}(\vec{k}_0,\omega_0,\vec{k}-\vec{k}_0,\omega-\omega_0) D_{NL}(-\vec{k}_0,-\omega_0,\vec{k},\omega)}{D_L(\vec{k}-\vec{k}_0,\omega-\omega_0)}$$

$$+ \frac{D_{NL}(-\vec{k}_0,-\omega_0,\vec{k}+\vec{k}_0,\omega+\omega_0) D_{NL}(\vec{k}_0,\omega_0,\vec{k},\omega)}{D_L(\vec{k}+\vec{k}_0,\omega+\omega_0)} \ . \tag{4.10}$$

It is noted that Eq. (4.10) with Eqs. (4.6) and (4.7) is quite general for electrostatic waves.

Hereafter, we restrict ourselves to the lower hybrid pump. We assume that the pump satisfies the cold plasma dispersion relation of lower hybrid wave,

$$\omega_0 = \omega_{LH}(1 + \frac{m_i}{m_e}\frac{k_{0\parallel}^2}{k_{0\perp}^2})^{1/2} \ . \tag{4.11}$$

Then, as $\Omega_i \ll \omega_0 \ll |\Omega_e|$, the pump can not move ions appreciably so that we neglect ion components in D_{NL}, whereas electrons are magnetized strongly enough that $k_\perp^2\rho_e^2 \ll 1$. We simplify Eq. (4.7) expanding Bessel functions in powers of η_e. In the limit of zero electron Larmor radius, we obtain, after symmetrizing about $(\vec{k}', \omega')$ and $(\vec{k}'', \omega'')$,

$$D_{NL}(\vec{k}',\omega',\vec{k}'',\omega'') = -\frac{1}{2}\frac{e}{T_e}\frac{\omega_{pe}^2}{k^2}\left[\frac{i}{\Omega_e}(k_y'k_x'' - k_x'k_y'')\right.$$

$$\times\int_{-\infty}^{\infty} du_{//}\,\frac{1}{k_{//}u_{//}-\omega}\left(\frac{\omega''}{k_{//}''u_{//}-\omega''} - \frac{\omega'}{k_{//}'u_{//}-\omega'}\right)f_{e_{//}}^{(0)}$$

$$\left.+\int_{-\infty}^{\infty} du_{//}\,\frac{1}{k_{//}u_{//}-\omega}\left(k_{//}'\frac{\partial}{\partial u_{//}}\frac{k_{//}''u_{//}}{k_{//}''u_{//}-\omega''} + k_{//}''\frac{\partial}{\partial u_{//}}\frac{k_{//}'u_{//}}{k_{//}'u_{//}-\omega'}\right)f_{e_{//}}^{(0)}\right] \quad . \tag{4.12}$$

$$f_{e_{//}}^{(0)} = \frac{1}{\sqrt{\pi}v_{Te}}\exp\left(-\frac{u_{//}^2}{v_{Te}^2}\right)$$

From Eq. (4.12), it is easily proved that symmetric relations hold as follows,

$$D_{NL}(\pm\vec{k}_0,\pm\omega_0,\vec{k},\omega) = \left(\frac{\vec{k}}{\vec{k}\pm\vec{k}_0}\right)^2 D_{NL}^{*}(\mp\vec{k}_0,\mp\omega_0,\vec{k}\pm\vec{k}_0,\omega\pm\omega_0) \quad , \tag{4.13}$$

where * denotes complex conjugate. Under the condition $\omega_0 \simeq \omega_{LH} \gg k_{//}v_{Te}$ and $\omega \pm \omega_0 \simeq \omega_{LH} \gg k_{//}v_{Te}$, we obtain

$$D_{NL}(\mp\vec{k}_0,\mp\omega_0,\vec{k}\pm\vec{k}_0,\omega\pm\omega_0)$$

$$= \pm\frac{i}{2}\frac{e}{m_e\Omega_e}(\vec{k}\times\vec{k}_0)\cdot\vec{e}_z\beta_{\pm}\chi e_{//}) \tag{4.14}$$

$$\mp\frac{1}{2}\frac{e}{m_e}\frac{\vec{k}_{0//}(\vec{k}_{//}\pm\vec{k}_{0//})}{(\omega\pm\omega_0)^2}(\alpha_{\pm}^{(1)}\chi_{e_{//}} + \alpha_{\pm}^{(2)}) \quad ,$$

where

$$\beta_{\pm} = \frac{\omega}{k_{//}^2}\left(\frac{k_{0//}}{\omega_0} - \frac{k_{//}\pm k_{0//}}{\omega\pm\omega_0}\right)\left(\frac{k_{0//}}{\omega} + \frac{k_{//}\pm k_{0//}}{\omega\pm\omega_0} + \frac{k_{//}}{\omega}\right) \quad , \tag{4.15}$$

$$\alpha_{\pm}^{(1)} = 1 + 2\frac{\omega}{k_{//}}\frac{k_{//}\pm k_{0//}}{\omega\pm\omega_0} \quad , \tag{4.16}$$

$$\alpha_{\pm}^{(2)} = \mp\frac{\omega_{pe}^2}{k^2}\frac{k_{//}}{\omega_0}\left(\frac{k_{0//}}{\omega_0} + 2\frac{k_{//}\pm k_{0//}}{\omega\pm\omega_0}\right) \quad , \tag{4.17}$$

$$\chi_{e_{//}} = \frac{\omega_{pe}^2}{k^2} \int_{-\infty}^{\infty} du_{//} \frac{k_{//} \partial f_{e_{//}}^{(0)} / \partial u_{//}}{\omega - k_{//} u_{//}} . \tag{4.18}$$

Thus, we obtain the four waves coupling dispersion relation for parametric instabilities of electrostatic waves excited by the pump of an electrostatic lower hybrid wave;

$$D_L(\vec{k},\omega) = \sum_{\pm} \left(\frac{\vec{k}}{\vec{k}\pm\vec{k}_0}\right)^2 \left\{ \left(\frac{\mu_{\perp}^{\pm}}{2}\right)^2 \beta_{\pm}^2 \chi_{e_{//}}^2 + \left(\frac{\mu_{//}^{\pm}}{2}\right)^2 \left(\alpha_{\pm}^{(1)} \chi_{e_{//}} + \alpha_{\pm}^{(2)}\right)^2 \right\}$$

$$\times \frac{1}{D_L(\vec{k}\pm\vec{k}_0, \omega\pm\omega_0)} , \tag{4.19}$$

here,

$$\mu_{\perp}^{\pm} = \frac{e}{m_e} \frac{\vec{k} \times \vec{\varepsilon}_0 \cdot \vec{e}_z}{\Omega_e(\omega \pm \omega_0)} , \quad \mu_{//}^{\pm} = -\frac{e}{m_e} \frac{(k_{//} \pm k_{0//}) \varepsilon_{0//}}{(\omega \pm \omega_0)^2} . \tag{4.20}$$

Eq. (4.19) holds as far as the pump is electrostatic and $\Omega_i \ll \omega_0 \ll |\Omega_e|$, since Eq. (4.19) has been derived without the relation (4.11). It should be pointed out that in the limit of diopole approximation ($\vec{k}_0 \to 0$), $\mu_{\perp}^{\pm} = (e/m_e)(k_y \varepsilon_{0x}/\Omega_e \omega_0)$, $\mu_{//}^{\pm} = -(e/m_e) k_{//} \varepsilon_{0//}/\omega_0^2$, $\beta_{\pm} = -1$, $\alpha_{\pm}^{(0)} = 1$, $\alpha_{\pm}^{(2)} = 0$, then, Eq. (4.19) recovers the dispersion relation derived under the dipole approximation [63].

§4-2 Effects of the finite wavelength of pump

In the limit of dipole approximation, parametric thresholds of electrostatic waves excited by the pump near the lower hybrid frequency are investigated precisely in a homogeneous plasma [45]. The lower hybrid wave excited externally decays into an another lower hybrid wave and a low frequency mode. Permissible low frequency modes are low frequency ion acoustic wave, high frequency ion acoustic wave, electrostatic ion-cyclotron wave and ion Bernstein wave. Also the importance of non-decaying ion quasi mode is noted [43]. In this section, it is shown that the non-dipole approximation has little influence on the threshold of these low frequency modes, while it affects significantly on high frequency modes. It is first noticed by Ott [44] that the decay of a lower hybrid wave into two other lower hybrid waves is permitted only when the finiteness of pump wavelength is taken into account. The present treatment extends that of Ott's which

is a cold plasma approximation to the case of finite temperature.

In this section, we restrict ourselves to the case when the pump is a lower hybrid wave, although the dispersion relation (4.19) holds for, for example, Gould-Trivelpiece mode [64], as noted in preceding section. Then, since $\mu_\perp/\mu_\parallel \simeq (k_\perp^2/k_\parallel^2)(\omega_{pe}/\Omega_e)\sqrt{m_e/m_i}$ and $k_\perp^2/k_\parallel^2 \gtrsim m_i/m_e$ for lower hybrid wave, we get $\mu_\perp \gg \mu_\parallel$. We retain only the first term on the right hand side of Eq. (4.19). Also we drop the response $(\vec{k}+\vec{k}_0,\ \omega+\omega_0)$ which is off-resonant. Then the dispersion relation becomes

$$D_L(k,\omega) = \left(\frac{\vec{k}}{\vec{k}-\vec{k}_0}\right)^2 \frac{\mu_\perp^2}{4}\,\beta^2\,\chi_{e_\parallel}^2\,\frac{1}{D_L(\vec{k}-\vec{k}_0,\omega-\omega_0)}\ , \tag{4.21}$$

where $\mu_\perp = \mu_\perp^-$, $\beta = \beta_-$.

The growth rate is given by

$$(\gamma-\gamma_1)(\gamma-\gamma_2) = \gamma_0^2\ , \tag{4.22}$$

with

$$\gamma_0^2 = -\left(\frac{\vec{k}}{\vec{k}-\vec{k}_0}\right)^2 \frac{\mu_\perp^2}{4}\,\beta^2\,\chi_{e_\parallel}^2\,\frac{1}{\frac{\partial}{\partial\omega_r}\mathrm{Re}D_L(\omega_r)}\,\frac{1}{\frac{\partial}{\partial\omega_r}\mathrm{Re}D_L(\omega_r-\omega_0)}, \tag{4.23}$$

$$\left.\begin{aligned}\gamma_1 &= -\mathrm{Im}\,D_L(\omega_r)/\partial\,\mathrm{Re}\,D_L(\omega_r)/\partial\omega_r\ ,\\ \gamma_2 &= -\mathrm{Im}\,D_L(\omega_r-\omega_0)/\partial\,\mathrm{Re}\,D_L(\omega_r-\omega_0)/\partial\omega_r\ ,\end{aligned}\right\} \tag{4.24}$$

The threshold is given by putting $\gamma = 0$ in Eq. (4.22),

$$\frac{\mu_\perp^2}{4} = -\left(\frac{\vec{k}-\vec{k}_0}{\vec{k}}\right)^2 \frac{\mathrm{Im}\,D_L(\omega_r)\,\mathrm{Im}\,D_L(\omega_r-\omega_0)}{\beta^2\chi_{e_\parallel}^2(\vec{k},\omega_r)}\ . \tag{4.25}$$

First, we investigate the effect of finite wavelength pump on coupling constants when $\omega \ll \omega_0$. We approximate $\chi_{e_\parallel}$ as

$$\left.\begin{aligned}\chi_{e_\parallel} &\simeq -\frac{k_\parallel^2}{k^2}\frac{\omega_{pe}^2}{\omega^2} \qquad \text{for } \frac{\omega}{k_\parallel} \gg v_{T_e}\ ,\\ \chi_{e_\parallel} &\simeq \frac{1}{k^2 d_e^2} \qquad \text{for } \frac{\omega}{k_\parallel} \ll v_{T_e}\ ,\end{aligned}\right\} \tag{4.26}$$

where $d_e = (\varepsilon_0 T_e/N_0 e^2)^{1/2}$ is the electron Debye length. From Eq. (4.15), it is obvious that the non-dipole effect depends sensitively on the parallel wavenumbers $k_{//}$ and $k_{0//}$. When $\omega/k_{//} \gg v_{T_e}$ (ion Berstein wave), the coupling constant including the effect of finite pump wavelength is $|\beta k_{//}^2/\omega^2|$. This is shown in Fig. 4.1(a). On the other hand $|\beta|$ shows the non-dipole effect for modes with $\omega/k_{//} \ll v_{T_e}$ (ion sound wave, electrostatic ion cyclotron wave, ion quasi mode). Fig. 4.1(b) illustrates $|\beta|$ versus $\omega/k_{//}$. Dotted curves in Fig. 4.1 (a) and (b) show the case of dipole limit ($\vec{k}_0 \to 0$). For modes with $\omega/k_{//} \ll v_{T_e}$ (kinetic modes; ion sound wave, electrostatic ion cyclotron wave, ion quasi mode), it is apparant from Fig. 4.1(b) that $|\beta|$ is nearly unity for $\omega/k_{//} < v_{T_e}$ provided that $\omega_0/k_{0//} \gg v_{T_e}$. Also there is little discrepancy between the dipole and non-dipole approximations in Fig. 4.1(a) as far as $0 < \omega/k_{//} \ll \omega_0/k_{0//}$ and $\omega_0/k_{0//} \gg v_{T_e}$.

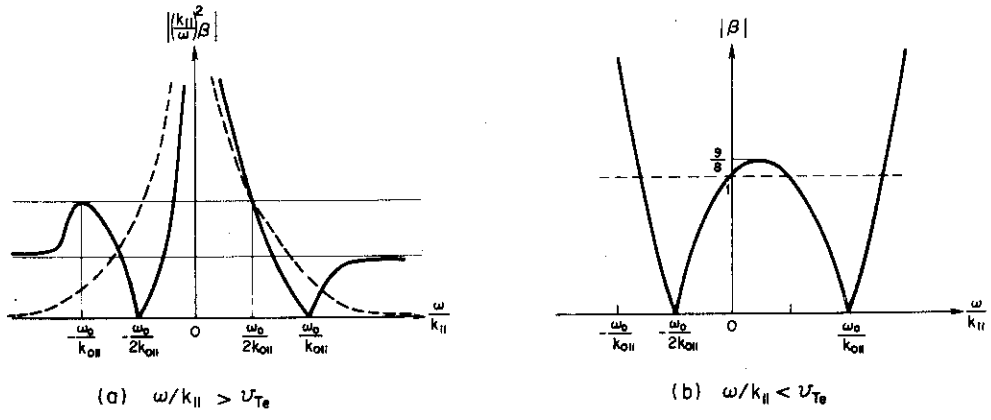

Fig. 4.1 Coupling constant versus $\omega/k_{//}$ in the case when $\omega \ll \omega_0$. The dotted curves show the dipole approximation. (a) for the modes with $\omega/k_{//} > v_{Te}$, (b) for the modes with $\omega/k_{//} < v_{Te}$.

Within the dipole approximation, parametric instabilities of low frequency modes (low frequency ion acoustic wave, high frequency ion acoustic wave, forward and backward electrostatic ion-cyclotron wave, ion Bernstein wave and ion quasi mode) have been investigated precisely [45]. In the present section, we consider a hot plasma with $T_e \simeq T_i \simeq$ keV as in the case of JT-60. The parallel phase velocity is much less than the light velocity (equivalently, $N_z \gg 1$) for the lower hybrid wave to be electrostatic, then,

$$c \gg \frac{\omega}{k_{\parallel}} \quad \frac{1}{k\rho_i} \sqrt{\frac{m_i}{m_e}} \quad \frac{\omega_{pe}}{\Omega_e} v_{T_i} \quad . \tag{4.27}$$

Here we have used the relation $k_{\parallel}^2/k^2 \lesssim m_e/m_i$ for lower hybrid wave. If $T_i \simeq$ keV, the inequality of (4.27) can hold only when $k\rho_i \gg 1$. However, the following relation holds:

$$\frac{\rho_i}{d_e} \simeq \frac{\Omega_e}{\omega_{pe}} \sqrt{\frac{T_i}{T_e}} \sqrt{\frac{m_i}{m_e}} \quad , \tag{4.28}$$

so that $d_e \ll \rho_i$ when $T_e \simeq T_i$. Even if $k\rho_i \gg 1$, electron Landan damping is expected to be small. The conditions exclude some possibilities and the most likely low frequency decay wave will be either a backward ion-cyclotron wave or a quasi mode if $\omega_0 < \sqrt{2}\ \omega_{LH}$ or only an ion cyclotron wave if $\omega_0 > \sqrt{2}\ \omega_{LH}$ [45]. By the results of Porkolab [42], including the effect of density inhomogeneity, the threshold for ion quasi mode is

$$\frac{u_0^2}{c_s^2} \simeq \frac{12\sqrt{2}\ \pi(1+\omega_{pe}^2/\Omega_e^2)^{1/2}\ \delta^{1/2} d_e}{R(1+\delta)^{1/2} L_N} \quad , \tag{4.29}$$

and for ion-cyclotron wave,

$$\frac{u_0^2}{c_s^2} \simeq \frac{4\omega_0^2}{\omega_{pi}^2} \frac{k_x}{k^2 L_N} \quad , \tag{4.30}$$

where $u_0 = \varepsilon_0/B_0$, $c_s = (T_e/m_i)^{1/2}$, $\delta = (k_{\parallel}/k_{\perp})^2 (m_i/m_e)$, $R = \sqrt{\pi}(\omega/k_{\parallel} v_{T_e}) \exp(-\omega^2/k_{\parallel}^2 v_{T_e}^2)$ and $L_N^{-1} = (1/N)(dN/dx)$. In the case of Fig. 2.1, $\omega_0 > \sqrt{2}\ \omega_{LH}$ for $x/a \gtrsim 0.75$. Near the point $x/a \simeq 0.75$, $N \simeq 2.5\times10^{19}$ m^{-3}, $T_e \simeq T_i \simeq 2.5$ keV, $L_N \simeq 0.357$ m. Choosing $\delta \simeq 1$ and $R \simeq 0.7$, we obtain the threshold $\varepsilon_0 \simeq 2.5\times10^5$ V/m for ion quasi mode and $\varepsilon_0 \simeq 3.5\times10^5$ V/m for ion-cyclotron mode, which are below the intensity of the perpendicular electric field predicted by linear theory as shown in Fig. 2.1(c).

Contrary to the case of low frequency modes, the finiteness of the pump wavelength is important to the excitation of high frequency mode. The typical example is the excitation of two lower hybrid waves which are driven to instability only when the finiteness of the pump wavelength is taken into account. In the cold plasma approximation, Eq. (4.23) gives the growth rate, for the instability of two lower hybrid wave,

$$\gamma_0^2 = -\frac{1}{16}\frac{e^2}{m_e^2}\frac{[\vec{k}\times\vec{\varepsilon}_0\vec{e}_z]^2}{k^2(\vec{k}-\vec{k}_0)^2}\frac{\omega_{pe}^2}{\Omega_e^2}\frac{1}{(1+\omega_{pe}^2/\Omega_e^2)^2}\frac{\omega-\omega_0}{\omega}$$

$$\times\left(\frac{k_{0\parallel}}{\omega_0}-\frac{k_\parallel-k_{0\parallel}}{\omega-\omega_0}\right)^2\left(\frac{k_\parallel}{\omega_0}+\frac{k_\parallel-k_{0\parallel}}{\omega-\omega_0}+\frac{k_\parallel}{\omega}\right)^2 \quad , \tag{4.31}$$

which recovers that of Ott's [44]. As shown in [44], an absolute instability of the lower hybrid wave decay is possible in an inhomogeneous plasma. The conditions necessary for absolute instability [65] are $v_{gx1}v_{gx2} < 0$. $\kappa'(x_0) = 0$, and

$$\gamma_0^2 > |v_{gx1}v_{gx2}|\ (\kappa'')^{2/3}. \tag{4.32}$$

Here, $k_{0x}(x_0) = k_{1x}(x_0) + k_{2x}(x_0)$ and $\kappa = k_{0x}(x) - k_{1x}(x) - k_{2x}(x)$ is the mismatch of the wavenumbers. For the lower hybrid wave, the group velocity is given by

$$\vec{v}_g = \left(-\frac{k_xk_z}{k^2}\vec{e}_x - \frac{k_yk_z}{k^2}\vec{e}_y + \vec{e}_z\right)\frac{\omega_{LH}k_z(m_i/m_e)}{k^2[1+(k_z/k)^2(m_i/m_e)]^{1/2}} . \tag{4.33}$$

Provided that $\omega_0 > 2\omega_{LH}(x_0)$, one can show that the conditions $\kappa'(x_0) = 0$, $v_{gx1}v_{gx2} < 0$ and the decay conditions,

$$\vec{k}_0 = \vec{k}_1 + \vec{k}_2 \quad ,$$

$$(1+\delta_0)^{1/2} = (1+\delta_1)^{1/2} + (1+\delta_2)^{1/2}, \tag{4.34}$$

$$\delta = \left(\frac{k_\parallel}{k_\perp}\right)^2\frac{m_i}{m_e} \quad ,$$

may be simultaneously satisfied at any point $x = x_0$ by an infinite number of decay wave pairs, $(\vec{k}_1,\omega_1)$ and $(\vec{k}_2,\omega_2)$ [44]. In the case of Fig. 2.1, as in the region where $x/a \gtrsim 0.9$, $\delta \gtrsim 3$, $\omega_{pj}(x) \gtrsim 0.5\omega_0$, the condition $\omega_0 > 2\omega_{LH}(x_0)$ can be satisfied. Assuming that $\kappa'(x_0) = 0$, we obtain

$$\kappa'' = \left\{k_{0x}\frac{4\alpha_0^2-1}{\alpha_0^4}\left(\frac{1+\delta_0}{\delta_0}\right)^2 - k_{1x}\frac{4\alpha_1^2-1}{\alpha_1^4}\left(\frac{1+\delta_1}{\delta_1}\right)^2 - k_{2x}\frac{4\alpha_2^2-1}{\alpha_2^4}\left(\frac{1+\delta_2}{\delta_2}\right)^2\right\}$$

$$\times\left\{\frac{d}{dx}\ln\omega_{LH}(x_0)\right\}^2, \tag{4.35}$$

where $\alpha = k_x/k$. Using Eqs. (4.23), (4.33) and (4.35), we can estimate the criterion Eq. (4.32). For $\delta_0 = 3.4$, $\delta_1 = \delta_2 = 0.1$, estimating Eq. (4.32) at the point $x/a \simeq 0.9$, we get the threshold $\varepsilon_0 \simeq (5\sim6)\times10^5$ V/m, which is comparable with the intensity of perpendicular electric field predicted by linear theory. Thus, we conclude that the parametric instability may occur almost all over the region before the turning point in the present case shown in Fig. 2.1.

§5. Tail Formation

The formation of high energy tail in a velocity distribution of ions has often been observed in experiments on lower hybrid resonance heating [66,67]. In order to explain the tail formation, we consider a nonlinear motion of an ion affected by a monochromatic electrostatic wave which has a frequency near an ion cyclotron harmonic and propagates perpendicularly to a uniform magnetic field. In case of oblique propagation, Smith and Kaufman [68] have recently shown the occurrence of stochastic acceleration along a magnetic field, which is followed by perpendicular acceleration because of energy conservation in the wave frame. However the threshold of the wave amplitude is so large when $k_{\parallel} v_T \ll \Omega_i$ that their results are not applicable to a lower hybrid wave. In this section, we show that because of the overlapping of islands in a phase plane, irreversible change in magnetic moment can take place even if $k_{\parallel}$ vanishes and no spatial inhomogeneity exists; this inhomogeneity has been essential for the irreversibility in many anologous studies on cyclotron heating in a mirror field [69-72].

§5-1 Stochastic behaviour of a phase point

We consider a motion of an ion in a uniform field $B_0\hat{z}$ in the presence of a monochromatic electrostatic wave $\phi \cos(kx-\omega t)$ propagating perpendicularly to the magnetic field. The Hamiltonian of a test ion takes a form,

$$H(x,y,p_x,p_y,t) = \{p_x^2+(p_y-m\Omega_i x)^2\}/2m + e\phi \cos(kx-\omega t) \ , \qquad (5.1)$$

where p_x and p_y are the canonical momenta : $p_x = mv_x$ and $p_y = mv_y + m\Omega_i x$. Since H is independent of y, the momentum p_y is a constant of motion. Defining the magnetic moment μ and the cyclotron phase θ by the relations,

where $\alpha = k_x/k$. Using Eqs. (4.23), (4.33) and (4.35), we can estimate the criterion Eq. (4.32). For $\delta_0 = 3.4$, $\delta_1 = \delta_2 = 0.1$, estimating Eq. (4.32) at the point $x/a \simeq 0.9$, we get the threshold $\mathcal{E}_0 \simeq (5\sim6)\times10^5$ V/m, which is comparable with the intensity of perpendicular electric field predicted by linear theory. Thus, we conclude that the parametric instability may occur almost all over the region before the turning point in the present case shown in Fig. 2.1.

§5. Tail Formation

The formation of high energy tail in a velocity distribution of ions has often been observed in experiments on lower hybrid resonance heating [66,67]. In order to explain the tail formation, we consider a nonlinear motion of an ion affected by a monochromatic electrostatic wave which has a frequency near an ion cyclotron harmonic and propagates perpendicularly to a uniform magnetic field. In case of oblique propagation, Smith and Kaufman [68] have recently shown the occurrence of stochastic acceleration along a magnetic field, which is followed by perpendicular acceleration because of energy conservation in the wave frame. However the threshold of the wave amplitude is so large when $k_{\parallel} v_T \ll \Omega_i$ that their results are not applicable to a lower hybrid wave. In this section, we show that because of the overlapping of islands in a phase plane, irreversible change in magnetic moment can take place even if $k_{\parallel}$ vanishes and no spatial inhomogeneity exists; this inhomogeneity has been essential for the irreversibility in many anologous studies on cyclotron heating in a mirror field [69-72].

§5-1 Stochastic behaviour of a phase point

We consider a motion of an ion in a uniform field $B_0\hat{z}$ in the presence of a monochromatic electrostatic wave $\phi \cos(kx-\omega t)$ propagating perpendicularly to the magnetic field. The Hamiltonian of a test ion takes a form,

$$H(x,y,p_x,p_y,t) = \{p_x^2+(p_y-m\Omega_i x)^2\}/2m + e\phi \cos(kx-\omega t) \ , \qquad (5.1)$$

where p_x and p_y are the canonical momenta : $p_x = mv_x$ and $p_y = mv_y + m\Omega_i x$. Since H is independent of y, the momentum p_y is a constant of motion. Defining the magnetic moment μ and the cyclotron phase θ by the relations,

$$\mu \equiv \frac{1}{2m\Omega_i}\{p_x^2 + (p_y - m\Omega_i x)^2\} = \frac{mv_\perp^2}{2\Omega_i} \quad , \tag{5.2}$$

$$\theta \equiv \arcsin\left(\frac{x - p_y/m\Omega_i}{\sqrt{2\mu/m\Omega_i}}\right) = \arctan\left(-\frac{v_y}{v_x}\right) \quad , \tag{5.3}$$

we may rewrite the Hamiltonian after the canonical transformation from (x, p_x) to (θ, μ),

$$H(\theta,\mu,t) = \mu\Omega_i + e\phi\cos(k\sqrt{2\mu/m\Omega_i}\sin\theta - \omega t) \tag{5.4}$$

$$= \mu\Omega_i + e\phi\sum_{\ell=-\infty}^{\infty} J_\ell(k\sqrt{2\mu/m\Omega_i})\cos(\ell\theta - \omega t) \quad , \tag{5.5}$$

here a series expansion of Bessel functions J_ℓ is applied.

By the use of an integer n nearest to ω/Ω_i, we again perform the canonical transformation from (θ,μ) to (ξ,M) defined by the generating function,

$$S(\theta,M,t) = (n\theta - \omega t)M \quad , \tag{5.6}$$

which contains the time explicitly. New variables and the Hamiltonian are given by

$$\xi \equiv n\theta - \omega t \quad , \tag{5.7}$$

$$M \equiv \mu/n \quad , \tag{5.8}$$

$$H(\xi,M,t) = (n\Omega_i - \omega)M + e\phi\sum_{\ell} J_\ell(k\sqrt{2nM/m\Omega_i})\cos\{\ell\xi/n + (\ell-n)\omega t/n\} \quad . \tag{5.9}$$

This Hamiltonian is expressed by a sum of a time-independent part $H_0(\xi,M)$ and time-dependent one $H_1(\xi,M,t)$;

$$H_0(\xi,M) = \delta\omega M + e\phi J_n(k\rho(M))\cos\xi \quad , \tag{5.10}$$

$$H_1(\xi,M,t) = e\phi\sum_{\ell\neq n} J_\ell(k\rho(M))\cos\{\ell\xi/n + (\ell - n)\omega t/n\} \quad , \tag{5.11}$$

here we have introduced, for simplicity,

$$\delta\omega \equiv n\Omega_i - \omega \ , \tag{5.12}$$

$$\rho(M) \equiv \sqrt{2nM/m\Omega_i} = v_\perp/\Omega_i \ . \tag{5.13}$$

When the wave amplitude is small, the time average of H_1 approaches zero because of small $d\xi/dt$ and dM/dt, and its contribution to an ion motion may be neglected [73]; therefore the motion derived from H_0 alone is considered [69,74]. The equations of motion obtained from Eq. (5.10) are

$$\frac{dk\rho}{dt} = -\frac{kn}{m\Omega_i\rho}\frac{\partial H_0}{\partial \xi} = \frac{kn}{m\Omega_i\rho}\, e\phi J_n(k\rho)\sin\xi \ , \tag{5.14}$$

$$\frac{d\xi}{dt} = \frac{\partial H_0}{\partial M} = \delta\omega + \frac{kn}{m\Omega_i\rho}\, e\phi J_n'(k\rho)\cos\xi \ , \tag{5.15}$$

and the qualitative phase trajectories are illustrated in Fig. 5.1. Tapped regions enclosed by separatrices can exist where $k\rho \gtrsim n$ if $\delta\omega$ is smaller than

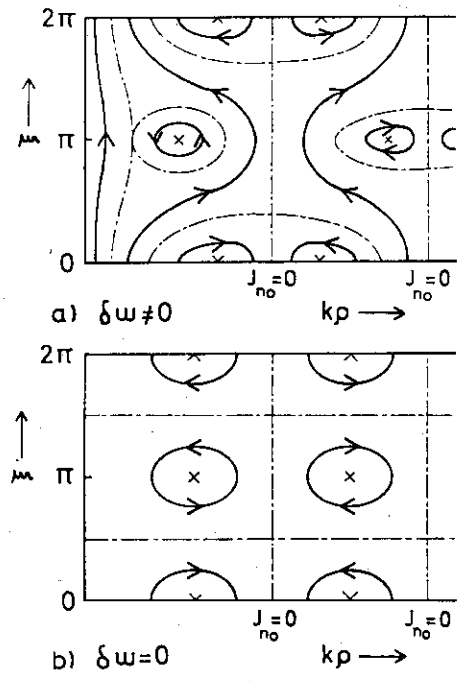

Fig. 5.1 Phase trajectory obtained from Eq.(5.10) for the case (a) $\delta\omega \neq 0$ and (b) $\delta\omega = 0$.

$(kn/m\Omega_i\rho)e\phi \max\{|J_n(k\rho)|\}$. With $\delta\omega$ approaching to zero, untrapped regions diminish and finally all ions are trapped in rectangular cells, which are enclosed by separatrices : $\xi = \pm\pi/2$ and $\rho = \rho^*$ where $J_n(k\rho^*) = 0$. We shall consider the case of hot ions ($v_\perp \gg \omega/k_\perp$) and a wave near an ion cyclotron harmonic. The former condition, $k\rho \gg n$, enables us to use the asymptotic expansion of J_n:

$$J_n \sim \sqrt{2/\pi k\rho}\ \cos\{k\rho - (2n+1)\pi/4\} \simeq \sigma\sqrt{2/\pi k\rho_0}\ \cos k\tilde{\rho}\ , \tag{5.16}$$

where ρ_0 satisfies $J_n'(k\rho_0) = 0$ and $\tilde{\rho} \equiv \rho - \rho_0 \ll \rho_0$. The quantity σ takes the value ± 1 depending on $k\rho_0$. Making use of the bounce frequency at the center of the trapped region,

$$\omega_t \equiv \frac{kn}{m\Omega_i\rho_0}\, e\phi|J_n(k\rho_0)| \simeq \frac{\omega_b^2}{\Omega_i}\,\frac{n}{(k\rho_0)^{3/2}}\,\sqrt{\frac{2}{\pi}}\ , \tag{5.17}$$

with $\omega_b^2 = k^2 e\phi/m$, we may express the latter condition by $\delta\omega \ll \omega_t$. Under these conditions, the equations of motion

$$dk\tilde{\rho}/dt = \sigma\,\omega_t \cos k\tilde{\rho} \sin\xi\ , \tag{5.18}$$

$$d\xi/dt = \delta\omega - \sigma\omega_t \sin k\tilde{\rho} \cos\xi\ , \tag{5.19}$$

may be simplified for an ion in the cell,

$$dk\tilde{\rho}/dt = \sigma\omega_t(q^2 - \sin^2 k\tilde{\rho})^{1/2}\ . \tag{5.20}$$

The quantity q defined by

$$q^2 = 1 - (kn/m\Omega_i\rho_0)^2(H_0/\omega_t)^2\ , \tag{5.21}$$

takes the value zero at the center of the cell and unity at the separatrix; and this quantity q will be used as the parameter of elliptic functions and elliptic integrals introduced below. Using Jacobian elliptic functions, we can express the solution to Eq. (5.20) as follows,

$$\sin k\tilde{\rho} = q\,\mathrm{sn}\{\omega_t(t - t_0), q\}\ , \tag{5.22}$$

$$\cos k\tilde{\rho} = \sigma_1\,\mathrm{dn}\{\omega_t(t - t_0), q\}\ , \tag{5.23}$$

$$\sin\xi = q\,\mathrm{cn}\{\omega_t(t-t_0),q\}/\mathrm{dn}\{\omega_t(t-t_0),\ q\} \quad , \tag{5.24}$$

$$\cos\xi = \sigma_2\sqrt{1-q^2}/\mathrm{dn}\{\omega_t(t-t_0),\ q\} \quad . \tag{5.25}$$

The quantities σ_1 and σ_2 which take the value ± 1, and the time t_0 depend on the initial value; however the initial conditions are not so important in the analysis that we assume $\sigma_1 = \sigma_2 = 1$ and $t_0 = 0$ for brevity.

Taking account of the periodicity of elliptic functions, we can express the motion derived from H_0 in terms of the action-angle variables (I, η):

$$dI/dt = 0 \ , \tag{5.26}$$

$$d\eta/dt = \Omega_t(I) = \{\pi/2F_0(q)\}\omega_t \ . \tag{5.27}$$

The relationship between the old and the new variables is given by the equations,

$$I(H_0) = \frac{1}{2\pi}\oint M d\xi = \frac{2}{\pi}\frac{m\Omega_i\rho_0}{kn}\int_0^q \frac{q}{\sqrt{1-q^2}}F_0(q)dq \ , \tag{5.28}$$

$$\eta(\xi,H_0) = \frac{\partial}{\partial I}\int^{\xi} M d\xi = \frac{\pi}{2}\frac{F\{\arcsin(q^{-1}\sin\xi),q)}{F_0(q)} \quad , \tag{5.29}$$

where compelte and incomplete elliptic integrals of the first kind are denoted by $F_0(q) = F(\pi/2,q)$ and $F(\psi,q)$, respectively. It is easy to see from Fig. 5.2 that the phase space area enclosed by a trajectory equals to the action I and the angle η means the phase on the trajectory, I = constant.

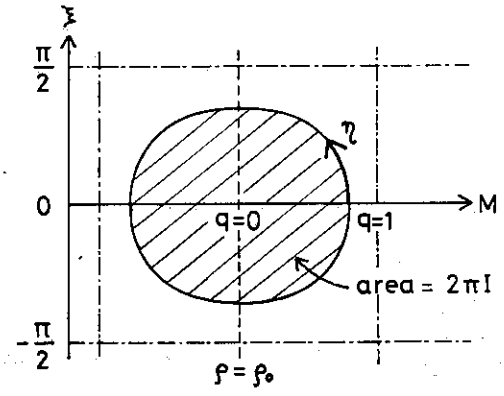

Fig. 5.2 Illustration of the relationship between the action-angle variables (I,η) and (ξ,M).

Since the time-dependent part of the Hamiltonian, H_1, has an explicit periodicity of period $(\ell-n)\omega/n$, the force derived from H_1 is able to resonate with the periodic motion determined from Eqs. (5.26) and (5.27) and to form islands on the resonant trajectory. When we use the asymptotic expansion of J_ℓ and take account of only the terms, $\ell = n+1$, dominant for the island formation, H_1 is approximated by

$$H_1 = -2e\phi\sqrt{2}/\pi k\rho_0 \sin k\tilde{\rho} \sin\xi \sin\{(\xi+\omega t)/n\} \quad . \tag{5.30}$$

Then using this simplified H_1, we find that dI/dt does not vanish;

$$\frac{dI}{dt} = \frac{dI}{dH_0}\left(-\frac{\partial H_0}{\partial M}\frac{\partial H_1}{\partial \xi} + \frac{\partial H_0}{\partial \xi}\frac{\partial H_1}{\partial M}\right) \tag{5.31}$$

$$= \frac{m\Omega_i\rho_0}{kn}\frac{2\omega_t^2}{\Omega_t}\left(\cos^2 k\tilde{\rho}\sin^2\xi - \sin^2 k\tilde{\rho}\cos^2\xi\right)\sin\left(\frac{\xi+\omega t}{n}\right) \tag{5.32}$$

$$= \sum_{-\infty}^{\infty} \Gamma_s \sin\{2(2s+1)\Omega_t t - \frac{\xi+\omega t}{n}\} \quad , \tag{5.33}$$

where

$$\Gamma_s = -\frac{m\Omega_i\rho_0}{kn}\omega_t\frac{8\pi}{F_0}\frac{(2s+1)r^{2s+1}}{1-r^{2(2s+1)}} \quad . \tag{5.34}$$

Here we have iterated $k\tilde{\rho}$ and ξ by the solution derived from H_0 and have used the series expansion [75] of Jacobian elliptic functions in terms of the nome: $r \equiv \exp\{-\pi F_0(q')/F_0(q)\}$ where $q'^2 = 1-q^2$. In case of our interest, $n \gg 1$, the time variation of $\xi/n \sim 0(\omega_t/n)$ can be neglected. Hence the resonance condition is given by

$$\Omega_t(I_r) = \frac{1}{2(2s+1)}\frac{\omega}{n} \simeq \frac{1}{2(2s+1)}\Omega_i \quad (s : \text{integer}) \quad . \tag{5.35}$$

Because of the I dependence of $\Omega_t(I)$, this resonance leads to the island formation on the resonant trajectory. Near the resonance $I = I_r$, the equations of motion are approximated by the expression,

$$d\Delta I/dt = \Gamma_s \sin\Delta\eta \quad , \tag{5.36}$$

$$d\Delta\eta/dt = 2(2s+1)\{d\Omega_t(I_r)/dI\}\Delta I \quad , \tag{5.37}$$

here the variables ΔI and $\Delta\eta$ are defined by

$$\Delta I \equiv I - I_r \quad , \tag{5.38}$$

$$\Delta\eta \equiv 2(2s+1)\{\Omega_t(I) - \Omega_t(I_r)\}t \quad , \tag{5.39}$$

and the nonresonant terms in Eq. (5.33) have been neglected. The first integral of Eqs. (5.36) and (5.37),

$$G = 2(2s+1)\{d\Omega_t(I_r)/dI\}\{(\Delta I)^2/2\} + \Gamma_s \cos\Delta\eta \quad , \tag{5.40}$$

gives the width of the island,

$$\Delta I_{max} = 2\left|\frac{\Gamma_s}{2(2s+1)(d\Omega_t(I_r)/dI)}\right|^{1/2} \quad ; \tag{5.41}$$

therefore the frequency width of the island is

$$\Delta\Omega_{t_{max}} = 2\left|\frac{(d\Omega_t(I_r)/dI)\Gamma_s}{2(2s+1)}\right|^{1/2} \quad . \tag{5.42}$$

On the other hand, the frequency spacing of adjacent resonances is obtained from Eq. (5.35) as follows,

$$\delta\Omega_t \equiv \Omega_t^{(s-1)} - \Omega_t^{(s)} = \left\{\frac{1}{2(2s-1)} - \frac{1}{2(2s+1)}\right\}\frac{n}{\omega} \sim \frac{4\Omega_t{}^2}{\Omega_i} \quad . \tag{5.43}$$

The explanation of the meaning of $\Delta\Omega_{t_{max}}$ and $\delta\Omega_t$ is shown in Fig. 5.3.

When adjacent islands overlap, i.e.,

$$K \equiv \left(\frac{2\Delta\Omega_{t_{max}}}{\delta\Omega_t}\right) = \frac{\Omega_i}{\omega_t{}^2}\frac{1}{\sinh\{\Omega_i F_0(q')/\omega_t\}}\frac{8}{\pi}\frac{E_0(q) - q'^2 F_0(q)}{q'q^2} \gtrsim 1 \quad , \tag{5.44}$$

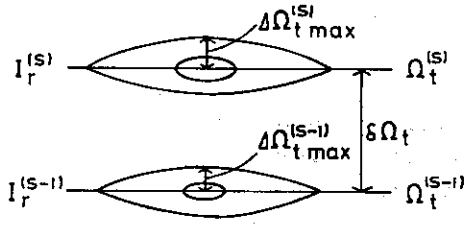

Fig.5.3 A sketch of the frequency width of islands $\Delta\Omega_t$ and the frequency spacing of adjacent resonance $\Delta\Omega_t$.

stochastic instability [76] occurs and the motion of a phase point becomes stochastic; here E_0 denotes the complete elliptic integrals of the second kind. It should be noted that if q approaches unity, the quantity K diverges provided that $\Omega_t/\Omega_i \neq 0$; therefore a stochastic layer always exists in the vicinity of a separatrix. The ratio R of the phase space area of the stochastic layer ($K > 1$) to the total phase space area of the cell $2\pi I(q = 1)$ can be calculated from Eqs. (5.28) and (5.44) as a function of ω_t/Ω_i,

$$R(\omega_t/\Omega_i) = 1 - I(q;K = 1)/I(q = 1) \ , \tag{5.45}$$

and is exhibited in Fig. 5.4. It is found that the ratio R begins to increase fairly abruptly when ω_t/Ω_i exceeds 0.15, which is regarded as a threshold for stochastic behavior of ion motions being appreciable. The saturation of R can be seen where $\omega_t/\Omega_i \gtrsim 0.5$; however, if we take account of the higher order resonance, $\ell = n \pm j$ ($j \geqq 2$), it is inferred that the ratio R keeps increasing to attain unity.

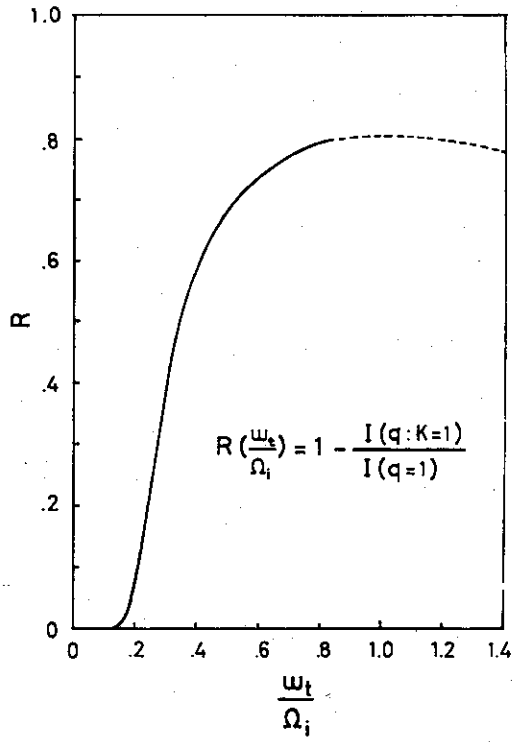

Fig.5.4 The ratio of the phase space area of the stochastic layer to the total space area of the cell.

In order to visualize the above consideration, numerical calculations are carried out according to Eq. (5.4). Two examples for different amplitudes are shown in Fig. 5.5; the bounce frequencies at the center are (a) ω_t/Ω_i = 0.13 and (b) 0.25. In each case ω/Ω_i is equal to 5 and the phase points are plotted at intervals of $\Delta t = 2\pi/\Omega_i$; theoretically predicted separatrix and the center of cell are indicated in the figures. In the case (a), most of phase points move periodically. On the contrary, in the case (b), islands at the resonance of $\Omega_t(I)/\Omega_i = 1/6$ are observed and the motion becomes highly irregular outside of the trajectory which starts from $(k\rho, \xi) = (8.15, 0.0)$.

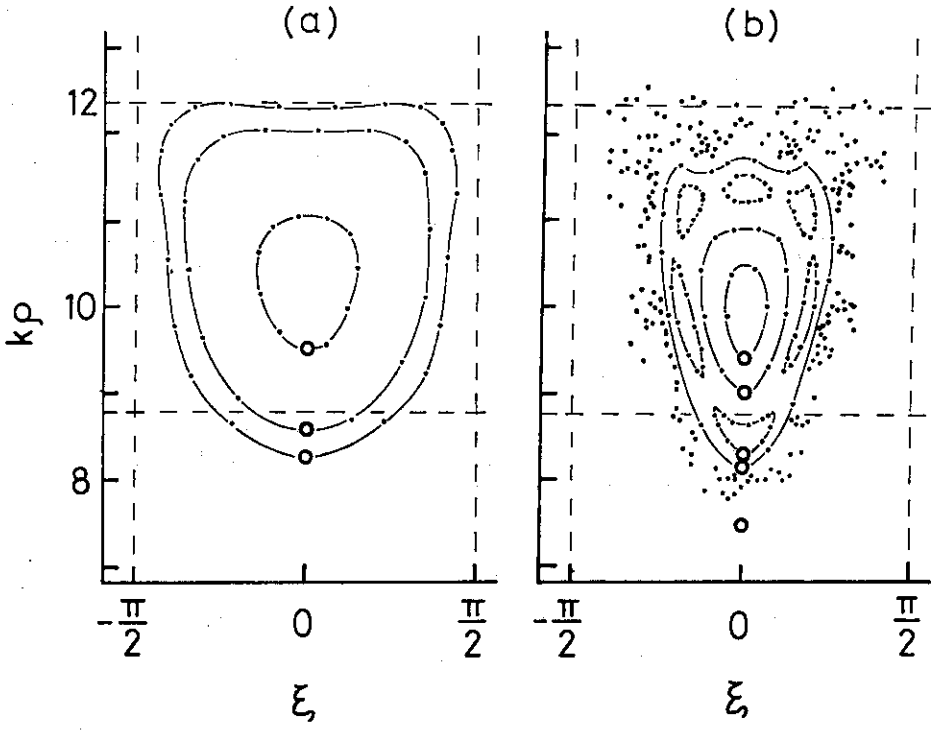

Fig. 5.5 Numerically calculated motions of phase points. Points are plotted at intervals of $2\pi/\Omega_i$; the initial points are indicated by circles. The frequency of the wave is 5 Ω_i and the amplitude are (a) $(\omega_b/\Omega_i)^2$=1 and (b) 2. The broken lines show the theoretically predicted separatrices.

§5-2 Tail formation and the threshold

Since the stochastic layer exists on both sides of a separatrix, it should be expected that diffusion of phase points from a cell to another cell takes place, when both stochastic layers in adjacent cell are appreci-

ably wide. The values of R and ω_t which characterize a cell become small with the increase of $k\rho_0$; therefore, diffusion in an ion perpendicular velocity distribution may not occur where ion energy exceeds a certain value.

Numerical calculations verify the discussions described above. At first, the motion of a test ion initially at $(k\rho,\xi) = (7.4, 0.0)$ is exhibited in Fig. 5.6, when the frequency and the amplitude are the same as Fig. 5.5(b).

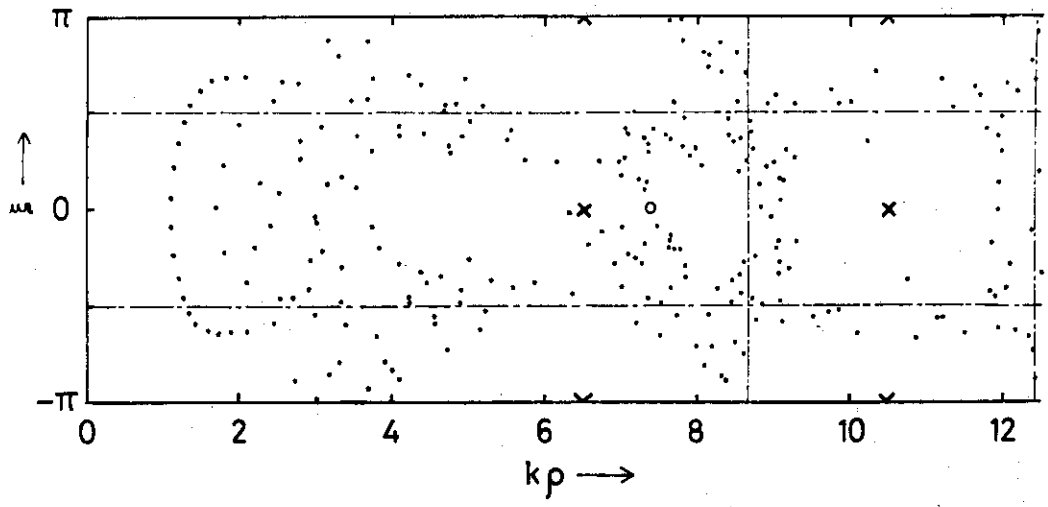

Fig. 5.6 Motion of a phase point. Parameters are the same as Fig. 5.5 (b), but the initial point differs from the previous case.

It can be seen that the phase points randomly wonder from a cell to an adjacent cell. Next the motions of ten ions are traced; their initial velocities are chosen as $k\rho = 2$, the frequency of the wave is $5\Omega_i$, and the amplitudes are (a) $(\omega_b/\Omega_i)^2 = 1$, (b) 1.5, and (c) 2. Figure 5.7 shows the time variation of the mean gyration radius defined by

$$\overline{k\rho}(t) = \frac{k}{\Omega_i}\left\{\frac{1}{10}\sum_{j=1}^{10} v_{\perp j}^2(t)\right\}^{1/2}, \tag{5.46}$$

where subscript j specifies an ion. We observe in Fig. 5.7 (a) that $\overline{k\rho}(t)$ oscillates with period about $200\ \Omega_i^{-1}$ but changes little in the value averaged over the time $200\ \Omega_i^{-1}$. In Fig. 5.8, we then exhibit the time evolution of the time-averaged distribution defined by

$$f(k\rho,t_{i_2}) = \frac{1}{i_2 - i_1 + 1}\sum_{i=i_1}^{i_2}\sum_{j=1}^{10}\delta(k\rho_j(t_i) - k\rho), \tag{5.47}$$

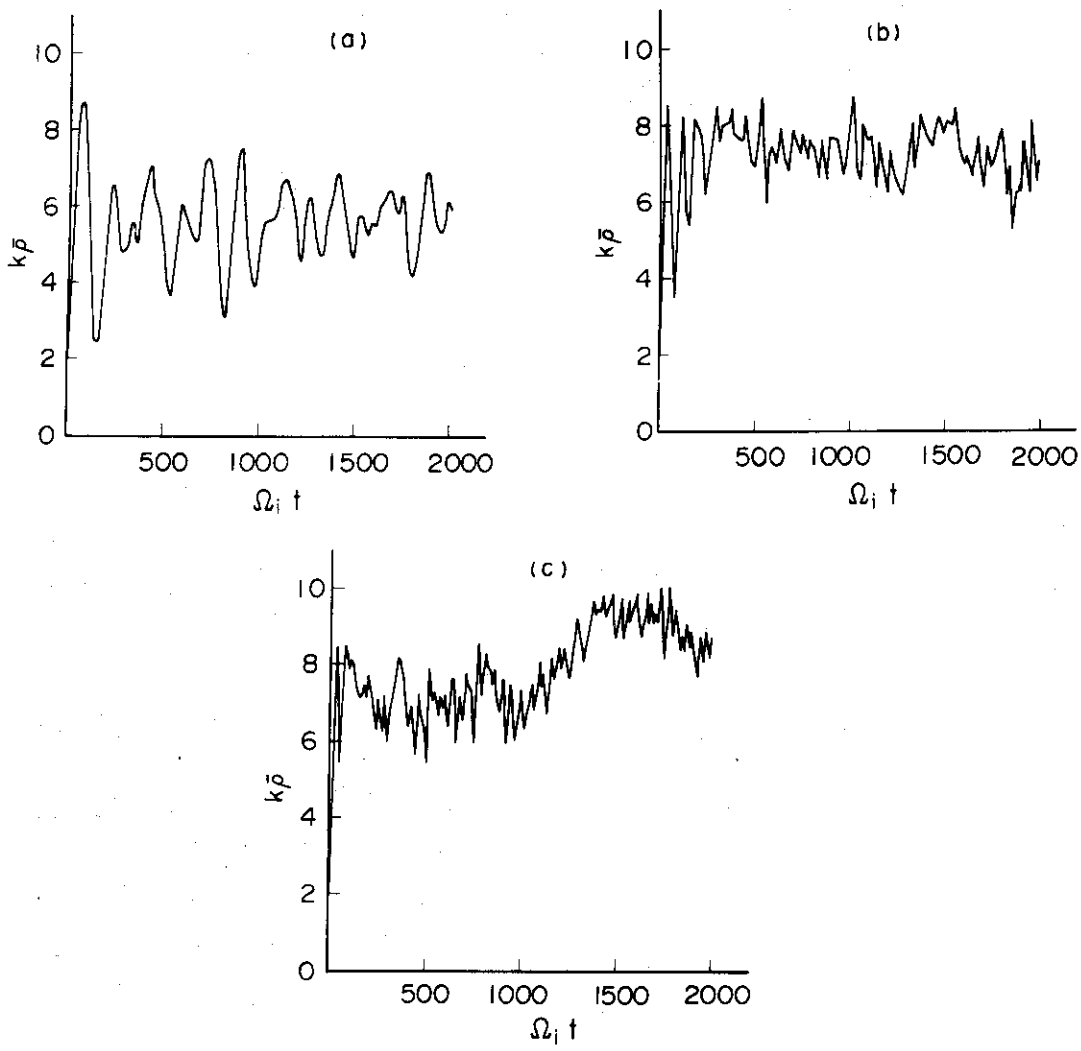

Fig. 5.7 Time variation of the mean gyration radius of ten ions, initially $k\rho = 2$. The frequency of the wave is 5 Ω_i and the amplitudes are (a) $(\omega_b/\Omega_i)^2 = 1$, (b) 1.5, and (c) 2.

where the time interval $\Delta t = t_{i+1} - t_i$ is equal to 2 Ω_i^{-1} and the duration for averaging $T = t_{i_2} - t_{i_1}$ is 200 Ω_i^{-1}. In the case (a), ions cannot be diffused into an upper cell placed over $k\rho^* = 8.7$ where $\omega_t/\Omega_i = 0.13$. On the other hand, a high energy tail is formed up to $k\rho^* = 12.3$ (case b) and up to $k\rho^* = 15.7$ (case c). The values of ω_t/Ω_i in each cell are tabulated in Table 5.1; the cells are separated by separatrices $k\rho = k\rho^*$ where $J_5(k\rho^*) = 0$. It is easy to see from these results that the limit of the tail is determined by the condition $\omega_t/\Omega_i \simeq 0.15$.

The upper limit of the tail is evaluated in case of the LHRH in JT-60. The frequency of the wave is about 17 Ω_i ($\Omega_i \simeq 4.8\times10^8$ sec^{-1}) and the amplitude is $(\omega_b/\Omega_i)^2 \simeq 3.5$ near the turning points: $\phi \simeq 5\times10^2$ V and $k_\perp \simeq 4\times10^3$ m^{-1}. The condition $\omega_t/\Omega_i \simeq 0.15$ gives the limit $k\rho \simeq 47$, i.e., the energy is about 160 keV.

Table 5.1 The values of ω_f / Ω_i

$k\rho^*$		0	8.7	12.3	15.7
$\left(\frac{\omega_b}{\Omega_i}\right)^2$	1.0	0.29	0.13	0.08	0.06
	1.5	0.43	0.19	0.12	0.08
	2.0	0.57	0.25	0.16	0.11

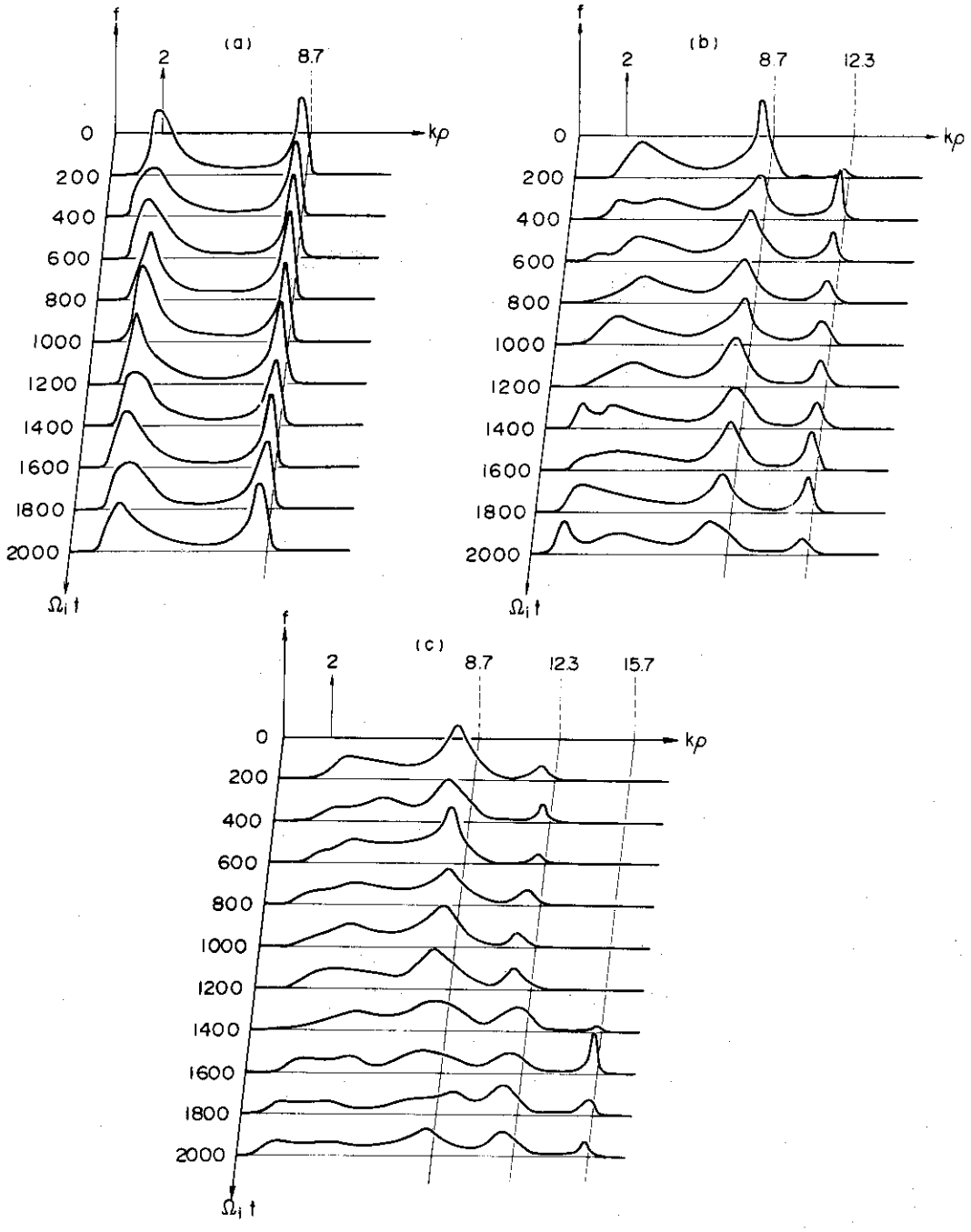

Fig. 5.8 Time-averaged distributions of ten ions. They are averaged over the duration 200 Ω_i^{-1}. The parameters are the same as Fig. 5.7.

§6. Summary and discussion

Here we will summarize the results of the preceding sections. First, it is shown that the requisite power for obtaining 7 keV plasma in JT-60 is about 10 MW. Assuming the scaling $\tau_E \propto Na^2$, we have W/T proportional to R. Therefore the ratio W/T for present tokamaks is comparable to that for JT-60.

Next, linear behaviors of lower hybrid waves are considered provided that the power is not so large. In a slab geometry, where the density gradient is taken into account, a lower hybrid wave, which satisfies the accessibility condition (Eq. (3.12)), is converted linearly to an outgoing wave before it reaches the resonance point. The conversion rate is obtained as Eq. (3.81). Damping mechanisms of the incident and outgoing waves are clarified. The electron Landau damping is the dominant one for $k_{\parallel} v_{Te} \sim \omega$, the ion cyclotron damping near the turning point is mostly effective if $\nu_{ii} < \Omega_i/(k_\perp \rho_i)^2$, and the collisional restored ion Landau damping is effective if $\Omega_i > \nu_{ii} > \Omega_i/(k_\perp \rho_i)^2$. The effects of the inhomogeneous magnetic field are also investigated. The wave propagates through a pass band difined as $|\omega - n\Omega_i(x)| > 4k_{\parallel} v_{Ti}$. The wave is damped in the vicinity of $\omega = n\Omega_i(x)$, and the spatially averaged absorption is compared to that by the unmagnetized ion Landau damping. The magnetic shear is not appreciable for the propagation or damping.

By ray tracing in a toroidal geometry, one can see in Fig. 3.28 that k is changed near the resonance surface in a cold plasma. On the other hand, the turning point shifts outwards in a warm plasma, and the effect of toroidicity can be negligible.

Parametric phenomena of lower hybrid waves are studied without dipole approximation. With respect to the excitation of low frequency waves, it is clarified that the finiteness of the pump wavelength does not affect on the threshold. The parametric thresholds in JT-60 are also calculated. In JT-60, the excitations electrostatic backward ion cyclotron modes and ion quasi modes dominate, of which thresholds are several 10^5 V/m.

Finally the posibility of the formation of the high energy ion tail is indicated when the external wave is sufficiently large. The upper limit of the tail is obtained by the condition $\omega_t/\Omega_i > 0.15$ (ω_t is given by Eq. (5.17)). A fairly good agreement is obtained between the theoretical result and that of numerical calculations (Fig. 5.8).

Acknowledgement

Authors would like to thank Dr. M. Tanaka and Prof. R. Itatani of Kyoto University for their encouragements and fruitful discussions. This work was partially supported by the Grand in Aids for Scientific Research of the Ministry of Education, Science and Culture in Japan.

References

1) M. Yoshikawa: IAEA Technical Committee Meeting on Large Tokamak Experiments, Dubna, 4~11, July, 1975. (Nuclear Fusion, 15 (1975) 909, compiled by A.H. Spans.)
2) T. Nagashima: private communication.
3) H. Kritz and O. Eldridge: Nuclear Fusion, 15 (1975) 465.
4) V. M. Glagolev: Plasma Physics, 14 (1972) 301, and ibid 14 (1972) 315.
5) S. S. Pesic: Plasma Physics, 15 (1973) 193.
6) P. M. Bellan and M. Porkolab: Phys. Fluids, 17 (1974) 1592.
7) M. D. Simonutti: Phys. Fluids, 18 (1975) 1524.
8) H. H. Kuehl and K. K. Ko: Phys. Fluids, 18 (1975) 1816.
9) I. Fidone: Phys. Fluids, 19 (1976) 334.
10) V. E. Golant: Sov. Phys. - Tech. Phys., 16 (1972) 1980.
11) M. Brambilla: Nuclear Fusion, 14 (1974) 327.
12) M. Krämer: Plasma Physics, 17 (1975) 373.
13) Y. N. Dnestrovski, D. P. Kostomarov, G. V. Pereverzev and A. V. Pogoshan: Fiz. Plasmi., 1 (1975) 623.
14) E. Lazzaro: Plasma Physics, 17 (1975) 1033.
15) J. J. Schuss: Phys. Fluids, 18 (1975) 1178.
16) P. L. Colestock and W. D. Getty: Phys. Fluids, 19 (1976) 1229.
17) T. H. Stix: Phys. Rev. Lett., 15 (1965) 878.
18) A. D. Piliya and V. I. Fedorov: Sov. Phys. - JETP, 30 (1970) 653.
19) T. Tang: Phys. Fluids, 13 (1970) 121.
20) B. N. Moore and M. E. Oakes: Phys. Fluids, 15 (1972) 144.
21) I. Fidone and R. B. Paris: Phys. Fluids, 17 (1974) 1921.
22) S. Weinberg: Phys. Rev., 126 (1962) 1899.
23) I. B. Bernstein: Phys. Fluids, 18 (1975) 320.
24) A. D. Piliya and V. I. Fedorov: Sov. Phys. - JETP, 33 (1971) 210.
25) R. J. Briggs and R. R. Parker: Phys. Rev. Lett., 29 (1972) 852.
26) K. Ohkubo, K. Ohasa and K. Matsuura: IPPJ-233, Institute of Plasma

Acknowledgement

Authors would like to thank Dr. M. Tanaka and Prof. R. Itatani of Kyoto University for their encouragements and fruitful discussions. This work was partially supported by the Grand in Aids for Scientific Research of the Ministry of Education, Science and Culture in Japan.

References

1) M. Yoshikawa: IAEA Technical Committee Meeting on Large Tokamak Experiments, Dubna, 4~11, July, 1975. (Nuclear Fusion, 15 (1975) 909, compiled by A.H. Spans.)
2) T. Nagashima: private communication.
3) H. Kritz and O. Eldridge: Nuclear Fusion, 15 (1975) 465.
4) V. M. Glagolev: Plasma Physics, 14 (1972) 301, and ibid 14 (1972) 315.
5) S. S. Pesic: Plasma Physics, 15 (1973) 193.
6) P. M. Bellan and M. Porkolab: Phys. Fluids, 17 (1974) 1592.
7) M. D. Simonutti: Phys. Fluids, 18 (1975) 1524.
8) H. H. Kuehl and K. K. Ko: Phys. Fluids, 18 (1975) 1816.
9) I. Fidone: Phys. Fluids, 19 (1976) 334.
10) V. E. Golant: Sov. Phys. - Tech. Phys., 16 (1972) 1980.
11) M. Brambilla: Nuclear Fusion, 14 (1974) 327.
12) M. Krämer: Plasma Physics, 17 (1975) 373.
13) Y. N. Dnestrovski, D. P. Kostomarov, G. V. Pereverzev and A. V. Pogoshan: Fiz. Plasmi., 1 (1975) 623.
14) E. Lazzaro: Plasma Physics, 17 (1975) 1033.
15) J. J. Schuss: Phys. Fluids, 18 (1975) 1178.
16) P. L. Colestock and W. D. Getty: Phys. Fluids, 19 (1976) 1229.
17) T. H. Stix: Phys. Rev. Lett., 15 (1965) 878.
18) A. D. Piliya and V. I. Fedorov: Sov. Phys. - JETP, 30 (1970) 653.
19) T. Tang: Phys. Fluids, 13 (1970) 121.
20) B. N. Moore and M. E. Oakes: Phys. Fluids, 15 (1972) 144.
21) I. Fidone and R. B. Paris: Phys. Fluids, 17 (1974) 1921.
22) S. Weinberg: Phys. Rev., 126 (1962) 1899.
23) I. B. Bernstein: Phys. Fluids, 18 (1975) 320.
24) A. D. Piliya and V. I. Fedorov: Sov. Phys. - JETP, 33 (1971) 210.
25) R. J. Briggs and R. R. Parker: Phys. Rev. Lett., 29 (1972) 852.
26) K. Ohkubo, K. Ohasa and K. Matsuura: IPPJ-233, Institute of Plasma

Physics, Nagoya University, Oct. 1975.

27) I. B. Bernstein: Phys. Rev., 109(1958) 10.

28) J. P. Dougherty: Phys. Fluids, 7 (1964) 1788.

29) J. P. M. Schmitt: J. Plasma Physics, 12 (1974) 51.

30) S. Ichimaru: "Basic Principles of Plasma Physics" (Benjamin, 1973).

31) B. A. Trubnikov: "Review of Plasma Physics" (Consultants Bureau, 1965), Vol. I.

32) P. M. Morse and H. Feshbach: "Methods of Theoretical Physics" (McGraw-hill, 1953), Pt. 1, 434.

33) V. M. Glagolev et al.: in Proc. 4th Intern. Conf. Plasma Physics and Controlled Nuclear Fusion Research, Wisconsin, 1971, IAEA-CN-28/L-6.

34) B. V. Galaktionov et al.: Sov. Phys. - Tech. Phys., 15 (1971) 1809.

35) W. M. Hooke and S. Bernabei: Phys. Rev. Lett., 29 (1972) 1218.

36) V. V. Alikaev et al.: in Proc. 6th Europ. Conf. on Controlled Nuclear Fusion and Plasma Physics, Moskow, 1 (1973) 63.

37) P. Bellan and M. Porkolab: Phys. Rev. Lett., 34 (1975) 124.

38) S. Bernabei, M. A. Heald, W. H. Hooke and F. J. Paoloni: Phys. Rev. Lett., 34 (1975) 866.

39) P. A. Raimbault and J. L. Shohet: Plasma Physics, 17 (1975) 327.

40) P. Bellan and M. Porkolab: Phys. Fluids, 19 (1976) 995.

41) M. Porkolab: Physica, 82C (1976) 86.

42) M. Porkolab: in a Symposium on Plasma Heating in Toroidal Devices, Varenna, Italy, 1974 (MATT-1069, Plasma Physics Laboratory, Princeton University, 1974).

43) M. Porkolab: Phys. Fluids, 17 (1974) 1432.

44) E. Ott: Phys. Fluids, 18 (1975) 566.

45) R. L. Berger and F. W. Perkins: Phys. Fluids, 19 (1976) 406.

46) R. L. Berger and L. Chen: MATT-1211, Plasma Physics Laboratory, Princeton University, 1976.

47) P. K. Kaw and Y. C. Lee: Phys. Fluids, 16 (1973) 155.

48) A. K. Sundaram and P. K. Kaw: Nuclear Fusion, 13 (1973) 901.

49) J. J. Thomson: Nuclear Fusion, 15 (1975) 237.

50) I. Fidone and G. Granata: Phys. Fluids, 19 (1976) 293.

51) Y. Y. Kuo and L. Chen" Phys. Fluids, 19 (1976) 1223.

52) A. Rogister: Phys. Rev. Lett., 34 (1975) 80.

53) A. Hasegawa and L. Chen: Phys. Fluids, 18 (1975) 1321.

54) A. Rogister and G. Hasselberg: Phys. Fluids, 19 (1976) 108.

55) L. Chen and R. L. Berger: MATT-1169, Plasma Physics Laboratory, Princeton University, 1975.

56) G. J. Morales and Y. C. Lee: Phys. Rev. Lett., 33 (1975) 1534.
57) P. K. Kaw: MATT-1208, Plasma Physics Laboratory, Princeton University, 1976.
58) J. M. Kindel, H. Okuda and J. M. Dawson: Phys. Rev. Lett., 29 (1972) 995.
59) E. Ott, J. B. McBride and J. H. Orens: Phys. Fluids, 16 (1973) 270.
60) M. H. Emery and G. Joyce: U. of Iowa 74-29, University of Iowa, 1974.
61) C. Chu, J. M. Dawson and H. Okuda: PPG-219, University of California, 1975.
62) P. L. Bhatnager, E. P. Gross and M. Krook: Phys. Rev., 94 (1954) 511.
63) T. Amano and M. Okamoto: J. Phys. Soc. Japan, 26 (1969) 529.
64) A. W. Trivelpiece and R. W. Gould: Journal of App. Phys. 30 (1959) 1784.
65) M. N. Rosenbluth: Phys. Rev. Lett., 29 (1972) 565.
66) I. P. Gladkovskii et al.: Sov. Phys. - Tech. Phys. 18 (1974) 1029.
67) V. V. Alikaev et al.: Sov. Phys. - Tech. Phys. 20 (1975) 327.
68) G. R. Smith and A. N. Kaufman: Phys. Rev. Lett. 34 (1975) 1613.
69) A. V. Timofeev: Nucl. Fusion 14 (1974) 165.
70) M. N. Rosenbluth: Phys. Rev. Lett. 29 (1972) 408.
71) F. Jaeger, A. J. Lichtenberg and M. A. Lieberman: Plasma Phys. 14 (1972) 1074.
72) M. A. Lieberman and A. J. Lichtenberg: Plasma Phys. 15 (1973) 125.
73) E. F. Jaeger and A. J. Lichtenberg: Ann. Phys. (N.Y.) 71 (1972) 319.
74) R. E. Aamodt and S. E. Bodner: Phys. Fluids 12 (1969) 1471.
75) M. Abramowitz and I. A. Stegun: "Handbook of Mathematical Functions (Dover Publications, Inc., New York, 1970)", P. 575.
76) G. M. Zaslavskii and B. V. Chirikov: Sov. Phys.-Usp. 14 (1972) 549.

Appendix A

I) Plasma dispersion function W(z)

The function W(z) is defined by

$$W(z) = \frac{1}{\sqrt{2\pi}} \int_C \frac{x}{x - z} \exp\left(-\frac{x^2}{2}\right) dx. \tag{A1}$$

The contour C is so chosen that the point z is always above C.

The convergent series for $|z| < 1$ is given by

$$W(z) = i\sqrt{\frac{\pi}{2}}\, z \exp\left(-\frac{z^2}{2}\right) + 1 - z^2 + \frac{z^2}{3} - \cdots\cdots + \frac{(-1)^n z^{2n}}{(2n-1)!!}\ , \tag{A2}$$

where $(2n-1)!! = (2n-1)(2n-3)\cdots\cdots 3\cdot 1$, and asymptotic series for large $|z|$ by

$$W(z) = i\sqrt{\frac{\pi}{2}}\, z \exp\left(-\frac{z^2}{2}\right) - \frac{1}{z^2} - \frac{3}{z^2} - \cdots\cdots - \frac{(2n-1)!!}{z^{2n}}\ . \tag{A3}$$

II) Function $\Lambda_n(\lambda)$

We define the function $\Lambda_n(\lambda)$ by

$$\Lambda_n(\lambda) = I_n(\lambda) e^{-\lambda}\ . \tag{A4}$$

For $\lambda \ll 1$, $\Lambda_n(\lambda)$ is approximated by

$$\Lambda_0(\lambda) \simeq 1 - \lambda + \frac{3}{4}\lambda^2 - \frac{5}{12}\lambda^3 + \frac{3}{16}\lambda^4 + \cdots\cdots, \tag{A5}$$

$$\Lambda_n(\lambda) \simeq \left(\frac{\lambda}{2}\right)^n / n!\ . \tag{A6}$$

If $\lambda \gg 1$ or $n \gg 1$, the following approximation holds,

$$\Lambda_n(\lambda) \simeq \frac{1}{\sqrt{2\pi}} \frac{1}{(n^2+\lambda^2)^{1/4}} \exp\left[(n^2+\lambda^2)^{1/2} - \lambda\right] \left(\frac{n}{\lambda} + \sqrt{\frac{n^2}{\lambda^2}+1}\right)^{-n}$$

$$\times \left\{1 + O\left(\frac{1}{\sqrt{n^2+\lambda^2}}\right)\right\} \quad ; \tag{A7}$$

especially for $\lambda \gg n \gg 1$, this is simplified to

$$\Lambda_n(\lambda) \sim \frac{1}{\sqrt{2\pi\lambda}} \exp\left(-\frac{n^2}{2\lambda}\right) . \qquad \text{(A8)}$$

The comparison between Eq. (A8) and the exact value $\Lambda_n(\lambda)$ is tabulated below for an example n = 30.

λ	$\Lambda_{30}(\lambda)$	(A8)
1	-	-
4	5.27×10^{-34}	2.76×10^{-50}
9	3.51×10^{-17}	2.56×10^{-23}
16	3.89×10^{-12}	6.09×10^{-14}
25	4.68×10^{-9}	1.22×10^{-9}
36	3.99×10^{-7}	2.48×10^{-7}
49	7.01×10^{-6}	5.85×10^{-6}
64	4.74×10^{-5}	4.41×10^{-5}
81	1.77×10^{-4}	1.71×10^{-4}
100	4.48×10^{-4}	4.43×10^{-4}

Appendix B

Using Eq. (3.38) and Appendix A, we obtain the summation of $\mathrm{Im}\, w_n(\omega^*)$ for $k_{\parallel}\rho_i \gg 1$ and $k_{\perp}\rho_i \gg 1$,

$$\bar{w} \equiv \sum_{n=-\infty}^{\infty} \mathrm{Im}\, w_n(\omega^*) = \sum_{n=-\infty}^{\infty} \sqrt{\frac{\pi}{2}} \frac{\omega^*}{k_{\parallel}\rho_i} \exp\left(-\frac{(\omega^*-n)^2}{2k_{\parallel}^2\rho_i^2} - \frac{n^2}{2k_{\perp}^2\rho_i^2}\right) . \qquad \text{(B1)}$$

By the following transformation,

$$k_{\perp}\rho_i = \frac{kv_{Ti}}{\Omega_i}\cos\theta \quad , \qquad k_{\parallel}\rho_i = \frac{kv_{Ti}}{\Omega_i}\sin\theta \quad , \qquad \text{(B2)}$$

Eq. (B1) becomes

$$\bar{w} = \sum_{n=-\infty}^{\infty} \frac{\omega\Omega_i}{2k^2v_{Ti}^2\sin\theta\cos\theta} \exp\left[-\frac{(\omega-n\Omega)^2\cos^2\theta + n^2\Omega^2\sin^2\theta}{2k^2v_T^2\sin^2\theta\cos^2\theta}\right]$$

$$= \sum_{n=-\infty}^{\infty} \frac{\omega}{2kv_{Ti}} \frac{\Omega_i}{kv_{Ti}\sin\theta\cos\theta} \exp\left[-\frac{\omega^2}{2k^2v_{Ti}^2}\right] \exp\left[-\frac{1}{2}\left(\frac{n\Omega_i - \omega\cos^2\theta}{kv_{Ti}\sin\theta\cos\theta}\right)^2\right]. \qquad \text{(B3)}$$

On the assumption that $\omega\cos^2\theta \gg kv_{Ti}\sin\theta\cos\theta \gg \Omega_i$ we may replace the summation by the integration as follows,

$$\bar{w} = \frac{\omega}{2kv_{Ti}} \exp[-\frac{\omega^2}{2k^2 v_{Ti}{}^2}] \int_{-\infty}^{\infty} dx \exp[-\frac{1}{2}(x - \frac{\omega\cos^2\theta}{kv_{Ti}\sin\theta})^2] , \tag{B4}$$

where

$$dx = \frac{\Omega_i}{kv_{Ti}\sin\theta\cos\theta} , \quad x = \frac{n\Omega_i}{kv_{Ti}\sin\theta\cos\theta} . \tag{B5}$$

Therefore the result of unmagnetised ion model can be recovered,

$$\bar{w} = \sqrt{\frac{\pi}{2}} \frac{\omega}{kv_{Ti}} \exp(-\frac{\omega^2}{2k^2 v_{Ti}{}^2})$$

$$= \mathrm{Im}\, W(\frac{\omega}{kv_{Ti}}) . \tag{B6}$$

Appendix C

Assuming the solution of the form

$$\phi(u) = \int_C g(p) e^{pu} dp , \tag{C1}$$

we look for the condition that the function g(p) and the contour C should satisfy. Substituting Eq. (C1) and

$$\frac{d^n\phi}{du^n} = \int_C g(p)\, p^n e^{pu}\, du . \tag{C2}$$

into Eq. (3.62) and integrating by part, we find

$$\int_C g(p)[p^4 + i\varepsilon p^2 + p + \mu + up^2]e^{pu}\, du$$

$$= \int_C g(p)[p^4 + i\varepsilon p^2 + p + \mu]e^{pu}\, du + [g(p)p^2 e^{pu}]_C - \int_C \frac{d}{dp}\, p^2 g(p)\, e^{pu}\, du$$

$$= \int_C [(p^4 + i\varepsilon p^2 + p + \mu)g(p) - \frac{d}{dp}(p^2 g(p))]e^{pu} du + [g(p)p^2 e^{pu}]_C = 0 . \tag{C3}$$

Therefore if g(p) is a solution of the first order differential equation,

$$(p^4 + i\varepsilon p^2 + p + \mu)g(p) = \frac{d}{dp}(p^2 g(p)) , \tag{C4}$$

and the contour C is so chosen that the value,

$$V(p) \equiv g(p)\, p^2\, e^{pu} \quad ,$$

has the same value at the end points, $\phi(u)$ becomes a solution of Eq. (3.62).